Concentration-dependent Recruitment of Mammalian Odorant Receptors

By

Xiaoyang Serene Hu

Department of Molecular Genetics & Microbiology
Duke University

Date:_____
Approved:

_____
Hiroaki Matsunami, Supervisor

_____
David Tobin

_____
Debra Silver

_____
Robert J. Lefkowitz

Dissertation submitted in partial fulfillment of
the requirements for the degree of
Doctor of Philosophy in the Department of
Molecular Genetics and Microbiology in the Graduate School
of Duke University

2019

ABSTRACT

Concentration-dependent Recruitment of
Mammalian Odorant Receptors

by

Xiaoyang Serene Hu

Department of Molecular Genetics & Microbiology
Duke University

Date:_____
Approved:

_____
Hiroaki Matsunami, Supervisor

_____
David Tobin

_____
Debra Silver

_____
Robert J. Lefkowitz

An abstract of a dissertation submitted in partial
fulfillment of the requirements for the degree of
Doctor of Philosophy in the Department of
Molecular Genetics and Microbiology in the Graduate School
of Duke University

2019

Copyright by
Xiaoyang Serene Hu
2019

Abstract

Deciphering natural odor plumes with dynamic changes in odor concentrations presents a common challenge to all animals. A fundamental challenge in studying the organization principles of the olfactory system to encode odor concentration information is the lack of comprehensively identified sets of activated odorant receptors (ORs) across an odorant concentration range inside freely behaving animals. In mammals, this has recently become feasible with high-throughput sequencing-based methods that identify populations of odorant activated ORs *in vivo*. In this study, we characterized the mouse OR repertoires activated by two odorants, acetophenone (ACT) and 2,5-dihydro-2,4,5-trimethylthiazoline (TMT), from 0.01% to 100% (v/v) concentrations. We also investigated the OR repertoires for structural derivatives of TMT (component of fox odor) such as 2-methyl-2-thiazoline (2MT) and 2,4,5-Trimethylthiazole (nTMT) and 2-sec-butyl-4,5-dihydrothiazole (SBT) for 1% and 100% (v/v) concentrations. We used a combination of *in vivo*, *in situ* and *in silico* approaches to investigate ORs with distinct sensitivities to the tested odorants. We examined Olfr923, which we identified to be one of the most sensitive ACT ORs based on our pS6-IP-Seq data. Using a mouse line that genetically labels Olfr923 positive axons, we provide evidence that ACT activates the Olfr923 glomerulus in the olfactory bulb. This study sheds light on the active process in which unique OR repertoires may collectively facilitate the discrimination of odorant concentrations. Together, these odorant receptors may shape the dynamic aspects of olfactory sensitivity and facilitate odorant intensity coding.

Dedication

To grandpa, who left us on May 9th, 2019 and would have been proud to see my Ph.D. defense. To grandma, who let me count every star in the night sky and sparked my interest in exploring the unknown.

Contents

Abstract iv

Contents vi

List of Figures xi

Acknowledgments xiii

1. Introduction 1

1.1 Olfaction is an important sense 1

1.2 Mammalian olfactory system 4

1.3 Phosphorylation of the ribosomal protein S6 6

1.4 Approaches to study OR responses *in vivo* 8

1.5 Zonal distribution of ORs 10

1.6 Concentration invariance in olfaction 11

1.7 Deorphanization of predator odors 12

1.8 Covalent modification of predator odor receptors 14

2. Updated method to identify ORs activated by odors *in vivo* 18

2.1 Introduction 18

2.2 Results 18

2.2.1 Modified pS6-IP-Seq enriched more ORs 19

2.2.2 Correlation between pS6-IP-Seq and *in vitro* OR responses 23

2.2.3 ROC classification of pS6-IP-Seq and *in vitro* OR responses 27

2.3 Conclusion and Discussion 28

3. Concentration-dependent OR recruitment 30

3.1 Introduction 30

3.2 Results 30

3.2.1 OR repertoires with different odorant concentrations 30

3.2.2 Most sensitive ORs may not be most robust responders at higher concentrations 32

3.2.3 Staining data confirms the pS6-IP-Seq OR enrichment 34

3.3 Conclusion and Discussion 38

4. Zonal activation of ORs is odor specific 41

4.1 Introduction 41

4.2 Results 41

4.2.1 RNA-Seq data relates to zonal index data 41

4.2.2 OR activation zones are odorant dependent 42

4.3 Conclusion and Discussion 43

5. Olfr923 as a model to evaluate pS6-IP-Seq 45

5.1 Introduction 45

5.2 Results 45

5.2.1 Olfr923 was not prominently downregulated in DREAM 45

5.2.2 ACT activated Olfr923 in the olfactory bulb 50

5.2.3 Modelling of ACT and Olfr923 *in silico* showed favorable free energy 52

5.3 Conclusion and Discussion 56

6. Predator odors and their chemical analogs 57

6.1 Introduction 57

6.2 Results..... 57

6.2.1 Freezing behavior paradigm 58

6.2.2 pS6-IP-Seq of TMT structural analogs 61

6.2.3 CRISPR/Cas9 knockout of TMT activated ORs 66

6.3 Conclusion and Discussion 70

7. Covalent modification of ORs 71

7.1 Introduction 71

7.2 Results..... 72

7.2.1 DTT inhibits some 2MT responsive ORs 72

7.2.2 Inhibition dependent OR and odorant 74

7.2.3 OR mutants show diminished response towards 2MT but not ACT 74

7.2.4 Clickable-TMT activated some ORs 78

7.3 Conclusion and Discussion 79

8. Conclusion 80

9. Methods 82

9.1 Animal protocol 82

9.1.1 Animals 82

9.1.2 Odor exposure 82

9.2 Olfr923-CRE Transgenic Mouse 83

9.2.1 Targeting of the Olfr923 locus 83

9.2.2 PCR Screening of Targeted ES Cells 84

9.2.3 ES Targeting 85

9.2.4 Olfactory bulb glomerulus visualization 85

9.3 GloSensor Assay 87

9.4 Immunohistology and in situ hybridizations 88

9.5 Next-generation sequencing 89

9.5.1 pS6-IP-Seq 89

9.5.2 RNA-Seq from dorsal and ventral olfactory epithelium 92

9.6 OR Mapping 92

9.6.1 OR gene definitions 93

9.6.2 OR sequence alignment 93

9.7 In silico modelling of Olfr923 94

9.7.1 Homology modelling 94

9.7.2 Molecular dynamics simulation 95

Appendix A 96

A.1 Detailed protocol for the updated pS6-IP-Seq 96

A.2 Detailed protocol for immunohistology and *in situ* hybridization 111

A.3 Protocol for Olfr376 gRNA designs 119

A.4 Cloning CRISPR guide sequences into pX330 121

A.5 Freezing Behavior Assay 123

Appendix B 125

B.1 Olfr1132 and Olfr491 cystine mutants 125

References 130

Biography 141

List of Figures

Figure 1: The mouse olfactory system 6

Figure 2: ORs are expressed in a zonal pattern at the olfactory epithelium 10

Figure 3: ORs responding to TMT/2MT may mediate the innate-fear response. 14

Figure 4: Ligands form covalent bonds with TRPA1 amino-acid residues 16

Figure 5: An illustration showing the updated pS6-IP-Seq method 20

Figure 6: The updated pS6-IP-Seq utilizes a monoclonal pS6 antibody 21

Figure 7: Comparison of Bowtie, Kallisto and STAR alignment 23

Figure 8: *In vivo* OR enrichment correlates with the *in vitro* activation data 25

Figure 9: pS6-IP-Seq enriched ORs show higher *in vitro* activation 27

Figure 10: ROC curves of support vector machine classifier performance 28

Figure 11: OR repertoires expand with increasing ACT concentrations 31

Figure 12: OR repertoires expand with increasing TMT concentrations 32

Figure 13: Volcano plots showing the enrichment of specific ACT and TMT ORs 34

Figure 14: pS6-IP-Seq enrichment data was verified via staining 35

Figure 15: Double-label *in situ* and immunostaining of OSNs 37

Figure 16: Additional 0.01% ACT responsive ORs showed pS6 colocalization 38

Figure 17: OR dorsal and ventral zonal distribution data based on RNA-Seq 41

Figure 18: ACT and TMT activated ORs have distinct zonal distributions 43

Figure 19: Olfr923 was not ACT responsive based on the DREAM technique 46

Figure 20: pS6 induction and downregulation of mRNA expression are correlated 48

Figure 21: ORs identified by DREAM have positive fold changes in pS6-IP-Seq 50

Figure 22: Exposure to ACT induces c-Fos expression in Olfr923 periglomerular neurons 51

Figure 23: c-Fos images for ACT exposed Olfr923 periglomerular neurons 52

Figure 24: Olfr923 is activated by ACT but not heptanal *in vitro* 53

Figure 25: *In silico* investigation of ACT binding to Olfr923 55

Figure 26: TMT structural analogs and mice freezing behavior 57

Figure 27: Predator naïve lab mice show freezing behavior towards 2MT 59

Figure 28: Mice Freezing behavior trials show concentration sensitivity 60

Figure 29: pS6-IP-Seq OR enrichment for TMT and its structural analogs 63

Figure 30: Lists of TMT and 2MT responsive ORs show some overlap 64

Figure 31: Triple homozygous mutants were generated with CRISPR 67

Figure 32: Non-target mutations were detected in genes such as Olfr153 68

Figure 33: Mosaicism was not detected in the CRISPR mouse 69

Figure 34: Freezing behavior was reduced in a triple knockout CRISPR mouse 70

Figure 35: Vapor-phase ACT or 2MT stimulation of pS6-IP-Seq enriched ORs 72

Figure 36: *In vitro* activation and inhibition of 2MT and its analogs is OR specific 74

Figure 37: Olfr1132 and Olfr491 cysteines to serine OR mutants 75

Figure 38: Olfr1132 and Olfr491 mutants showed a reduced response to 2MT 76

Figure 39: TMT and click-TMT activated slightly different sets of ORs *in vitro* 79

Figure 40: Homologous recombination of the Olfr923 targeting vector 84

Figure 41: Alignment of amino acid residues for 2MT responsive ORs 125

Acknowledgments

Thank you, Dr. Hiroaki Matsunami, for your support and guidance. This thesis would not have been possible without your mentorship. I am especially grateful to my committee members Dr Tobin, Dr Silver and Dr. Lefkowitz for their indispensable advice on this journey. My friends, coauthors, and colleagues at Duke also made this five-year marathon most remarkable.

I would like to thank my parents and grandparents, for their continuous support through my Ph.D. Their love and wisdom have guided me through the most challenging hours. I am most lucky to have met Frank Qian in my first semester at Duke. We have been inseparable since and had a wonderful 5 years pursuing our PhDs together. He is always incredibly supportive, and I would not have gotten this far without him. I am excited for our next stage of lives together.

1. Introduction

1.1 Olfaction is an important sense

The ability for organisms to sense the external world is essential for survival. Sensory systems equipped with peripheral neurons express protein receptors that detect and transmit information such as smells, colors and sounds from the external environments to the brain.

The nervous system is organized to encode external information across various sensory modalities. In the human visual system, three types of light receptors (S-cone, M-cones, and L-cones) have distinct sensitivities to different sections of the light spectrum, allowing for fine-tuned color discrimination (Nathans, 1987). In the human gustatory system, distinct receptors in the taste bud cells formulate the perception of our five basic taste qualities (sweet, bitter, salty, sour, sweet, and umami) (Lindemann, 1996). The human olfactory system has around 400 distinct odorant receptors dedicated to the task of distinguishing between the thousands of volatile odors that we encounter in the environment (Malnic et al., 2004).

Chemosensation refers to an organism's detection of an environmental chemical stimulus that is interpreted into a neurological signal (Bargmann, 2006a). The process of chemosensation has existed for a long time – from prehistoric to the evolutionarily recent. Primitive forms exist in nematode worms, emerged during the Cambrian explosion 500 million years ago. For instance, the well-studied invertebrate C. elegans possess a well-developed chemosensory system and dedicate 5% of its genes for detecting a wide variety

of volatile (olfactory) and water-soluble (gustatory) cues (Troemel et al., 1995; Bargmann, 1998, 2006b).

Without exception, every animal species studied to date has a form of chemosensation which allows it to sense the external environment. This includes insects, such as the fruit fly through their antennae (Clyne et al., 1999; Vosshall et al., 1999), fish through their frontal olfactory organs (Kasumyan, 2004), and humans through our noses (Bushdid et al., 2014). The basic units of olfaction are remarkably conserved from aquatic fishes to land-dwelling mammals (Laberge and Hara, 2001; Niimura et al., 2014). This repetitive theme in the evolution of olfactory biology signals a fundamental need for organisms to sense their chemical surroundings.

Despite a central theme in the evolution of chemosensation, there is significant diversity observed in the basic unit of olfaction – the receptors that recognize chemical ligand (Buck and Axel, 1991). Large receptor repertoires have been identified not only in vertebrates (Godfrey et al., 2004; Malnic et al., 2004; Niimura et al., 2014) but also in invertebrates (Clyne et al., 1999; McKenzie and Kronauer, 2018) suggesting that an evolutionary process creating enough diversity to establish the remarkable discriminatory capacity of chemosensory system (Dryer, 2000; Adipietro et al., 2012; Jiang and Matsunami, 2015).

The use of odors has been found in many facets of animal and human life. While perfume houses such as Coco Channel launch their signature perfumes every summer; male orchid bees collect environmental scents to create their own “perfume” (Eltz et al.,

1999; Mitko et al., 2016); female moths emit chemical signals to advertise reproductive viability (Christensen et al., 1989), and house cats rub facial pheromones to mark territory (Soini et al., 2012).

The sense of smell allows organisms to discriminate odor quality (identity) and also perceive changes in quantity (intensity) at different concentrations (Beets, 1970; Polak, 1973). The ability to successfully detect and interpret these cues maximize fitness and survival of an organism. In the continuous struggle for calories, a predator and his prey interact via varying emotional states to avoid danger and find food. Emotional reactions are carefully wired within specialized sensory systems, giving animals the appropriate behavioral response to survive and thrive. This is especially true in the prey species, where detection of olfactory messages plays an important role in the induction of innate-fear behaviors, which include hide, fight or flight (Kavaliers and Choleris, 2001). How the olfaction system is organized to serve these complex, yet essential functions is explored in this thesis.

Discriminating between different odors is the first hallmark feature in our sense of smell. The ability to read odor concentration is the second function in our sense of smell. Consistent with our experience, the perceived quality of an odorant shift from weak to strong at different concentrations (Gross-Isseroff and Lancet, 1988). Aromas from food, pheromones from mates and scents from predators often span a dynamic range in concentrations. Tracking the concentrations of these odors therefore, serves nutritional, reproductive and protective purposes - allowing animals to make appropriate behavioral

decisions. For instance, depending on how far the predator is, an animal can choose between hiding versus running away.

1.2 Mammalian olfactory system

G protein-coupled receptors (GPCRs) comprise a large receptor protein family that detect physiological stimuli including light, hormones, odorants, and neurotransmitters through the activation of G protein-based transduction cascades (Alexander et al., 1975; Dohlman et al., 1991; Dryer and Berghard, 1999). The mammalian olfactory system, capable of detecting and discriminating a large number of different odorous volatile molecules, begins at the nasal passage, where millions of olfactory sensory neurons (OSNs) line the main olfactory epithelium. Lining the cilia of the OSNs are olfactory receptors (ORs), which form the largest and most heterogeneous set of receptors within the GPCR family (Buck and Axel, 1991; Dryer and Berghard, 1999). The diverse collection of ORs are encoded by ~400 and ~1100 intact OR genes in humans and mice, respectively (Buck and Axel, 1991; Healy et al., 1997; Zhang and Firestein, 2002; Godfrey et al., 2004; Malnic et al., 2004; Ibarra-Soria et al., 2014; Niimura et al., 2014). Mature OSNs express only one type of the available ORs at a high level (Chess et al., 1994; Malnic et al., 1999; Hanchate et al., 2015; Saraiva et al., 2015; Tan et al., 2015; Scholz et al., 2016).

Functional responses were recorded for single OSNs using electrophysiological techniques in the form of action potentials generated from exposure to specific odorants (Firestein, 1996). Odor perception is initiated by the activation of a specific OR set within the large repertoire of G-protein coupled odorant receptors (Malnic et al., 1999). Early data

collected from frogs suggested that individual OSNs can recognize and respond to a set of structurally different odorant molecules, while an odorant can activate multiple OSNs with different response intensities dependent on odorant concentrations (Duchamp-Viret and Duchamp, 1997). The qualitative tuning of OSNs with broad molecular ranges indicated that an odorant was encoded by a unique set of OSNs that responded with distinct sensitivities.

As OSNs expressing the same OR send convergent axonal projections to form glomeruli in the olfactory bulb, OR activations are translated into glomerular activation patterns which are further processed within the olfactory bulb (Figure 1) and olfactory cortical areas (Ressler et al., 1994; Vassar et al., 1994; Mombaerts et al., 1996; Rubin and Katz, 1999; Wachowiak and Cohen, 2001; Oka et al., 2006; Miyamichi et al., 2011; Sosulski et al., 2011; Storace and Cohen, 2017; Wilson et al., 2017). Different odorants are perceived by complex combinatorial OR codes dependent on each receptor's unique ligand recognition profile (Malnic et al., 1999). In mice, there are approximately 1100 intact OR genes, most of which recognize structurally related volatiles and thus are considered to be "narrowly tuned"(Godfrey et al., 2004; Nara et al., 2011; Yu et al., 2015). Odorants are represented by combinatorial codes whereby a given odorant at a specific concentration activates a specific combination of ORs, which in turn activate a specific combination of glomeruli (Malnic et al., 1999; Rubin and Katz, 1999; Bozza et al., 2002; Oka et al., 2006; Saito et al., 2009).

Previous studies found an increase in the recruitment of active ORs (inside OSNs) and glomeruli (inside the olfactory bulb) as a response to higher odorant concentrations (Rubin and Katz, 1999; Fried et al., 2002; Khan et al., 2010; Wilson et al., 2017)(Jiang et al., 2015). Broadly tuned OSNs responding to a certain odorant can respond to additional odorants at higher odorant concentrations. There is, however, insufficient research to determine the identity of these ORs and their collective responses at different odorant concentrations *in vivo*. This limited our ability to draw conclusions on how odor identity and intensity information are encoded by specific ORs.

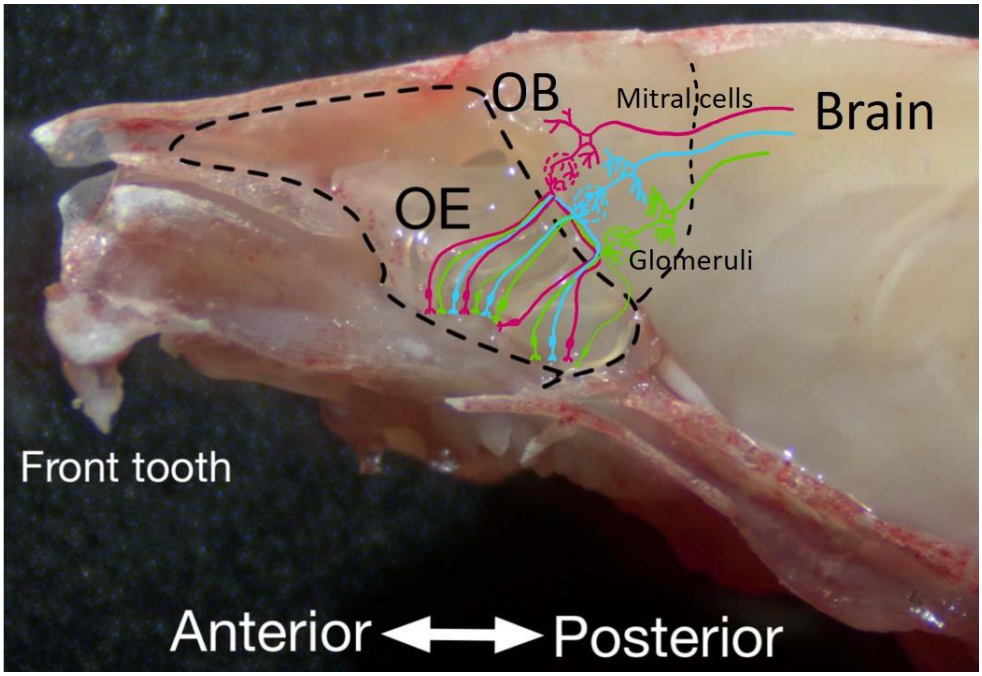

Figure 1: The mouse olfactory system. Olfactory epithelium (OE), olfactory bulb (OB).

1.3 Phosphorylation of the ribosomal protein S6

The identification of clear OR targets for a given odorant has been a long-standing problem in olfaction. Since the first discovery of the OR gene superfamily in 1991, similar chemosensory receptors have been found in various species across the tree of life (Buck

and Axel, 1991; Clyne et al., 1999; Godfrey et al., 2004; Malnic et al., 2004; Niimura et al., 2014). The functions of these receptors, however, had been uncharacterized until the successful functional expression and screening of these OR in various cell expression systems (Katada et al., 2003; Saito et al., 2004; Minic et al., 2005; Zhuang and Matsunami, 2008). Functional cloning of these ORs allowed for the pairing of odorant ligands to specific receptors.

The Matsunami lab has been a pioneer in pairing odorants to its repertoire of responding OR partners for both mice and human ORs via the *in vitro* heterologous cell system cAMP-mediated luciferase reporter gene assay (Saito et al., 2004; Zhuang and Matsunami, 2008; Kida et al., 2018). Recently, we developed a transformative *in vivo* genomic method to comprehensively screen for ORs that are activated by particular odorants via mRNA profiling at the olfactory epithelium (Jiang et al., 2015). This method made use of the S6 ribosomal subunit which was found to be phosphorylated in odorant activated OSNs (Knight et al., 2012). Briefly, the phospho-S6 ribosomal protein is immunoprecipitated (pS6-IP) and mRNA physically associated with the subunit (from mice OR) is captured for deep sequencing. The harvested mRNA is then processed into cDNA libraries and detected via next-generation sequencing. The sequencing output is then carefully analyzed between control and odorant-stimulated samples to reveal OR genes that are differentially enriched as a result of selective OSN activation. Immunostaining for pS6 is now adopted in the field of olfaction and visual systems to

study neuron activation in OSNs and retinal cells (Asakawa et al., 2017; Milner and Do, 2017; Sharma et al., 2017).

1.4 Approaches to study OR responses *in vivo*

Over the years, multiple technologies have developed to study the activation of OSNs and ORs by odorants (Peterlin et al., 2014). The first mammalian OR to be matched *in vivo* with its odorant ligands was the rat olfactory receptor I7. An adenovirus-mediated gene transfer drove up exogenous rat OR-I7 expression in OSNs, followed by ex vivo electrophysiological recordings showing substantial greater response of I7 towards odorants such as octanal (Zhao et al., 1998). This methodology offers moderate throughput in which odorants are delivered to the ex vivo olfactory epithelium in vapor phase.

Systems mentioned above in which targeted ORs are expressed in OSNs somewhat recapitulate the olfaction system. However, such OSN-based expression systems are relatively low throughput and only allowed for the screening of a few ORs (Zhao et al., 1998; Touhara et al., 1999; Bozza et al., 2002; Feinstein et al., 2004). Large scale, heterologous-based screening thus holds the promise of providing an efficient model for studying the combinatorial code involving hundreds of different ORs.

Calcium imaging of dissociated olfactory epithelium has been used to detect physiological odorant activation of OSNs by measuring the temporal and spatial properties of Ca^{2+} influx (Restrepo et al., 1993; Tareilus et al., 1995). OR activation leads to a G protein-coupled signaling cascade and an increase in intracellular cAMP. This initiates

the opening of the olfactory cyclic nucleotide-gated ion channels and mediates the influx of Ca^{2+} and Na^{+} ions to depolarize the OSN (Jones and Reed, 1989; Breer and Boekhoff, 1992; Reed, 1992; Pierce et al., 2002). This OR signal transduction pathway form the basis for functional readout of OR response through a variety of *in vitro* heterologous expression systems.

A challenge in studying OR function *in vitro* is that many ORs are resistant to heterologous expression when expressed alone. In HEK293T cells, it has been found that some ORs fail to exit the endoplasmic reticulum and do not functionally expressed at the cell surface (Lu et al., 2003). The Matsunami lab identified receptor transporting proteins (RTP1 and RTP2) to facilitate OR trafficking to the cell surface (Saito et al., 2004). The later adoption RTP1S which is a shorter and more potent form of RTP1 significantly enhanced our ability to functionally express ORs *in vitro* (Zhuang and Matsunami, 2008).

Besides pS6-IP-Seq, there are two recent high-throughput approaches to study OR responses *in vivo*: one is the Kentucky Method based on activation-dependent S100a5 expression (McClintock et al., 2014). Another is the DREAM technique (deorphanization of receptors based on expression alterations of mRNA levels) which is based on OR-specific transcriptional downregulation after odor stimulation (von der Weid et al., 2015). DREAM and pS6-IP-Seq identified overlapping, but not identical sets of ORs (Jiang et al., 2015; von der Weid et al., 2015). In insects, these differences are attributed to underlying differences between S6 phosphorylation and OR downregulation following OR activation (Koerte et al., 2018).

1.5 Zonal distribution of ORs

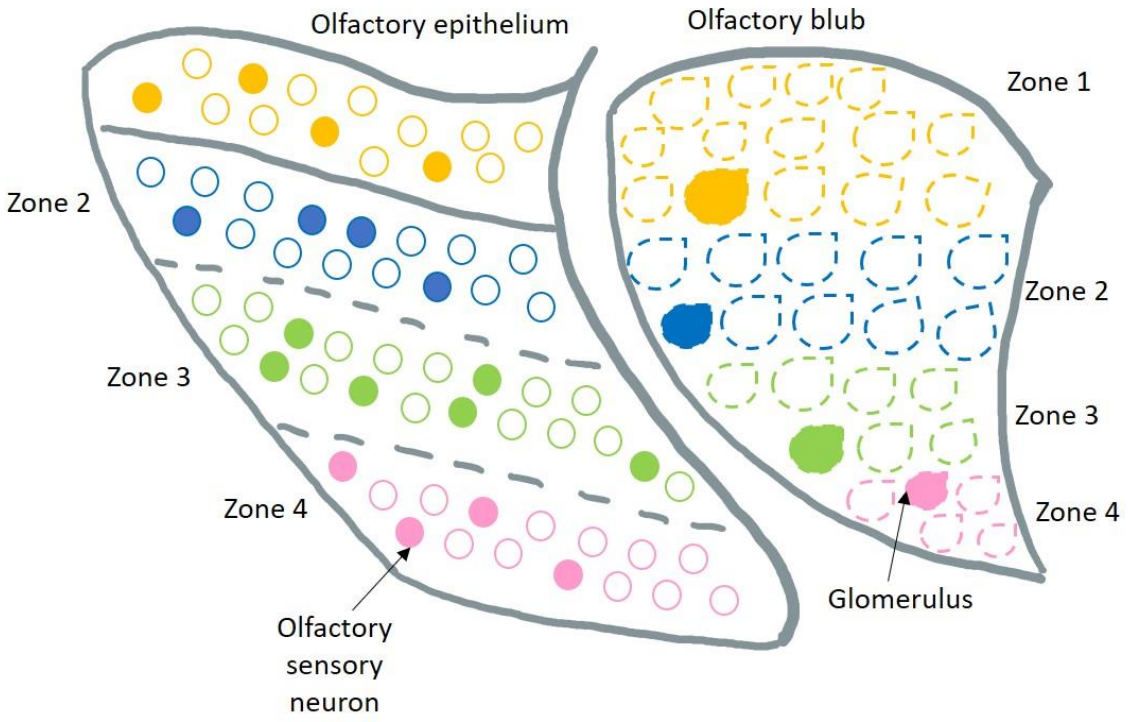

Figure 2: ORs are expressed in a zonal pattern at the olfactory epithelium. Modified based on Yamaguchi et al., 2006.

The olfactory system is organized at multiple levels. The first level of organization occurs at the olfactory epithelium, where different OR are expressed in distinct, yet partially overlapping, regions along the dorsomedial–ventrolateral (DV) axis (Figure 2). This spatially segregated, OR expression was first discovered in rodents (Ressler et al., 1993; Vassar et al., 1993) and subsequently observed in the zebrafish (Weth et al., 1996), the fly (Vosshall et al., 1999), followed by primates (Horowitz et al., 2014). This OR expression pattern was initially divided into four discrete "zones" (Ressler et al., 1993; Vassar et al., 1993) but was later determined to be more overlapping continuous (Norlin et al., 2001; Miyamichi et al., 2005). The olfactory system exhibits additional spatial

organization where the axons of OSNs expressing the same OR project onto fixed glomeruli at the olfactory bulb (Ressler et al., 1994; Vassar et al., 1994; Mombaerts et al., 1996; Wang et al., 1998). These projections were mapped by in situ hybridization (Ressler et al., 1994; Vassar et al., 1994; Tsuboi et al., 1999) and labelled with marker genes such as green fluorescent protein and lacZ (Mombaerts et al., 1996; Wang et al., 1998; Feinstein and Mombaerts, 2004). Together, these glomeruli form a topographic map of the hundreds of ORs expressed in the olfactory system.

1.6 Concentration invariance in olfaction

ORs can respond to a set of odorants at different levels of specificity and affinity, suggesting that a change in the concentration of an odorant can alter the resulting combinatorial receptor code (Kajiya et al., 2001). It has also been shown that more OSNs, and likely more unique ORs, fire at higher concentrations of an odor (Ma and Shepherd, 2000). These may explain our experience that the quality and intensity of some scents are perceived differently between low and high odorant concentrations (Gross-Isseroff and Lancet, 1988).

A fundamental form of perceptual invariance in chemosensation is concentration invariance which refers to the ability of an organism to recognize the same odor over a range of different odor concentrations (Uchida and Mainen, 2007). As changes in odorant concentration can result in a change in the number of OSNs and glomeruli activated, this raising the interesting question of how different patterns of OSNs and glomerular activation can lead to similar olfactory percepts.

It has been recently found that odorant information was transformed from a representation that was highly concentration-dependent in the olfactory bulb to a representation that was largely concentration invariant in the piriform cortex. In the Fleischmann et al., 2017 paper, the group analyzed piriform neural activity over a 100-fold concentration range of ACT and found a concentration-invariant subnetwork of piriform neurons which are significantly modulated by odorant identity but not concentration. Datta et al., 2017 reported the presence of concentration invariant neurons in pICoA and PCx when mice were exposed to TMT (Iurilli and Datta, 2017). They found that most neural responses in both plCoA and PCx changed as concentrations rose, but these changes generally unfolded in a non-monotonic manner regardless of the odor tested, suggesting that information about odor identity and concentration may be in part decoupled at the single-neuron level in both brain areas. These concentration-invariant piriform neurons complement our discovery of specific low odorant concentration responsive ORs which were reliably activated across a large concertation range.

1.7 Deorphanization of predator odors

Early humans had much to fear for in the wild, but they could not simply cower in caves. They needed to find food, win mates, and run from carnivores such as the megantereon (extinct saber-toothed cat) or chasmaporthetes (extinct hunting hyenas) (Lee-Thorp et al., 2000). It seems that not only are small prey animals inherently fearful; humans and primates experience innate fear too. For instance, in the 1940s, psychologist Donald Hebb found that young chimpanzees born in captivity are instinctively frightened

by snakes, even though they had never seen them before. Humans too, tend to associate snakes with danger. As such, they are much better at identifying snakes during visual detection tasks as compared to nonthreatening stimuli such as frogs or caterpillars (Lobue and DeLoache, 2008). In such instances, humans utilized an innate perceptive ability to focus on threatening stimuli and respond quickly with the emotion of fear. The amygdalae, which reacted effectively to potential threats, allowed our ancestors to excise caution, run from danger, and protect their offspring.

In mice, olfactory cues from predators are known to be crucial for detecting overt and potential threats (Papes, Logan et al. 2010, Isogai, Si et al. 2011). Olfactory cues communicate the presence of danger to the frightened mouse via scents released by the predators (kairomones) or threatened conspecifics (Apfelbach, Blanchard et al. 2005). Often, these aversive odorants are predator-derived (eg. fox odor). To understand how these semiochemicals communicate the message of fear, we need to figure out how the identity of these odorants is encoded at the receptor level. While the field has made progress in identifying functional brain compartments of the olfactory system mediating this behavior, it is still largely unclear which receptors are involved in the detection of such cues, partly due to difficulty in the tracking of OR activation in vivo upon odorant stimulation at a population level. We thus investigated the concentration-dependent combinatorial OR code of predator related odorants such as TMT and 2MT inside the predator naïve lab mice (Figure 3).

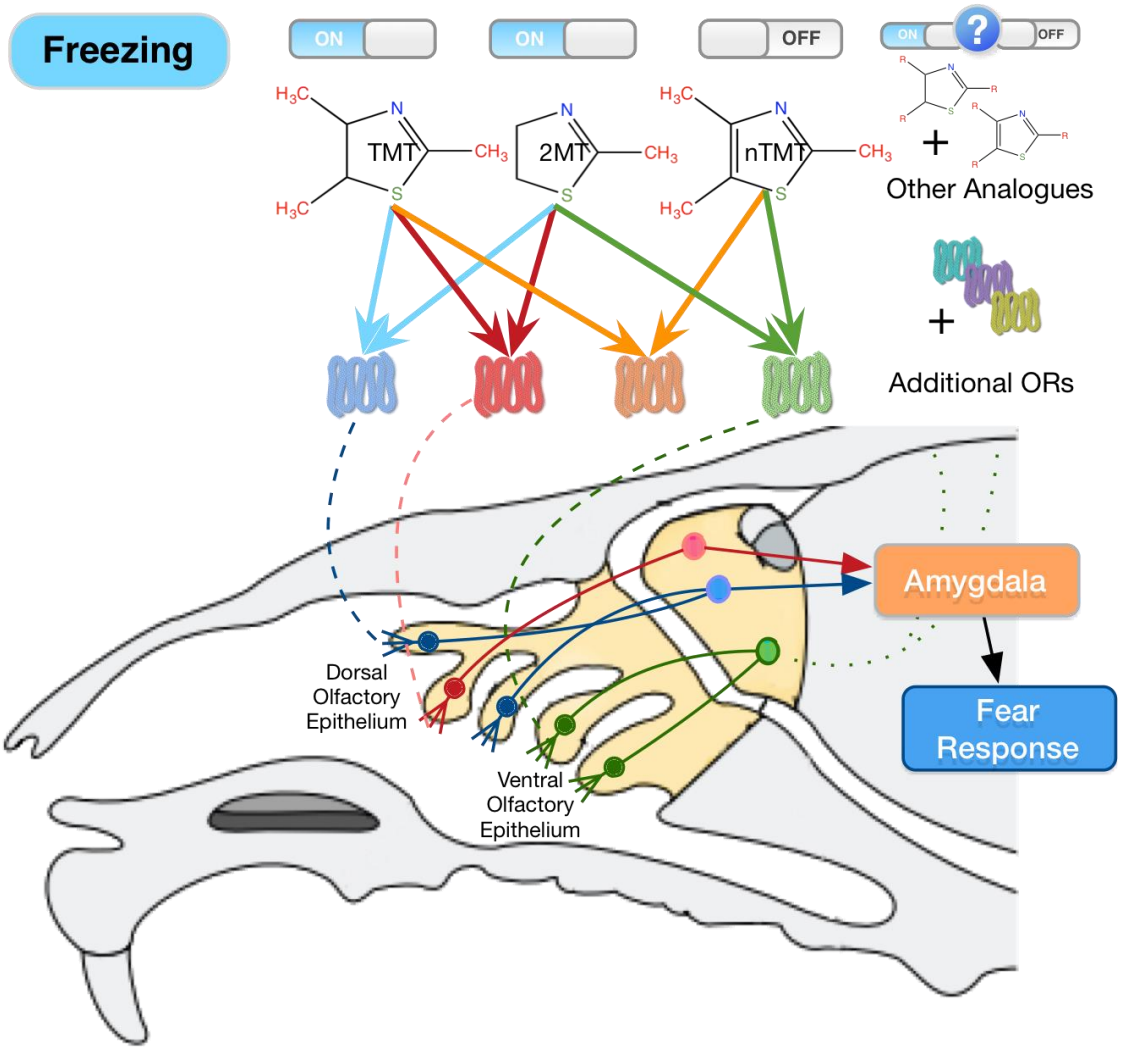

Figure 3: ORs responding to TMT/2MT may mediate the innate-fear response.

1.8 Covalent modification of predator odor receptors

Recently, a paper found Olfr1019 to responsive to TMT and implicated with predator odor driven immobility (Saito et al., 2017). By photoactivation of the Olfr1019 glomerulus, they are able to induce prolonged immobility responses in the channelrhodopsin knock-in mice mouse. In contrast, control mice continued to demonstrate natural behaviors, such as, walking, stopping, exploring and grooming,

despite photoillumination of the olfactory bulb. The study also compared immobility responses to TMT between Olfr1019-knockout and wild-type mice. When subjected to 10% TMT exposure, the wild-type mouse demonstrated clear fear responses such as immobility. The Olfr1019-knockout mice showed lower immobility towards TMT than that of the wild-type mice (Saito et al., 2017). It is important, however, to note that immobility was lowered, but not abolished, suggesting the role of additional ORs and receptors in relaying predator information that elicits freezing behavior.

In 2018, another study conducted a large-scale recessive genetics screen of ethylnitrosourea (ENU)-mutagenized mice (Wang et al., 2018). They found that mutants which lost Trpa1 (a pungency/ irritancy receptor) showed diminished TMT/2MT and evoked innate fear/defensive responses. They subsequently generated Trpa1−/− mice which failed to effectively activate known fear/stress brain centers upon 2MT exposure while still able to smell and conditionally learn to fear 2MT. It was shown that Trpa1 acts as a chemosensor for 2MT/TMT and Trpa1-expressing trigeminal ganglion neurons and contribute critically to 2MT-evoked freezing behavior.

Trp-channels are weakly selective cation channels that respond to the binding of extracellular or intracellular ligands (noxious agents such as wasabi) and changes in temperature (Tobin et al., 2002; Bautista et al., 2005; Jabba et al., 2014). Trpa1 ligands such as wasabi are known to be electrophiles, activating the channel by forming covalent bonds with specific cysteine or lysine amino-acid residues. Each subunit of the Trpa1 contains six membrane-spanning α-helical domains, S1–S6 (purple color rods), and their

constriction regulates the influx of Ca^{2+}. A coiled-coil domain in the cytoplasmic C terminus is surrounded by 'ankyrin repeats', which has been suggested to contain the cysteine residues targeted by electrophilic Trpa1 activators. The ankyrin repeats (ARs) (green color rods) at the amino-terminal end (N) provide a large cytoplasmic surface for interactions with noxious ligands (Figure 4.0).

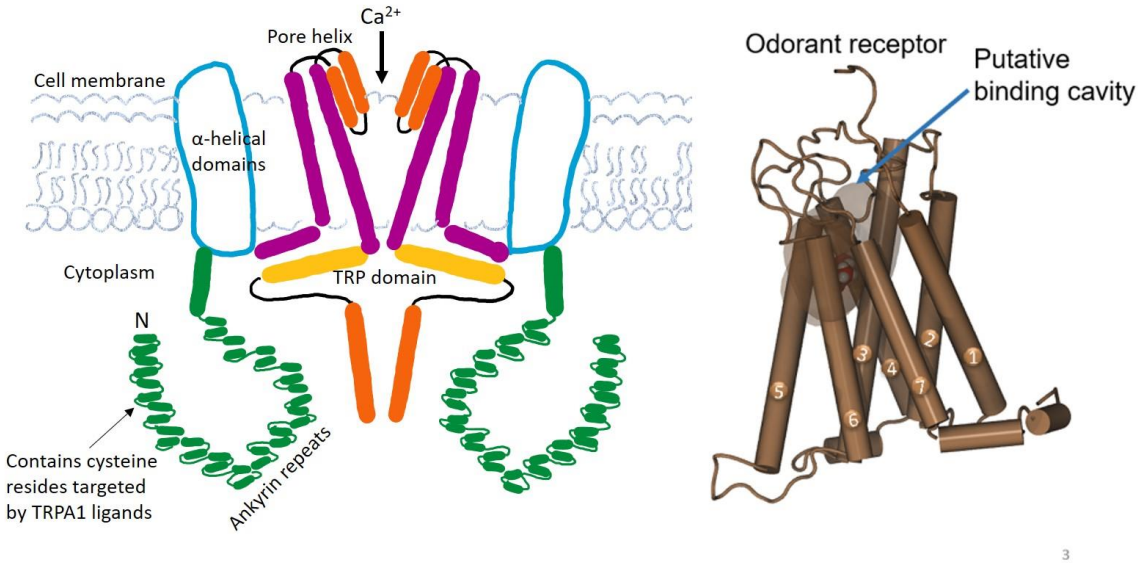

Figure 4: Ligands form covalent bonds with TRPA1 amino-acid residues. Modified based on Paulsen et al., 2015, Nature.

Wang et al. found Trpa1 to be a chemosensor for 2MT/TMT. They transfected the Trpa1-P2A-mCherry construct into HEK293T cells and performed Ca^{2+} imaging upon exposure to 1, 10, 100 and 1000 μM of 2-methyl-2-oxazoline, 2MT, or TMT. Both TMT and 2MT, but not 2-methyl-2-oxazoline (a structurally related but non-fear inducing odorant) evoked Ca^{2+} transients in the transfected HEK293T cells in a dose-dependent manner. They also inhibited Trpa1 by HC-030031 treatment and abolished the 2MT evoked Ca^{2+} transients.

The docking of an odorant molecule into the canonical binding cavity exerts stress to the protein structure, leading conformational changes (Kato et al., 2008; Peterlin et al., 2008) and toggling of the amino acid residues such as the ionic lock (de March et al., 2015). When an odorant molecule fits stably in the binding cavity, the ligand is recognized, triggering conformational change and the OR is activated. This process is largely based on van der Waals forces, hydrogen bonding and hydrophobic interactions(Ahmed et al., 2018); covalent bonds has not been found to be involved in the OR activation/ligand docking process. We thus performed selective activation and inhibition of predator related odorants to look for evidence of possible covalent modification in OR-ligand pair interactions.

2. Updated method to identify ORs activated by odors *in vivo*

2.1 Introduction

The mammalian olfactory system begins at the nasal passage, where millions of OSNs are zonally distributed within the main olfactory epithelium. Odor detection is mediated by a large repertoire of ORs, and mature OSNs express a single dominant OR gene (Ressler et al., 1993; Hanchate et al., 2015). ORs constitute the largest family of seven transmembrane G-protein-coupled receptors, and the mice genome encode for over 1000 intact OR genes (Buck and Axel, 1991; Dryer and Berghard, 1999). Different odorants are perceived by complex combinatorial OR codes dependent on each receptor's unique chemical partners (Malnic et al., 1999; Godfrey et al., 2004; Nara et al., 2011; Yu et al., 2015). Together, specific repertoires of ORs are activated by a volatile odor, the corresponding OSN neural activity is converted into a segregated map in the olfactory bulb initiating the olfactory transduction cascade to downstream brain regions and cortical neurons (Stettler and Axel, 2009).

To understand how mammalian ORs encode odorant concentrations, we carried out high-throughput *in vivo* screens via phosphorylated ribosomal protein S6 immunoprecipitation followed by RNA-Seq (pS6-IP-Seq). This characterized comprehensive OR responses and changes in OR activation patterns against ACT and TMT from 0.01% to 100% (v/v).

2.2 Results

2.2.1 Modified pS6-IP-Seq enriched more ORs

We identified ORs activated by ACT and TMT at varying odorant concentrations *in vivo*. This is made possible through a recently developed *in vivo*-based method which identifies ORs expressed in activated OSNs via mRNA profiling (Jiang et al., 2015). This method made use of the finding that the phosphorylation of the ribosomal protein S6 is an indicator of neuronal activation (Knight et al., 2012; Biever et al., 2015). Immunoprecipitation of ribosome-mRNA complex containing phospho S6 (pS6-IP also known as phosphoTRAP) followed by next-generation sequencing identifies OR mRNAs present in odorant activated OSNs (Figure 5).

We updated the pS6-IP-Seq method as originally described by Jiang et al., in an effort to profile ORs expressed in active OSNs that respond to lower concentrations of odorants (Jiang et al., 2015). Figure 5A shows the updated pS6-IP-Seq pipeline. Similar to the Jiang et al. publication, we habituated and stimulated a mouse for one hour with 10 μl of odorant at a given starting odorant concentration (Jiang et al., 2015). We replaced the polyclonal antibody against pS6 with a monoclonal alternative to improve immunoprecipitation consistency. We updated annotations of OR genes to also include untranslated regions (UTRs) containing Bowtie aligned transcripts (Langmead et al., 2009; Li et al., 2009). As an example, figure 5B shows coding region (CDS) annotation and updated annotation (CDS + UTR) for an ACT OR, Olfr923. Figure 5C also shows Olfr923's transcripts read depth aligned with STAR based on the new OR annotation (see Methods for details) (Dobin et al., 2013; Bray et al., 2016).

The updated OR annotations now include 1385 UTR annotated ORs, largely based on the work of Ibarra-Soria et al. (Ibarra-Soria et al., 2014). To complete this set of OR definitions, we made three additional modifications: reannotation of 58 coding exonal ORs genes to include noncoding UTRs, correction of a misannotated OR (Olfr151) and addition of four previously unannotated ORs from the refGene database (O'Leary et al., 2015). More ORs were significantly enriched (FDR corrected $p<0.05$) at 1% and 100% ACT and TMT with the UTRs included gene annotations, compared to ORs reported by Jiang et al. (Jiang et al., 2015), suggesting a more sensitive detection of OR enrichment with the updated pS6-IP-Seq method (Figure 5B, D).

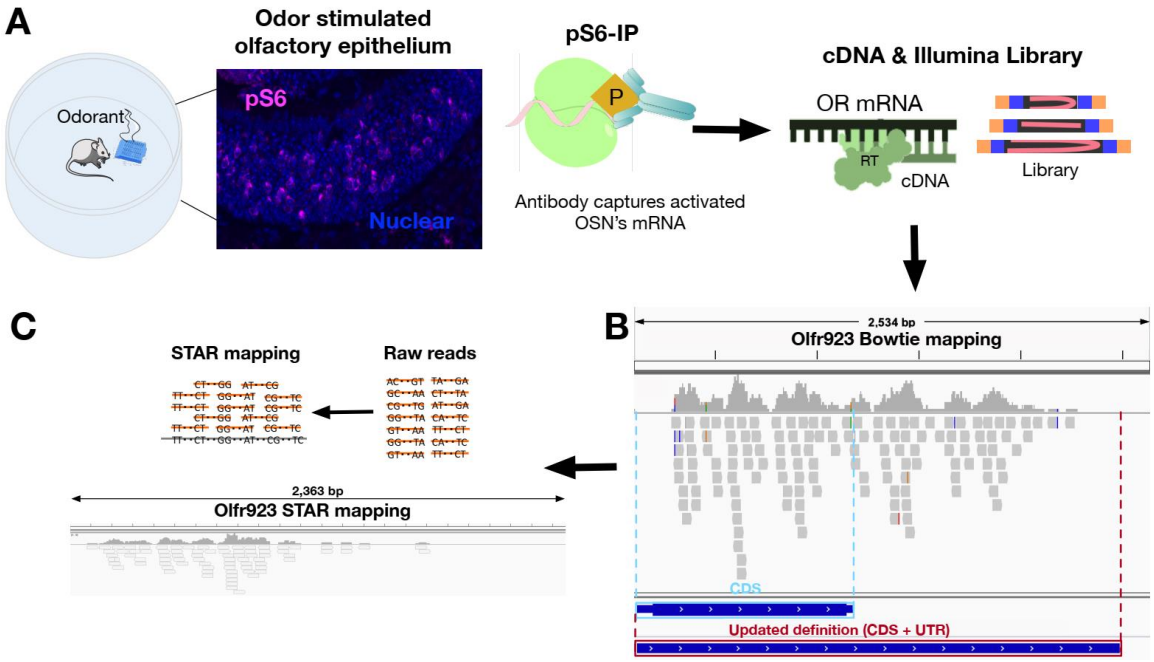

Figure 5: An illustration showing the updated pS6-IP-Seq method. (A) Following odorant stimulation, a monoclonal pS6 antibody captures mRNA from activated OSNs that is processed into an Illumina library. (B) Olfr923's OR gene annotation include CDS + transcribed UTRs. (C) STAR aligns and quantifies OIlfr923 transcript reads at the mouse olfactory epithelium.

A new essential monoclonal antibody for the pS6 subunit was tested alongside the original polyclonal antibody in a controlled experiment where olfactory epithelium

tissues from 3 ACT stimulated mice were combined and then treated separately with 20µl and/or 6µl of polyclonal and monoclonal antibodies respectively. Statistical regression on the normalized read counts of 1248 mice OR genes (Figure 6) has confirmed that the new monoclonal antibody is not only comparable to the old polyclonal antibody but also more cost-effective. Our data suggest that the monoclonal antibody captures mRNA species from the OR family with greater efficiency than the previous polyclonal antibody: only 1/3 of the monoclonal antibody (6µl) is needed to achieve comparable mRNA profiling to that of 20µl polyclonal antibody. The slope of the OR read counts linear regression line is close to 1.0 (monoclonal ≈ polyclonal), supporting the null hypothesis of no significant difference between the antibodies. Additionally, the monoclonal antibody is specific to only one epitope, and hence a more reliable candidate for immunoprecipitation with less batch to batch variation.

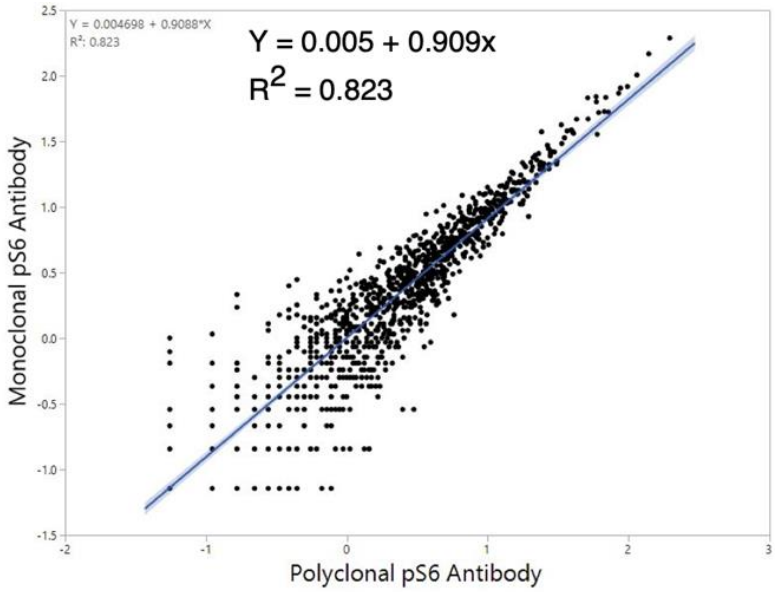

Figure 6: The updated pS6-IP-Seq utilizes a monoclonal pS6 antibody. Scatter plot comparing the immunoprecipitated mRNA counts (normalized) for 1248 OR genes. X-axis: olfactory epithelium processed with 20 µl of polyclonal anti-pS6 antibody. Y-axis: olfactory epithelium processed with either 20 µl or 6 µl of monoclonal anti-pS6 antibody.

Multiple alignment methodologies exist for alignment of sequenced RNA reads to the mouse genome. We tested Bowtie, Kallisto and STAR and found that each has their own advantages and shortcomings. Bowtie was used in the Jiang et al., publication and it takes up to three days to map pS6-IP-Seq data files. We then adopted Kallisto pseudoalignment to quantify our sequencing reads. Kallisto rapidly determines the compatibility of reads to target genes based on our transcriptome index, without the need for alignment (Bray et al., 2016). With Kallisto, each pS6-IP-Seq data file can be processed within 30 mins. However, we found that Kallisto inflated the reads for around 20 ORs by assigning high numbers of low complexity reads (Figure 7B). For instance, when you compare the ACT readcounts from Bowtie versus the readcounts from Kallisto, you see an OR with close to zero reads based on Jiang et al., 2015 jump to nearly 5000 reads (Figure 7B). We thus decided to switch our and quantification pipeline from Kallisto to STAR alignment with RSEM quantification. STAR is a highly modifiable alignment (no pseudoalignment) algorithm that uses a genome reference with transcript alignments being indexed as chromosome coordinates indicated by our custom GTF annotations (see methods). STAR aligns lesser reads per OR than Kallisto, with a maximum of around 800 reads (Figure 7C), this however, does not affect the outcome of our differential expression analysis and very similar sets of ORs were enriched across Bowtie, Kalliso and DREAM (Figure 7).

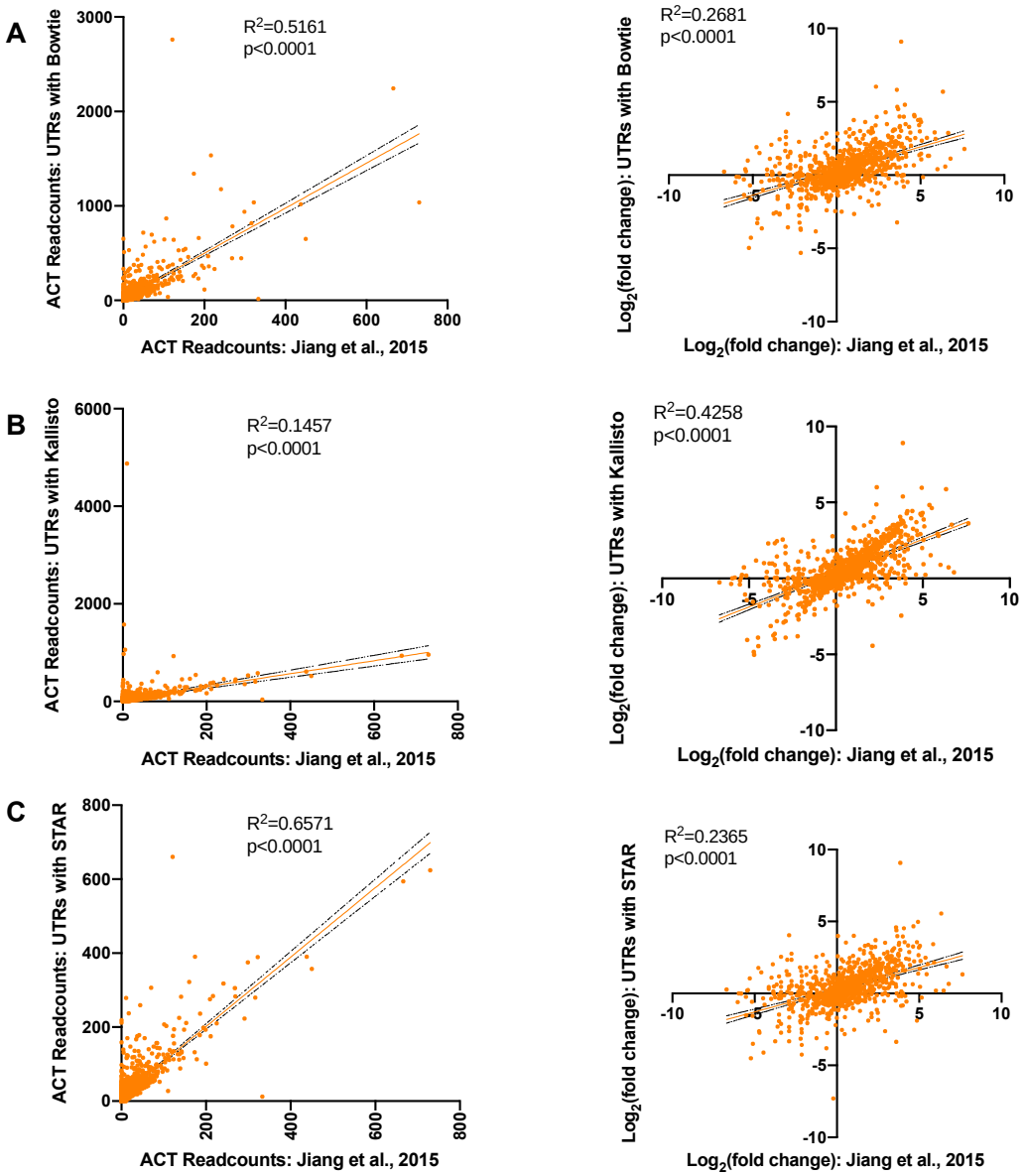

Figure 7: Comparison of Bowtie, Kallisto and STAR alignment using an ACT pS6-IP-Seq dataset from Jiang et al., 2015.

2.2.2 Correlation between pS6-IP-Seq and *in vitro* OR responses

The *in vitro* responses of a panel of 500 ORs against ACT based on cAMP-mediated luciferase reporter gene assays in heterologous cells were reported to be correlated with the enrichment of ORs from pS6-IP-Seq (Jiang et al., 2015). Here we compared our new *in*

vivo ACT pS6-IP-Seq dataset to the *in vitro* ACT dataset reported by Jiang et al. (Jiang et al., 2015). We first investigated whether significantly enriched ORs grouped using *in vivo* pS6-IP-Seq (orange circles) showed higher *in vitro* activation at three different concentrations of ACT (3uM, 30uM, and 300uM), compared to the "not *in vivo* enriched" OR group (gray circles) (Figure 8A).

From 0.01% to 1% ACT, we saw that the *in vivo* pS6-IP-Seq enriched ORs (orange circles) Log_2FC and normalized *in vitro* activation were consistently higher than *in vivo* non-responders (grey circles) as seen from the dotted red lines (Figure 8C). The average ± SEM for log_2FC values of the *in vivo* enriched ORs were 1.74 ± 0.15, whilst that of non-enriched ORs were 0.16 ± 0.09. The average ± SEM for *in vitro* activation of the *in vivo* enriched ORs were 29.43 ± 7.22, whilst that of non-enriched ORs were 5.05 ± 0.40 (Figure 8D).

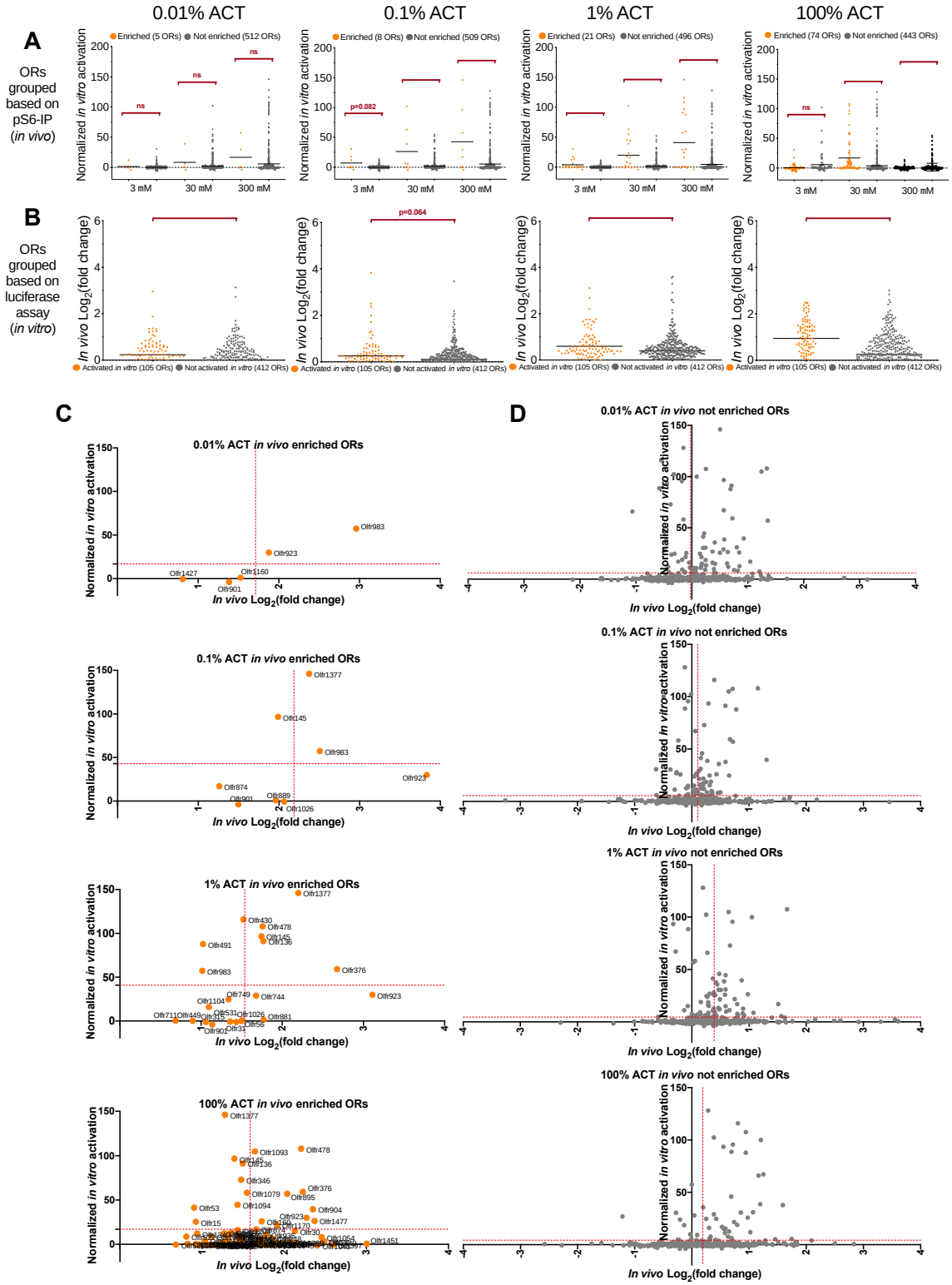

Figure 8: ***In vivo*** **OR enrichment correlates with the** ***in vitro*** **activation data. (A)** ***In vitro*** **Hana3A cell lines cAMP-mediated reporter data for 517 out of the 1088 pS6-IP-Seq mapped intact ORs are classified into** ***in vivo*** **pS6-IP-Seq ACT enriched (orange, FDR corrected p<0.05 and $\log_2$ fold**

change > 0) and not enriched groups (grey, FDR corrected p>0.05 or log_2 fold change < 0). *In vitro* normalized fold increase in luciferase signals were plotted for each OR groups across four ACT concentrations. 100% is based on the fold of increase of Olfr1126 activated by 300 μM ACT. 0% is determined by the fold of increase of empty rho-pCI vector stimulated with 3 μM ACT. Black bars represent mean. *p<0.05, **p<0.01, ***p<0.001 by Mann–Whitney test (*in vivo* enriched ORs compared to not enriched ORs). (B) *In vivo* pS6-IP-Seq fold enrichment was plotted for each OR groups across four ACT concentrations. ORs are classified based on *in vitro* cAMP-mediated reporter data into activated (orange, fold luciferase induction at 300 μM ACT > 2.33) and not activated groups (grey, fold luciferase induction at 300 μM ACT < 2.33). Black bars represent mean. **p<0.01, ***p<0.001 by Mann–Whitney test (*in vitro* enriched ORs compared to not enriched ORs). (C) Plotting individual pS6-IP-Seq enriched ORs fold change data against their *in vitro* activation data at 0.01%, 0.1%, 1% and 100% starting concentrations of ACT. Red dotted line indicates average values between the plotted ORs. (D) Plotting individual pS6-IP-Seq not enriched ORs fold change data against their *in vitro* activation data at 0.01%, 0.1%, 1% and 100% starting concentrations of ACT. Red dotted line indicates average values between the plotted ORs.

Additionally, we created a graph for each ACT concentration, with FDR corrected p-values on the X axis, and *in vitro* responses on the Y axis to provide a sense how FDR corrected p-values correlates with *in vitro* responses (Figure 9). Overall, 89 out of the 138 *in vivo* enriched ORs were tested *in vitro* and 46 (52%) were activated. Consistent with the results of Jiang et al., we found that the *in vivo* enriched OR group has a significantly higher *in vitro* activation from 0.1% to 100% ACT, but there are instances where *in vivo* enriched ORs do not show *in vitro* responses, and vice versa (Jiang et al., 2015). Similarly, we observed that the ORs grouped based on *in vitro* luciferase assay activation (orange circles) has a significantly higher pS6-IP-Seq fold enrichment at all the ACT concentrations tested, compared to the "not *in vitro* activated" OR group (gray circles) (Figure 9). 46 out of the 105 *in vitro* activated ORs were also enriched *in vivo* based on pS6-IP-Seq.

From 0.01% ACT to 100% ACT, we saw that Olfr923 showed higher than average (blue line) *in vitro* activation (Figure 9). At 0.1% ACT, Olfr145 (OR with biggest mRNA fold change decrease based on DREAM) also showed higher than average (blue line) *in*

vitro activation. Olfr1377 (consistently enriched *in vivo* at 0.1% ACT above) showed the highest normalized *in vitro* activation amongst all 516 tested ORs (Figure 9).

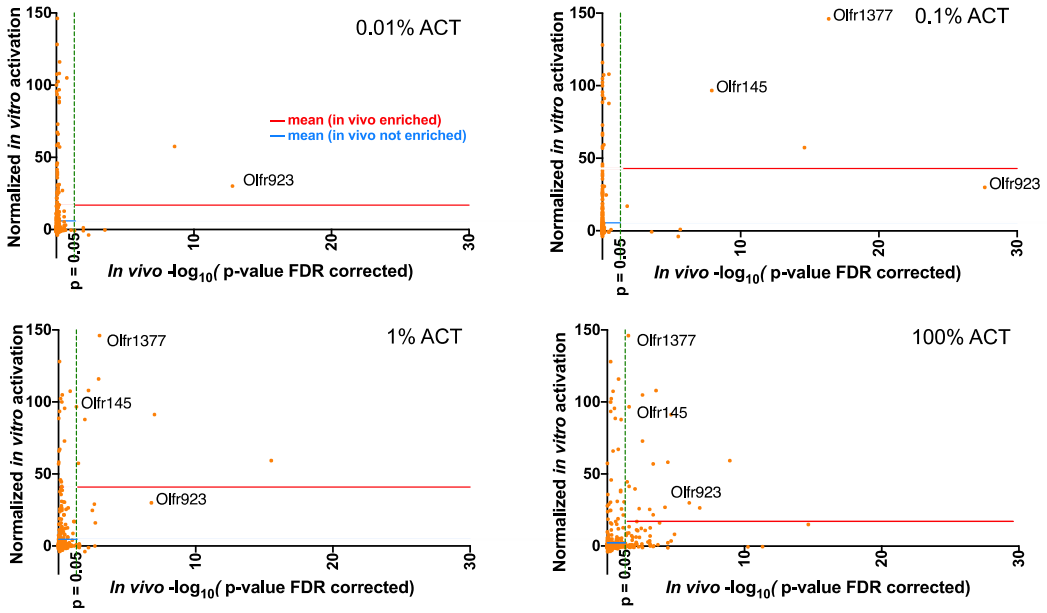

Figure 9: pS6-IP-Seq enriched ORs show higher *in vitro* activation. Individual OR have their FDR corrected p-values plotted against *in vitro* activation data. Green dotted line indicates FDR corrected p=0.05 line (ORs to the right have FDR corrected p<0.05, ORs to the left have FDR corrected p>0.05). Red and blue lines indicate mean *in vitro* activation values for *in vivo* enriched and not enriched ORs.

2.2.3 ROC classification of pS6-IP-Seq and *in vitro* OR responses

Receiver operating characteristic (ROC) curves was used to see how well OR pS6-IP-Seq enrichment (*in vivo*) correlates OR luciferase response (*in vitro*). In Figure 10, for 100% ACT, the classifier performance (area under the ROC curve, AUC) = 0.738 ($P = 1.5 \times 10^{-14}$, Wilcoxon rank-sum test, one tailed against H0: classifier performs no better than random). In Figure 10, we see that the AUC values at 1% and 100% ACT is above > 0.73 ($P < 0.001$, Wilcoxon rank-sum test, one tailed against H0: classifier performs no better than random).

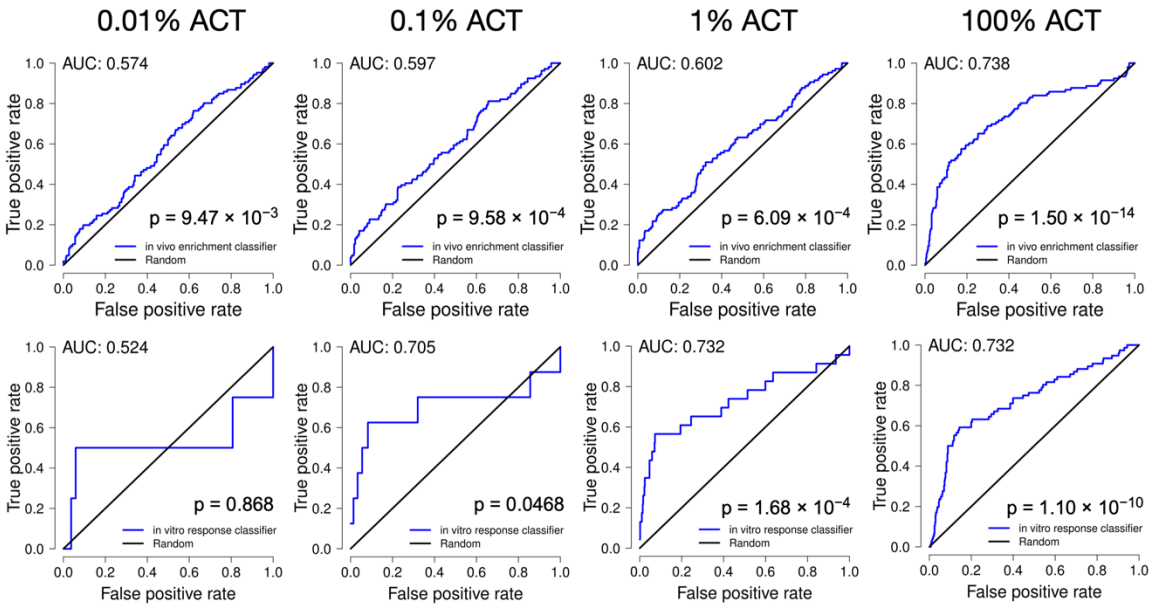

Figure 10: ROC curves of support vector machine classifier performance showing area under the curve and p-values based on Wilcoxon rank-sum test, one tailed against H0: classifier performs no better than random.

2.3 Conclusion and Discussion

To more accurately describe the concentration-dependent combinatorial OR code, we report an updated pS6-IP-Seq method to profile mRNA expression in odor activated OSNs. We utilized a monoclonal pS6 antibody, streamlined the library preparation methods (Knight et al., 2012; Jiang et al., 2015), and adopted STAR for efficient sequence reads mapping (Dobin et al., 2013). We can now identify more ORs at given odor concentrations and at lower and more physiologically relevant odor concentrations. The updated pS6-IP-Seq can be adopted to identify responsive ORs across a wide range of monomolecular odorants, odorant mixtures, and complex natural odors to further our understanding of peripheral odor coding (Isogai et al., 2018).

Our OR lists overlap with a majority of the ORs identified by the Jiang et al. publication (Jiang et al., 2015). Out of the total 86 ACT responsive ORs reported by Jiang

et al., 51 of these ORs were also identified by our current study. The vast majority of the non-overlapping ORs exhibit a positive Log_2FC, indicating that these ORs were enriched but did not reach our statistical criteria (FDR corrected $p<0.05$). It is also likely that the difference in antibodies against pS6 (i.e. polyclonal antiserum in Jiang et al. vs monoclonal antibodies in the current study) contribute some differences (Jiang et al., 2015). Changes in the bioinformatics pipelines also contribute to differences.

3. Concentration-dependent OR recruitment

3.1 Introduction

An increase in the number of ORs mapped based on the Jiang et al., 2015 data suggests that the updated pS6-IP-Seq method may allow us to identify activated ORs at lower odorant concentrations than what has been previously reported (Jiang et al., 2015). To test this, we stimulated mice with 0.01%, 0.1%, 1% and 100% (v/v) of ACT and TMT (Figure 11A), performing the updated pS6-IP-Seq at each condition (n=3; see Methods for details).

3.2 Results

3.2.1 OR repertoires with different odorant concentrations

At the lowest starting concentration, 0.01%, ACT enriched 6 ORs (FDR corrected $p<0.05$) (Figure 11B). The number of ORs recruited increased from 6 to 115 (Figure 11B) when the starting odorant concentration was increased from 0.01% to 100%. This shows that more ORs were activated at higher concentrations of odorants. Trace amine associated receptors (Taars), a small family of chemosensory receptors activated by volatile amines (Liberles and Buck, 2006) were not significantly enriched by the tested odorants.

To investigate the phylogenetic relationship of ORs responding to an odorant, we plotted enriched ORs on protein sequence-based phylogenetic trees (Figure 11C). As the odorant concentrations increase, more diverse sets of ORs are enriched (Figure 11C), consistent with findings previously reported (Jiang et al., 2015).

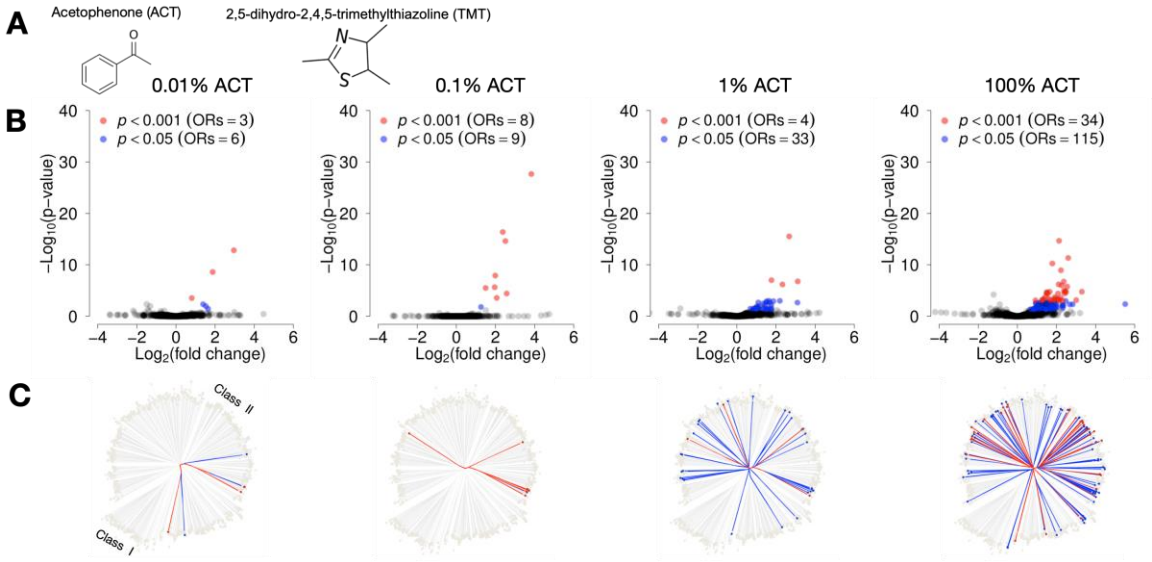

Figure 11: OR repertoires expand with increasing ACT concentrations. (A) Chemical structure of ACT and TMT. (B, D) Volcano plots showing the $\log_2$ fold change and $-\log_{10}$ p-value of OR genes from 0.01% to 100% ACT. OR differential expression values are based on pS6-IP-Seq with odorant stimulated and unstimulated C57BL6 mice. ORs significantly enriched by pS6-IP-Seq with fold change > 1 are colored in blue and red based their p-values (FDR corrected). N = 3 mice were used for each odorant condition. (C) Protein sequence distance trees generated using similarity based on pairwise distances from aligned OR protein sequences. Each end of the branches represents an OR placed alongside its closest neighbors. Both class 1 (bottom left ¼ the tree) and class 2 (remaining ¾ of the tree) ORs are shown. ORs significantly enriched by ACT and at each odorant concentrations are labelled in red (p<0.001) and blue circles (p<0.05).

We performed the same experiment and analyses for another odorant, TMT. The number of ORs recruited increased from 3 to 68 for TMT (Figure 12A) when the starting odorant concentration was increased from 0.01% to 100% TMT. Similar to ACT, more diverse sets of ORs are enriched as the odorant concentrations increase (Figure 12B). These findings are consistent with earlier studies based on glomerular activation in the olfactory bulb (Rubin and Katz, 1999; Wachowiak and Cohen, 2001; Fried et al., 2002; Wilson et al., 2017) and complement these studies by identifying ORs that respond to a wide range of concentrations of odorant.

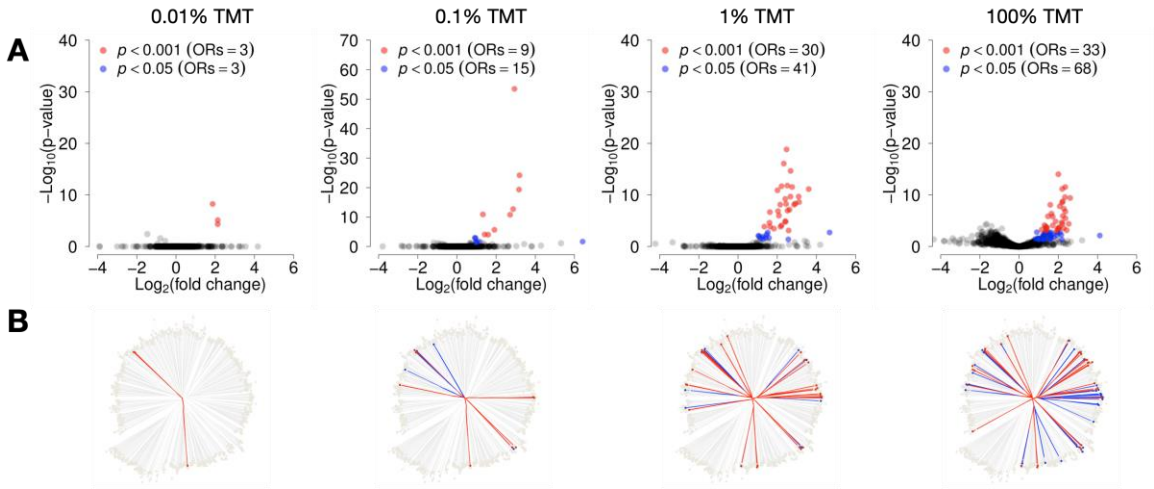

Figure 12: OR repertoires expand with increasing TMT concentrations. (A)Volcano plots showing the $\log_2$ fold change and $-\log_{10}$ p-value of OR genes from 0.01% to 100% TMT. ORs significantly enriched by pS6-IP-Seq with fold change > 1 are colored in blue and red based their p-values (FDR corrected). N = 3 mice were used for each odorant condition. (B) Protein sequence distance trees generated using similarity based on pairwise distances from aligned OR protein sequences. Each end of the branches represents an OR placed alongside its closest neighbors. ORs significantly enriched by TMT at each odorant concentrations are labelled in red (p<0.001) and blue circles (p<0.05).

3.2.2 Most sensitive ORs may not be most robust responders at higher concentrations

At 0.01% starting concentration of ACT, Olfr923 was the most significantly enriched OR with the largest $\log_2$ fold change (Log_2FC) amongst significantly enriched ORs (FDR corrected $p=1.56*10^{-13}$, $\text{Log}_2\text{FC}=2.96$) (Figure 13A), suggesting it is among the most sensitive ORs that recognize ACT. Olfr923 remained significantly enriched from 0.1% to 100% ACT (FDR corrected p-value $p<0.001$) (Figure 13A). However, the rank order of Olfr923 in terms of FDR corrected p-values and Log_2FCs went down at 1% and higher concentrations of ACT (Figure 13A). Olfr983 is the second most significantly enriched OR with the second largest Log_2FC amongst significantly enriched ORs at 0.01% ACT (FDR corrected $p=2.55*10^{-9}$, $\text{Log}_2\text{FC}= 1.88$) (Figure 13A). Similarly, the rank order of Olfr983's activation also went down at higher starting concentrations of ACT (Figure 13A). In

contrast, Olfr907 and Olfr898, ORs with the largest and second largest Log_2FCs among significantly enriched ORs at 100% ACT, were not significantly enriched at 1% and lower starting concentrations of ACT (Figure 13A). Olfr30, the most significantly enriched OR at 100% ACT, was also not significantly enriched at 1% and lower starting concentrations of ACT. In addition, Olfr376, the most significantly enriched OR at 1% ACT, was also not significantly enriched at 0.1% and lower concentrations of ACT. These results suggest that sensitive ORs responding at lower odorant concentrations may not be the most robust responders at higher odorant concentrations, and vice versa.

We observed similar trends with TMT. The rank order of three significantly enriched ORs at 0.01% TMT (Olfr1395, Olfr165 and Olfr1297) also went down in terms of FDR corrected p-values and Log_2FCs at 1% and 100% starting concentrations of TMT (Figure 13B). In contrast, Olfr837 and Olfr506, ORs with the largest and the second largest Log_2FCs among ORs significantly enriched ORs at 100% TMT, were not significantly enriched at 0.1% and 0.01% TMT (Figure 13B). Lastly, Olfr531 and Olfr376, the most and the second most significantly enriched OR at 100% TMT, were not significantly enriched at 0.01% (Figure 13B).

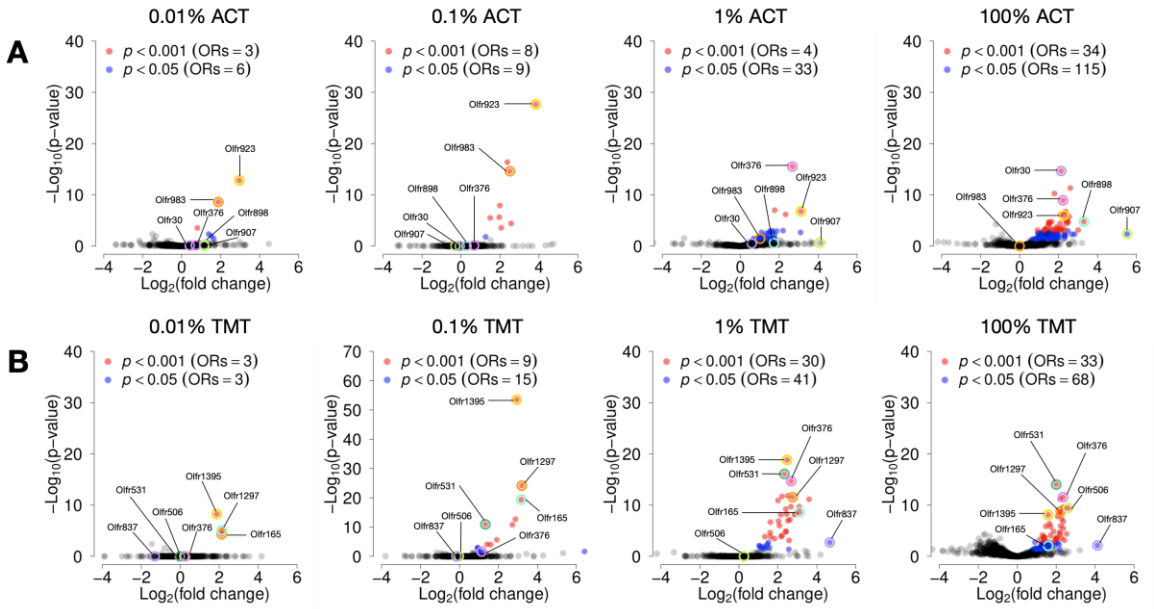

Figure 13: Volcano plots showing the enrichment of specific ACT and TMT ORs. (A) Six ACT responsive ORs - Olfr923, Olfr983, Olfr376, Olfr898, Olfr907, Olfr30 are labelled. (B) Seven TMT responsive ORs - Olfr1395, Olfr1297, Olfr165, Olfr531, Olfr506, Olfr837, Olfr376 are labelled.

3.2.3 Staining data confirms the pS6-IP-Seq OR enrichment

To validate pS6 induction for OSNs in a set of significantly enriched ORs, we conducted in situ hybridization and pS6 immunostaining for ORs responsive at 0.01% starting odorant concentrations. Consistent with our pS6-IP-Seq data, both Olfr923 and Olfr983, but not Olfr376-expressing OSNs (serving as a control) showed significantly higher pS6 signals at 0.01% ACT compared to no odor controls (Figure 14A, C and Figure 15). Violin plots for Olfr1427 and Olfr901 (pS6-IP-Seq enriched at 0.01% ACT) show significantly higher pS6 signals in staining at 1% and higher starting ACT concentrations (Figure 16). In situ hybridization and pS6 immunostaining also confirmed the activation of Olfr1395, Olfr1297 and Olfr165-expressing OSNs towards TMT (Figure 14B, D and Figure 15). Consistent with our pS6-IP-Seq data, Olfr376-expressing OSNs did not show significantly higher pS6 signals at 0.01% starting concentration of TMT (Figure 14D and

Figure 15). As a negative control, we also stained for the pS6 intensity of Olfr1395 when mice were exposed to ACT instead of TMT. Consistent with our pS6-IP-Seq's differential expression data for ACT, Olfr1395 did not show significantly higher pS6 signals at any tested ACT concentrations (Figure 16). Together, our data verified a set of sensitive ORs for ACT and TMT.

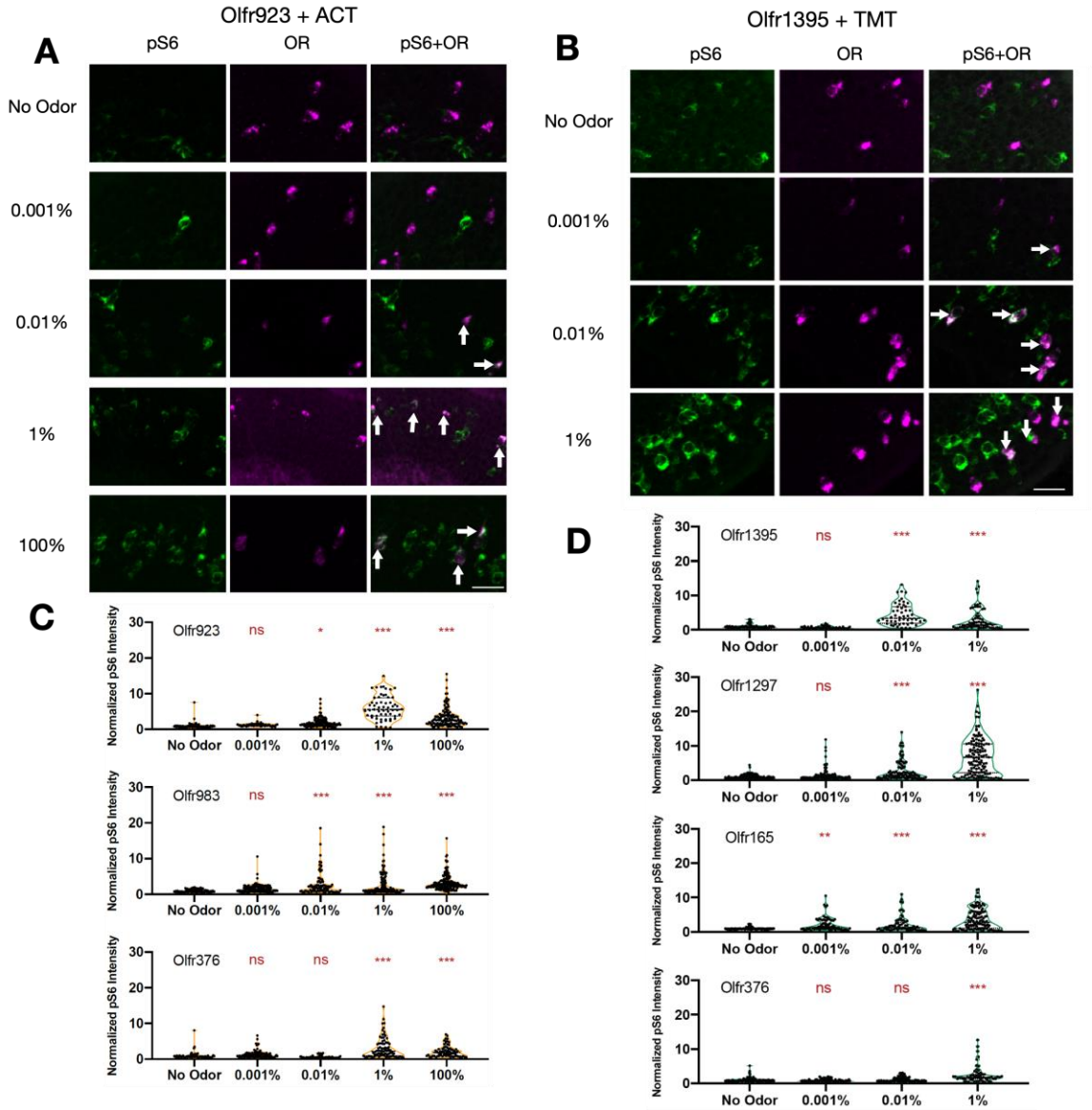

Figure 14: pS6-IP-Seq enrichment data was verified via staining. (A, B) Fluorescence microscopy images showing double-label *in situ* of Olfr923 and Olfr1395 OSNs. Green is antibody staining

for pS6, magenta is the digoxigenin probe signal. Colocalizations are marked by white arrows, representing odorant activated OSNs. Scale bar represents 25 μm. (C, D) Violin plots showing the normalized pS6 intensity for digoxigenin-labelled OSNs based on colocalization, each dot represents a probe labelled OSN. Orange and green colors outline ACT and TMT violin plots respectively. Quantification of the staining data reveals significant difference in normalized pS6 intensity as a result of odorant stimulation. *p<0.05, **p<0.01, ***p<0.001 by one-way ANOVA, Dunnett's post hoc test (various odorant concentrations are compared to no odor controls) for each probe. N = 1–3 mice.

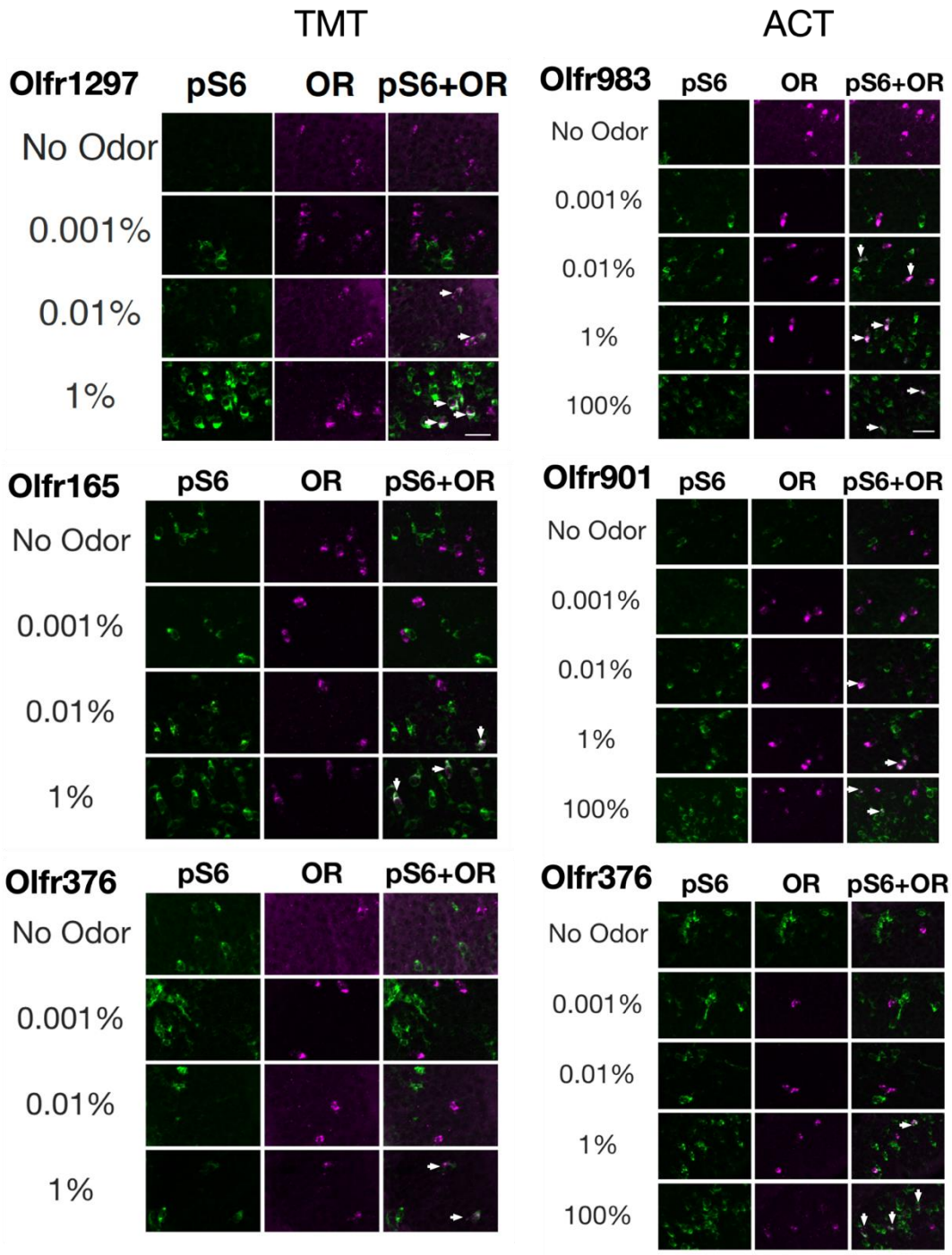

Figure 15: Double-label *in situ* and immunostaining of OSNs. Magenta is the digoxigenin OR probe signal, green is antibody staining for pS6. Colocalizations are marked by white arrows. Colocalization is observed at starting concentrations of 0.01% odorant and above. Scale bar represents 25 μm.

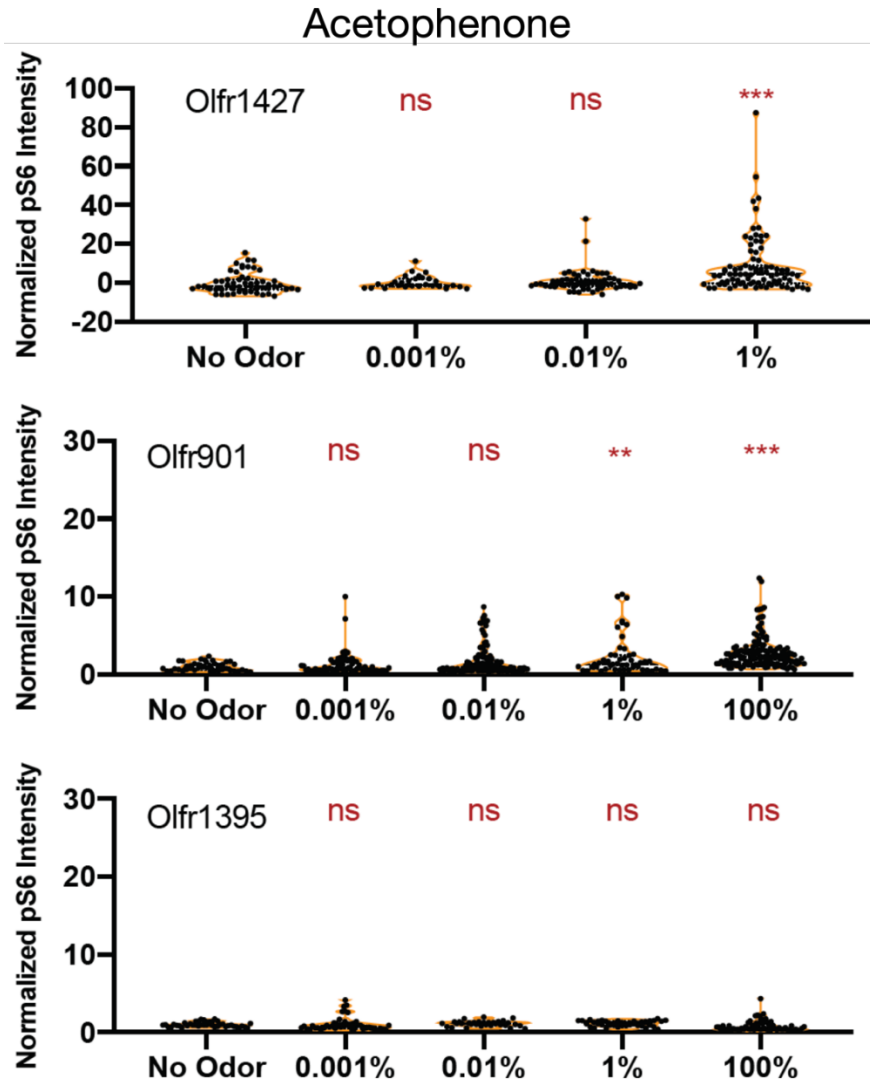

Figure 16: Additional 0.01% ACT responsive ORs showed pS6 colocalization. Olfr1427 and Olfr901 were ORs enriched by 0.01% ACT based on pS6-IP-Seq. Olfr1395 (significantly enriched by TMT based on pS6-IP-Seq) serves as a negative control for ACT. **p<0.01, ***p<0.001 by one-way ANOVA, Dunnett's post hoc test (various starting odorant concentrations are compared to no odor controls) for each probe. N = 1–3 mice.

3.3 Conclusion and Discussion

Our data support the notion that higher concentration of odorants activates more ORs (Fried et al., 2002; Mainland et al., 2014). In the vast majority of cases, ORs significantly enriched with odor stimulation at a low concentration are also enriched at higher concentrations. However, there are some instances where ORs show significant

enrichment only at lower concentrations. The statistical criteria based on the FDR corrected $p<0.05$ cut-off does not represent the critical boundary between responsive ORs and non-responsive ORs. It serves as a selection criterion to identify populations of responsive ORs activated backed by statistical confidence. It is also likely that the proportional nature of RNA-Seq contributes to apparent lower fold changes at the higher odorant concentration. With future advancements in next-generation sequencing data collection and analysis, we expect refinement in the list of enriched ORs.

Humans perceive the same odor with higher intensity and varying degree of pleasantness as odor concentration increases (Moskowitz et al., 1976; Anderson et al., 2003). In some cases, odor quality and/or pleasantness shift when different concentrations of the same odorant are presented (Gross-Isseroff and Lancet, 1988), though there is no such report for ACT and TMT. Higher concentrations of odorants that results in higher OSN spiking rates (Rospars et al., 2000; Bhandawat et al., 2005; Grosmaitre et al., 2006) are likely to result in higher S6 phosphorylation as shown in the retinal cells (Milner and Do, 2017). This cascade of events, could, in turn, contribute to the neural representation of elevated odor intensity. Higher concentration of odors activate additional, lower affinity ORs at the olfactory epithelium, resulting in more glomerular activations in the olfactory bulb (Fried et al., 2002; Khan et al., 2010). These additionally recruited, low-affinity ORs may drive differences in odor quality and perceived intensity by modulating neuronal firing in higher olfactory areas (Stettler and Axel, 2009). In this study, we identified a set of ORs responding to both low and high concentrations odorant and another set of ORs

recruited only at high odorant concentrations. In the future, resources provided in this study will be useful in defining the roles of high- and low- affinity ORs by targeting specific ORs to manipulate in reference to their *in vivo* activation profiles.

In summary, our study comprehensively identifies ORs responding to varying concentrations of odorants and contributes to the understanding of how odorant concentration information is encoded at the receptor level in the peripheral olfactory system. Identifying ORs responding to both low to high odorant concentrations will be valuable in future studies evaluating the contribution of high- and low- affinity ORs towards odor perception.

4. Zonal activation of ORs is odor specific

4.1 Introduction

The distribution of OSNs expressing a given ORs is confined within continuous and partially overlapping spatial zones along the dorsomedial (dorsal) – ventrolateral (ventral) axis on the olfactory epithelium (Ressler et al., 1993; Vassar et al., 1993; Miyamichi et al., 2005; Tan and Xie, 2018). To test if active ORs for each odorant show bias in their zonal distributions, we conducted an RNA-Seq using dorsal and ventral olfactory mucosa (see Methods for details).

4.2 Results

4.2.1 RNA-Seq data relates to zonal index data

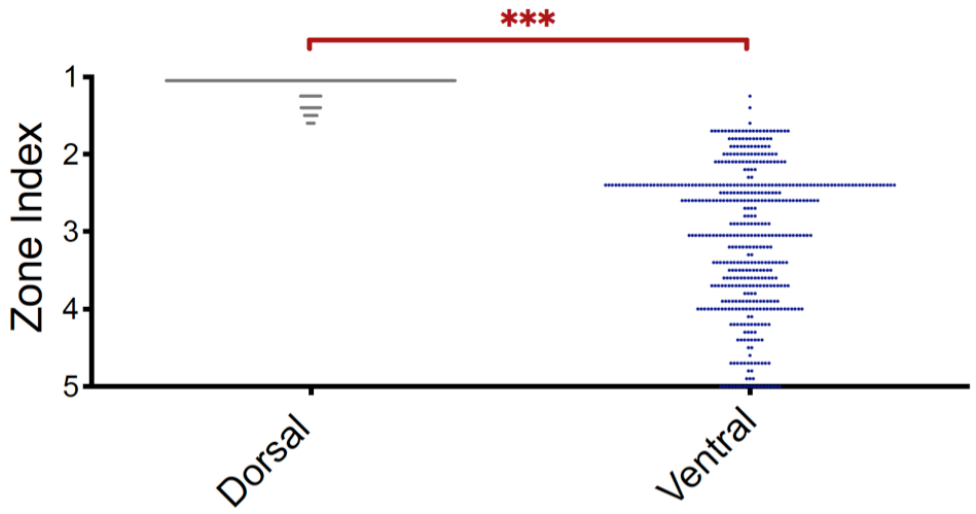

Figure 17: OR dorsal and ventral zonal distribution data based on RNA-Seq is correlated with the zonal index data by Tan et al. where their zonal index increases progressively from dorsal to ventral. ***p<0.001 by Mann–Whitney test (dorsal compared to ventral).

We found 412 and 558 ORs to be significantly enriched in dorsal and ventral zones, respectively. Out of the 117 unclassified ORs, 45 ORs were unclassified due to low

expression. The vast majority of the remaining ORs (70/73) are assigned to zonal index positions between 1.5 to 2.5 (1 being most dorsal and 5 being most ventral) in Tan et al., 2018, suggesting that the these unclassified ORs are expressed in areas close to the dorsal/ventral boundary (Figure 17). Our RNA-Seq data classifying the ORs into dorsal and ventral zones is consistent with the zone index data reported by Tan et al. ($p<0.001$, Mann-Whitney test) (Tan and Xie, 2018) (Figure 17).

4.2.2 OR activation zones are odorant dependent

Comparing between the distribution of responsive dorsal and ventral ORs for ACT and TMT at different concentrations, we found that ACT responsive ORs as a group are more dorsally distributed than TMT responsive ORs from low to high odorant concentrations (Figure 18), suggesting that biased zonal populations of ORs are responding to each of the tested odorants.

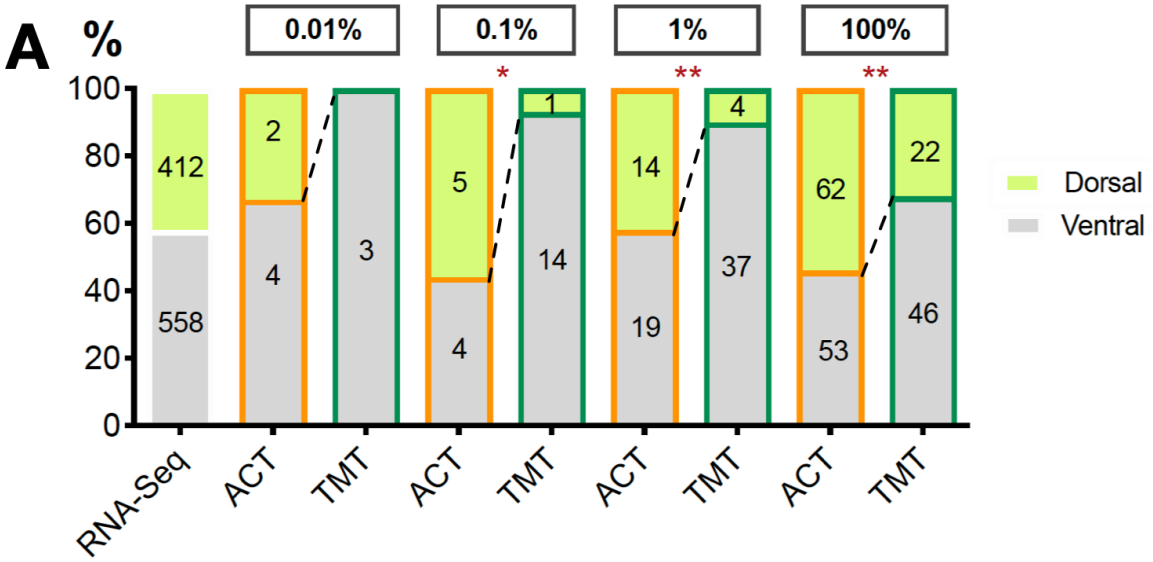

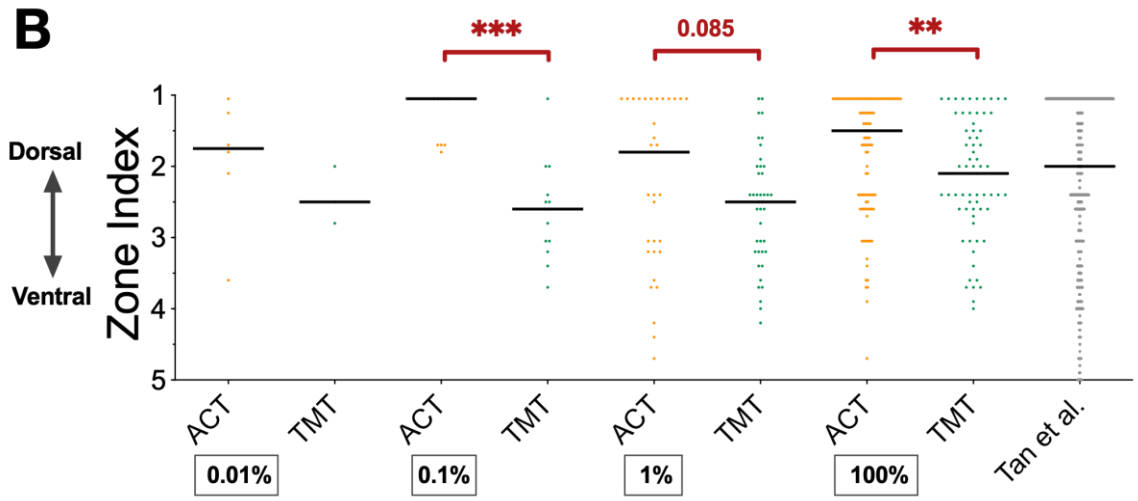

Figure 18: ACT and TMT activated ORs have distinct zonal distributions. (A) Stacked bar graphs showing the zonal location of ACT and TMT activated ORs across various concentrations. Orange and green colors outline ACT and TMT graphs respectively. *p<0.05, **p<0.01, by Fisher's exact test (ACT compared to TMT). N = 3 mice olfactory epithelium were used in RNA-Seq to determine OR zonal positions. (B) The OR zonal index distribution for ORs activated by ACT or TMT shows statistical difference between odorants. **p<0.01, ***p<0.001 by Mann–Whitney test (ACT compared to TMT).

4.3 Conclusion and Discussion

Another dimension of smell encoding, besides keeping track of odorant concentrations, is for neurons to also represent concentration differences of a given odor (Parabucki et al., 2019). Despite facing a dynamic environment where they encounter hundreds to thousands of volatile odors at various concentration gradients, humans and animals are capable of maintaining stable odor quality perception across concentrations (Krone et al., 2001; Wachowiak and Cohen, 2001; Uchida and Mainen, 2007; Mainland et al., 2014; Sirotin et al., 2015; Wilson et al., 2017).

What is not yet clear is how odor identities are encoded and maintained despite massive differences in the activated OR repertoires across concentrations. Stable odor ratio information (Uchida and Mainen, 2007), input-output transformation at the level of

the olfactory bulb (Storace and Cohen, 2017) and early activated ORs during the first sniff (Wilson et al. 2017) are implicated in concentration invariance. Sensitivity of ORs, as well as abundance and positions of OSNs expressing individual ORs within the olfactory epithelium (zonal expression), can play a role in determining the timing of neuronal activation at the level of glomeruli in the olfactory bulb (Schneider et al., 1966; D'Hulst et al., 2016). Our datasets reporting ORs responding to low concentrations of odorants, in conjunction with a number of OSNs expressing different ORs which correlates with OR mRNA abundance (Ibarra-Soria et al., 2014) together with zonal expression of ORs (Ressler et al., 1993; Vassar et al., 1993; Miyamichi et al., 2005; Tan and Xie, 2018) can provide valuable information in targeting a specific set of ORs to investigate their role in odor coding.

5. Olfr923 as a model to evaluate pS6-IP-Seq

5.1 Introduction

The DREAM technique is another method for the *in vivo* identification of odor activated ORs. DREAM relies on the transcriptional downregulation of individual ORs after ~five hours of odor exposure (von der Weid et al., 2015). Using DREAM, von der Weid et al. (2015) identified 44 ORs to be responsive at 5% ACT, with Olfr145 as the best responder. To examine the similarity and differences between pS6-IP-Seq and DREAM, we also performed a 5-hour ACT stimulation in the lab, and looked for OR mRNA downregulation.

Based on pS6-IP-Seq, we found Olfr923 to be the most sensitive and significantly enriched ACT OR (Figure 11). As an independent approach to demonstrate *in vivo* activation of Olfr923 expressing OSNs by ACT, we generated an IRES-Cre gene knock-in mice at the Olfr923 locus and crossed them with Rosa26-lox-stop-lox-tdTomato reporter mice to label the Olfr923 glomerulus (Madisen et al., 2010).

5.2 Results

5.2.1 Olfr923 was not prominently downregulated in DREAM

To understand the apparent differences between DREAM and pS6-IP-Seq, we carried out DREAM using 5% ACT and quantified OR mRNAs with RNA-Seq. Using the same odor stimulation setup as pS6-IP-Seq but with a 5 hour exposure, our DREAM data replicated that Olfr145 (ACT OR reported with the largest RNA-Seq fold change decrease) (von der Weid et al., 2015) decreased in transcripts at 5% ACT (Figure 19, left panel, fold change 0.57, $p<0.001$). In addition, Olfr145 was also enriched based on our new pS6-IP-

Seq datasets at 0.1%, 1%, and 100% ACT (Figure 8). Olfr923, however, was not significantly downregulated at 5% ACT (Figure 19, left panel, fold change 0.86, p=1.00). At 0.01% ACT stimulation, both Olfr145 and Olfr923 were not significantly downregulated (Figure 19, right panel). The inventors of DREAM have suggested that we should instead use older mice (around 3 months) and to have at least n=5 in order to replicate the mRNA downregulation of Olfr923 DREAM data.

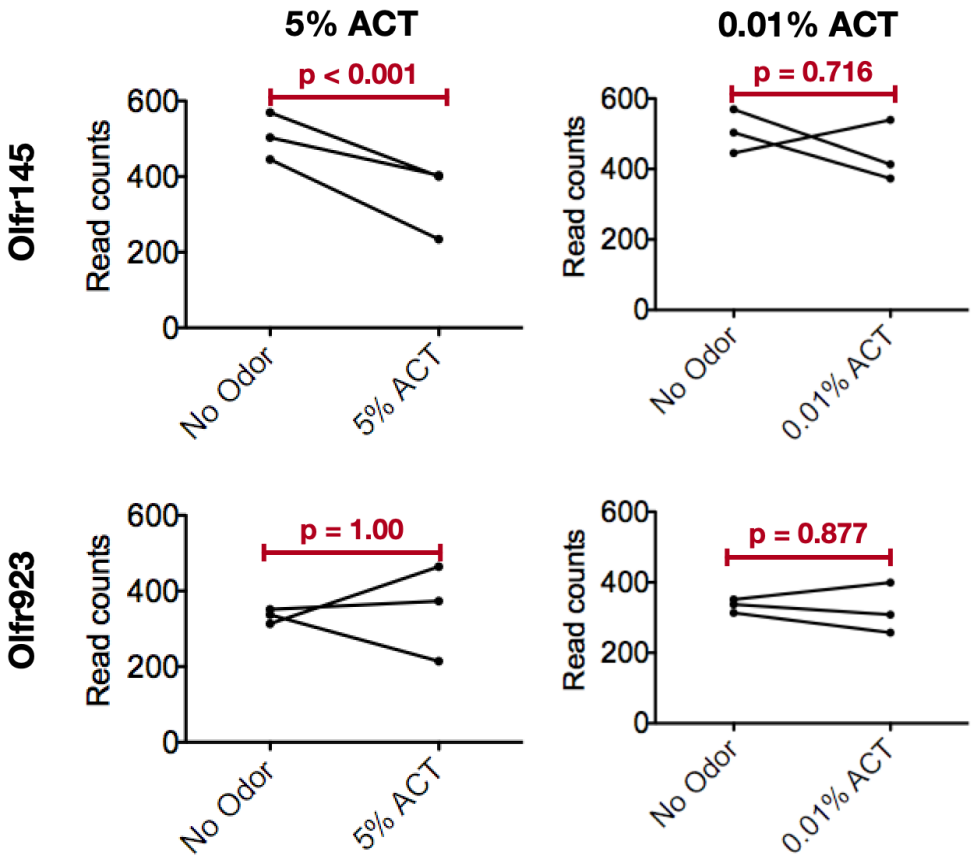

Figure 19: Olfr923 was not ACT responsive based on the DREAM technique. DREAM OR mRNA reads were plotted for 5% and 0.01% ACT after 5 hours of odorant exposure. Olfr145 is significantly downregulated at 5% ACT in DREAM, but not at 0.01% ACT. Olfr923 is not significantly downregulated in both the 5% and 0.01% ACT conditions. P-values are uncorrected based on RNA-Seq differential expression analysis (no odor compared to ACT). N = 3 mice were used for each odorant condition. Dots connected with a horizontal line represent littermates.

To understand the relationship between DREAM and our updated pS6-IP-Seq, we focused on 44 ORs whose mRNA expressions were downregulated by 5% ACT (von der Weid et al., 2015). We remapped the sequence data using our updated OR definitions and performed differential expression analysis using the same bioinformatics pipeline as our pS6-IP-Seq datasets (see Methods for details). Consistent with the von der Weid et al. study, all 44 of the 5% ACT responsive ORs were downregulated. Comparing the DREAM data with our Log_2FC values based on pS6-IP-Seq, a majority of the 44 ORs showed positive Log_2FC values in pS6-IP-Seq (Figure 20). Overall, 19 out of the 44 ORs showed significant enrichment at least in one of the tested concentrations in our pS6-IP-Seq data. Log_2FC values were negatively correlated between DREAM at 5% ACT and pS6-IP-Seq from 0.01% to 1% ACT (p-values < 0.05 and R^2 range from 0.11 to 0.25, Figure 20), while Log_2FC values were weakly correlated between DREAM at 5% ACT and pS6-IP-Seq at 100% ACT (p-value =0.2356 and R2 = 0.03, Figure 20). Altogether, our analysis suggests that the degrees of pS6 induction and downregulation of mRNA expression are moderately correlated. We also looked at the pS6-IP-Seq data of ORs that were differentially expressed solely in the DREAM dataset, we found that at least 21 out of the 26 ORs showed positive Log_2FC (Figure 21), suggesting that these ORs likely had S6 phosphorylation and were responding to ACT.

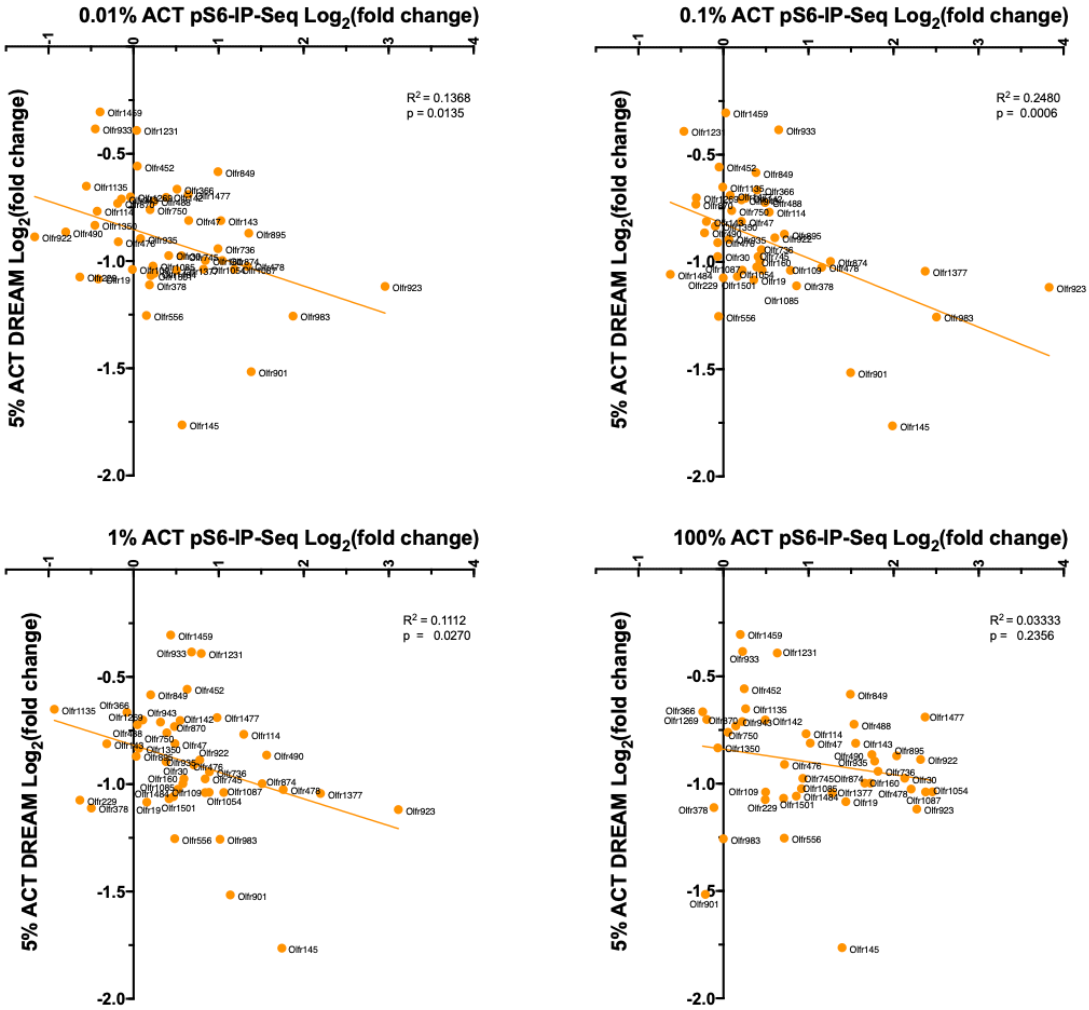

Figure 20: pS6 induction and downregulation of mRNA expression are correlated. Individual ORs pS6-IP-Seq fold changes based on 0.01%, 0.1%, 1% and 100% ACT are compared to the DREAM 5% ACT fold changes (sequence data realigned using the updated UTRs with coding exons annotation and STAR bioinformatics pipeline). All 44 of the previously reported 5% ACT DREAM responsive ORs were shown. R^2 and p-values are based on linear regression.

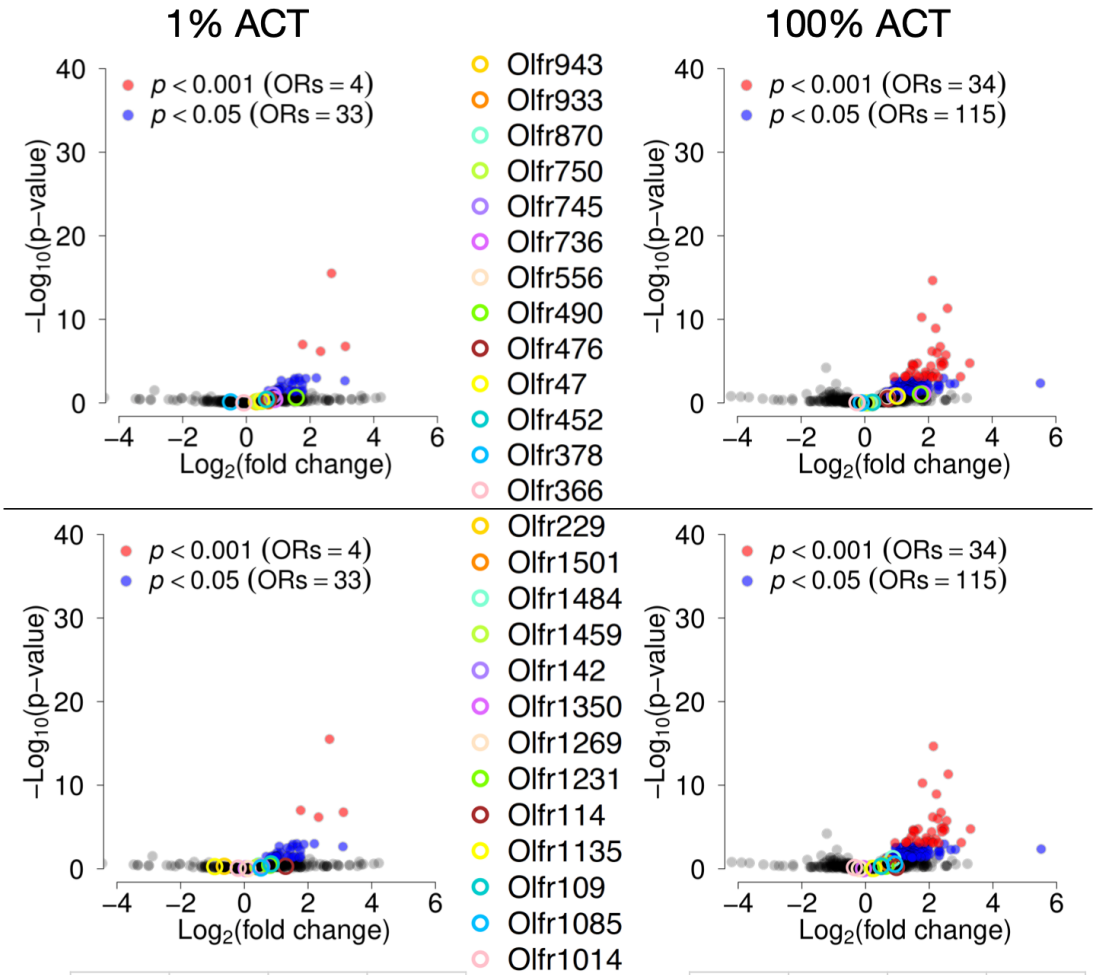

ORs	logFC	Uncorrected p-value	FDR
Olfr943	0.86	0.01	0.06
Olfr933	1.82	0.01	0.08
Olfr870	1.75	0.01	0.09
Olfr750	0.93	0.02	0.15
Olfr745	1.02	0.03	0.16
Olfr736	0.71	0.05	0.21
Olfr556	0.71	0.05	0.22
Olfr490	0.92	0.07	0.27
Olfr476	0.72	0.08	0.30
Olfr47	0.50	0.16	0.48
Olfr452	0.63	0.16	0.49
Olfr378	0.49	0.21	0.55
Olfr366	0.49	0.23	0.56
Olfr229	0.97	0.38	0.69
Olfr1501	-0.35	0.38	0.70
Olfr1484	0.24	0.54	0.84
Olfr1459	0.22	0.56	0.85
Olfr142	0.20	0.65	0.90
Olfr1350	0.26	0.65	0.90
Olfr1269	-0.24	0.67	0.91
Olfr1231	0.22	0.72	0.93
Olfr114	-0.20	0.77	0.95
Olfr1135	0.15	0.77	0.95
Olfr109	-0.07	0.82	0.97
Olfr1085	-0.11	0.83	0.97
Olfr1014	0.05	0.89	0.99

ORs	logFC	Uncorrected p-value	FDR
Olfr943	0.32	0.39	0.72
Olfr933	0.68	0.18	0.56
Olfr870	0.48	0.31	0.66
Olfr750	0.39	0.26	0.63
Olfr745	0.84	0.01	0.12
Olfr736	0.89	0.07	0.37
Olfr556	0.48	0.14	0.51
Olfr490	1.56	0.02	0.22
Olfr476	0.71	0.06	0.36
Olfr47	0.49	0.22	0.59
Olfr452	0.63	0.07	0.37
Olfr378	-0.50	0.41	0.75
Olfr366	-0.08	0.88	0.97
Olfr229	-0.63	0.14	0.51
Olfr1501	0.42	0.23	0.60
Olfr1484	0.47	0.10	0.44
Olfr1459	0.44	0.20	0.57
Olfr142	0.55	0.17	0.55
Olfr1350	0.06	0.84	0.96
Olfr1269	0.11	0.86	0.96
Olfr1231	0.80	0.06	0.37
Olfr114	1.30	0.14	0.50
Olfr1135	-0.93	0.17	0.55
Olfr109	0.84	0.02	0.26
Olfr1085	0.52	0.48	0.79
Olfr1014	-0.19	0.59	0.84

Figure 21: ORs identified by DREAM have positive fold changes in pS6-IP-Seq. Volcano plots showing the pS6-IP-Seq data at 1% and 100% ACT of 26 ACT ORs found to be differentially expressed solely in the DREAM technique. Out of the 44 ORs identified by DREAM at 5% ACT, 19 ORs were also identified by STAR.

5.2.2 ACT activated Olfr923 in the olfactory bulb

To ask whether the Olfr923 glomeruli in the olfactory bulb were activated, we conducted c-Fos immunostaining in periglomerular cells induced by odor stimulation (Guthrie et al., 1993). Mice exposed to 0.01% starting concentration of ACT displayed a significant increase in c-Fos induction in periglomerular cells surrounding the Olfr923 glomeruli compared to no odor controls both in terms of cell counts and percentages of c-Fos-positive cells ($p < 0.05$ paired t-test, one-tailed) (Figure 22 and Figure 23), suggesting ACT activates Olfr923 OSNs and also the Olfr923 glomeruli.

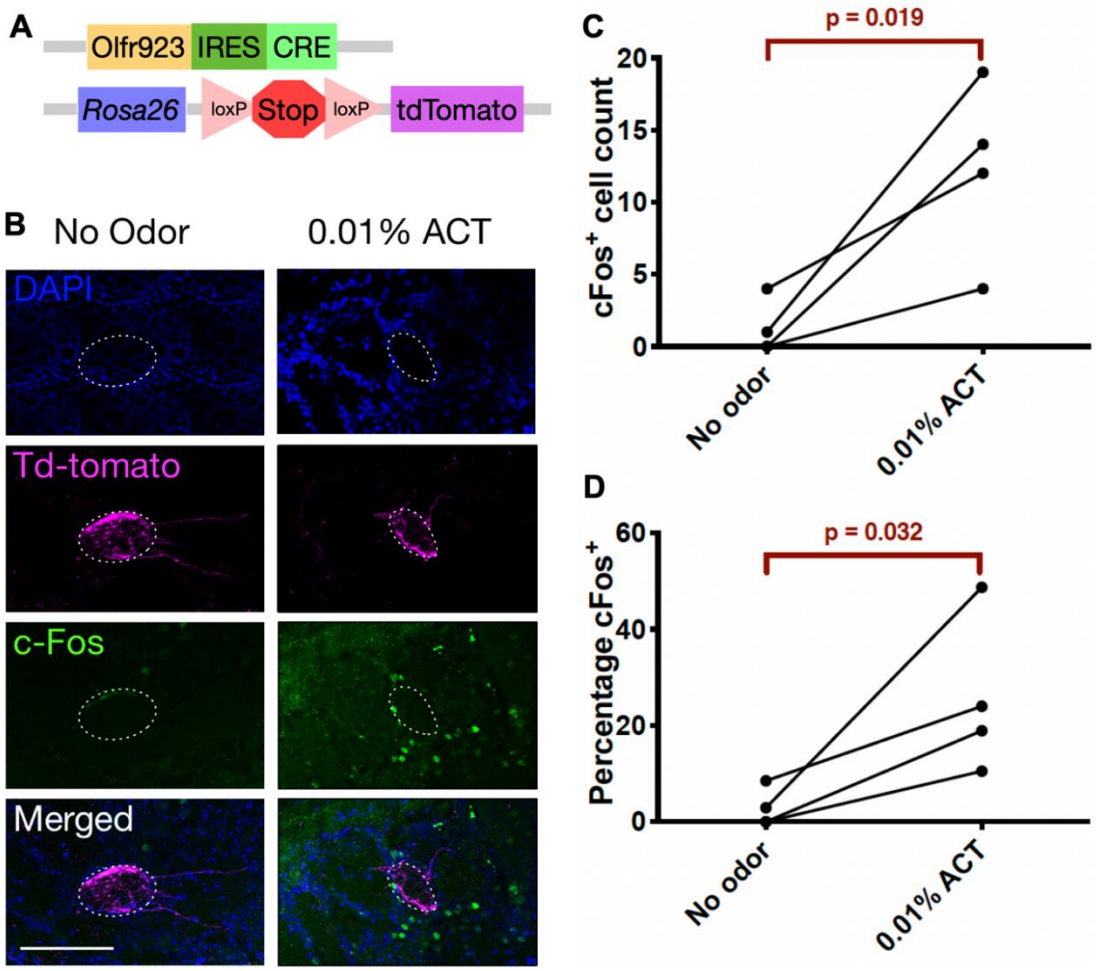

Figure 22: Exposure to ACT induces c-Fos expression in Olfr923 periglomerular neurons. (A) Schematic drawing of the Olfr923-Cre transgenic mouse targeting vector. (B) Fluorescence microscopy image showing the Olfr923 mouse glomerulus. Magenta is Olfr923 labelled by td-tomato, green is periglomerular neurons stained for c-Fos, blue is DAPI nuclear staining. Scale bar represents 100 μm. Tissue sections with the greatest density of td-tomato fibers at the glomeruli were used for staining. (C) c-Fos-positive periglomerular cell counts around the Olfr923 glomeruli. (D) Percentage of c-Fos-positive periglomerular cells, calculated by the number of c-Fos-positive over the total number of DAPI labelled Olfr923 periglomerular cells. (C) P-values are based on paired t-test, one-tailed (no odor compared to 0.01% ACT). N = 4 mice were used for each odorant condition. Dots connected with a horizontal line represent samples that were stained on the same day.

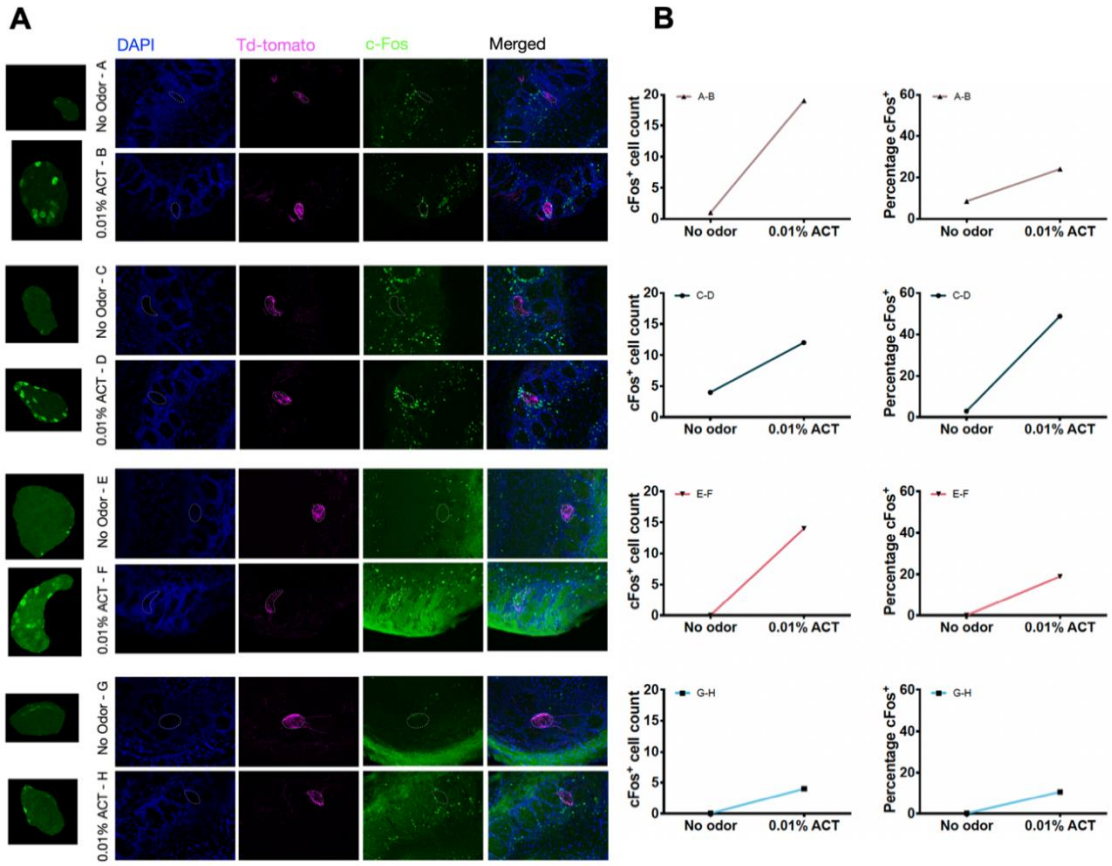

Figure 23: c-Fos images for ACT exposed Olfr923 periglomerular neurons . (A) Fluorescence microscopy images of the olfactory bulb. Blue is DAPI nuclear staining, magenta is Olfr923 labeled by td-tomato, green is periglomerular neurons stained for c-Fos. Merged images show periglomerular c-Fos activity around the Olfr923 glomeruli. Scale bar represents 100 μm. (B) Individual quantification of the c-Fos activity for each glomerulus, quantified areas are shown in as cropped glomeruli images on the left. Dots connected with a horizontal line represent samples that were stained on the same day.

5.2.3 Modelling of ACT and Olfr923 *in silico* showed favorable free energy

Our *in vivo* and *in situ* data consistently showed ACT to be an activator for Olfr923. Lastly, we asked if Olfr923 has evidence for structural properties that are favorable for ACT binding. Heptanal is a non-agonist of Olfr923 as previously reported (Ibarra-Soria et al., 2017). We first aimed to confirm Olfr923 activation *in vitro* using the GloSensor assay system to monitor the real time response of Olfr923 against ACT and heptanal. ACT or

heptanal was dissolved into medium and odor-mediated cAMP induction was monitored in real time. Increases of over time were observed when Olfr923 was exposed to ACT, an indication of Olfr923 activation by ACT, while no significant luminescence increase was observed when Olfr923 was exposed to heptanal (Figure 24A). To quantify Olfr923 activations, we analyzed the area under the curve (AUC) of the normalized luminescence and generated dose response curves, confirming differential activation of Olfr923 by ACT and heptanal (Figure 24B).

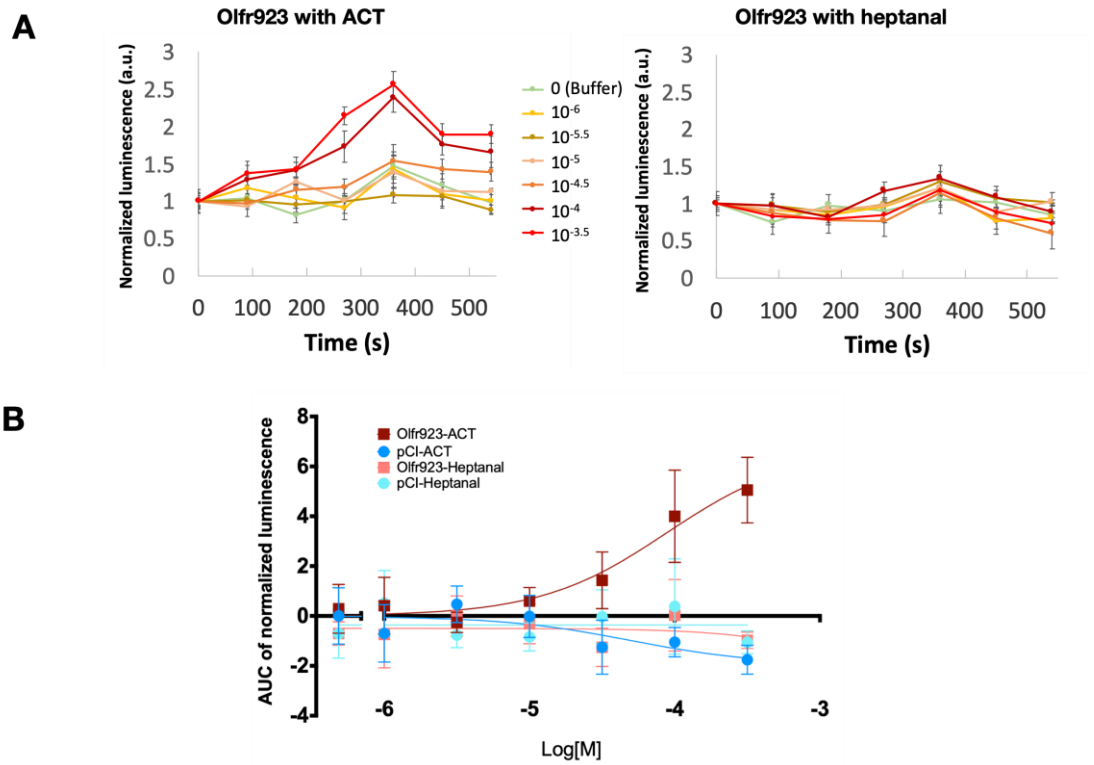

Figure 24: Olfr923 is activated by ACT but not heptanal *in vitro*. (A) Liquid-phase ACT and heptanal stimulation of Olfr923 with the GloSensor assay system Luminescence in each well was measured once every 90 s for 6 cycles and the values were normalized with the initial value for Olfr923-pCI and response of the pCI control at the given time point. N = 3 wells were used for each concentration. Error bars indicate standard error of the mean (SEM). (B) Area under the curve (AUC) indicates the sum of normalized luminescence (normalized to pCI vector+ buffer condition) from initial response to final response. Error bars indicate SEM.

A three-dimensional model of Olfr923 was then built by homology modeling. ACT was docked into the canonical binding cavity of Olfr923, and heptanal serves as a negative control. Heptanal is a non-agonist of Olfr923 as previously reported (Ibarra-Soria et al., 2017). This complex was embedded in a membrane model, solvated in water and submitted to multiple molecular dynamics simulations. After several steps of minimization, equilibration and 800ns of production with no constraints, ACT remained closely associated with the canonical binding cavity (Figure 25A). However, heptanal exited the binding cavity to enter into the lipid bilayer that compose the membrane, suggesting a low ligand-OR binding cavity affinity (Figure 25B). Olfr923 bound to ACT has a favorable negative $\Delta G_{binding}$ (Figure 25C). In contrast, heptanal has an unfavorable positive $\Delta G_{binding}$ (Figure 25C) ($p=0.0371$ paired t-test, one-tailed).

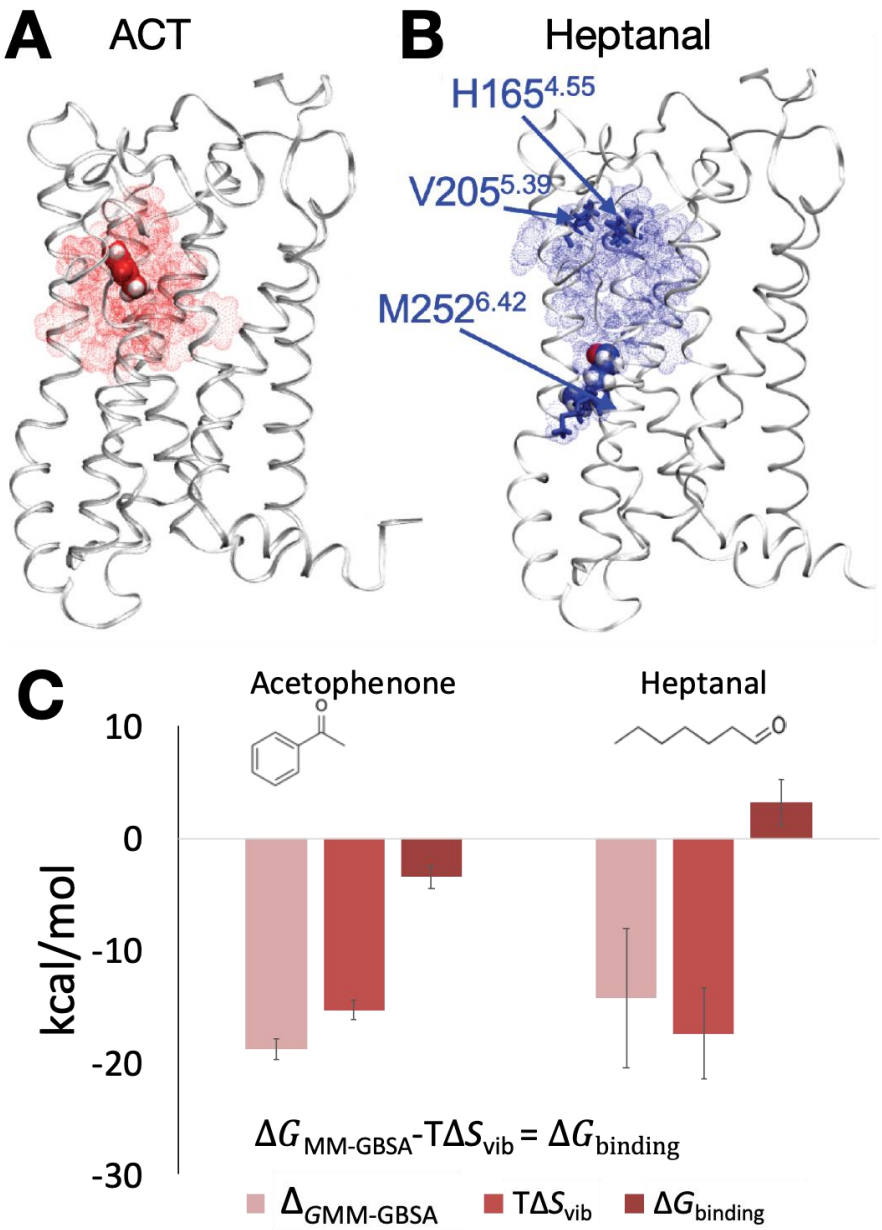

Figure 25: ***In silico*** **investigation of ACT binding to Olfr923. The three-dimensional structure of Olfr923 was built by homology modeling and bound to ACT (red,** A**) and heptanal (blue,** B**). Helices are represented in white ribbons and the odorant molecules are shown in Van der Walls volumes. The residues interacting with the odorant molecule during molecular dynamics simulations are highlighted by dotted clouds in the corresponding color (ACT-red, heptanal-blue). Residues specific to heptanal binding, H165$^{4.55}$, V205$^{5.39}$ and M252$^{6.42}$ (Ballesteros-Weinstein numbering shown in superscript) (Ballesteros and Weinstein, 1995), are represented in blue licorice.** (C) **Computed enthalpy $\Delta G_{MM\text{-}GBSA}$, entropy $T\Delta S_{vib}$, and free energy of binding $\Delta G_{binding}$ for heptanal and ACT bound to Olfr923. *p<0.05 by paired t-test (ACT compared to heptanal). N = 3 simulations per odorant.**

5.3 Conclusion and Discussion

The DREAM technique identifies odor responsive ORs based on a decrease in OR mRNA abundance after odor stimulation (von der Weid et al., 2015). Our analysis suggests that, OR responses based on *in vitro* assays and the two *in vivo*-based assays (pS6-IP-Seq and DREAM) correlated each other yet they did not show strong linear correlations. For example, Olfr923 is one of the most sensitive and robust ORs responding to ACT based on pS6-IP-Seq, ranking top in terms of Log_2FC amongst significantly enriched ORs from 0.01% to 1% ACT. Olfr923 ranked 36th out of the 44 responsive ORs based on 5% ACT DREAM RNA-Seq fold change in the publication, Olfr923 now ranks 5th when our bioinformatics pipeline is used to reanalyze the 5% ACT DREAM RNA-Seq data (von der Weid et al., 2015) (Figure 20). When tested *in vitro* via the luciferase assay, Olfr923 ranked 32nd out of the 105 responsive ORs based on fold luciferase induction with 300 μM ACT (Jiang et al., 2015). Difficulties in functionally expressing certain ORs in heterologous cells partly explains the differences. Future mechanistic understanding of how odorant activation drives S6 phosphorylation or OR mRNA decrease should help explain these differences across the *in vivo* and *in vitro* OR response studies. In addition, the abundance of ORs can also be widely varied (Ibarra-Soria et al., 2014). Some ORs with low read counts did not reach the set significance (FDR corrected $p>0.05$) in spite of large fold changes. A deeper sequencing read depth will help determine whether these ORs are bona fide ORs responding to the tested odorants.

6. Predator odors and their chemical analogs

6.1 Introduction

3,5-Trimethyl-3-thiazoline (TMT), which is secreted from the red fox anogenital gland, triggers an innate, odor-driven defensive response in mice (Fendt et al., 2005; Kobayakawa et al., 2007). This unconditioned inborn aversion is hardwired in the mouse brain and is observed even in the predator-naïve laboratory mice (Fendt et al., 2005). Curiously, a TMT synthetic structural analog, 2MT induces highly robust freezing in mice (Kobayakawa et al., 2007; Isosaka et al., 2015) (Figure 26). To study the role of odorant-OR interactions behind these predator odors, we investigated OR responsive *in vivo* and *in vitro* for TMT and its structural analogs. Here, we employed open-field behavior test, pS6-IP-Seq and OR specific fluorescent *in situ* hybridization and cAMP-mediated GloSensor assays to study the combinatorial coding of predator related odorants.

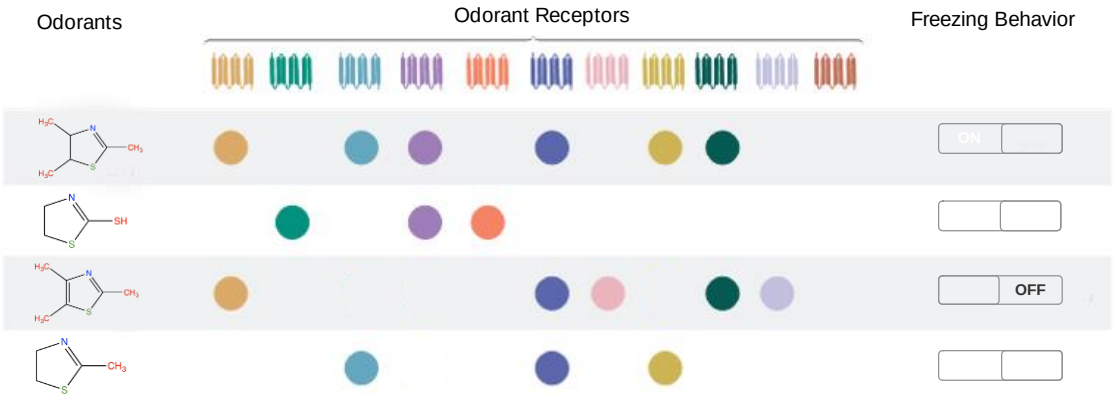

Figure 26: TMT structural analogs and mice freezing behavior. (Hypothetical combinatorial OR code of the four odorants and whether it elicit freezing behavior in mouse.

6.2 Results

6.2.1 Freezing behavior paradigm

Laboratory studies that were done on mice showed that predator odors have distinctive behavioral effects on mice in the form of freezing and suppression of feeding or grooming behaviors (Apfelbach et al., 2005). We have successfully established an odor-driven open-field behavioral paradigm in the lab to study defensive behaviors. In Figure 27, we quantified robust mice freezing response towards 1% 2MT in randomized behavioral trials. Each time block of exposure is 10 minutes, Tissue-Tek cassette containing no odorant is presented first, followed by one odorant (2MT or ACT). Behavior traces were videotaped and the FreezeScan program from Clever Sys Inc was used to score the freezing responses. we conducted a global ANOVA considering the factors of odorant, gender and age (n=8). There was a main effect of odorant, reflecting significant differences in percentage freezing time between the 2MT exposed group, when compared against control or ACT.

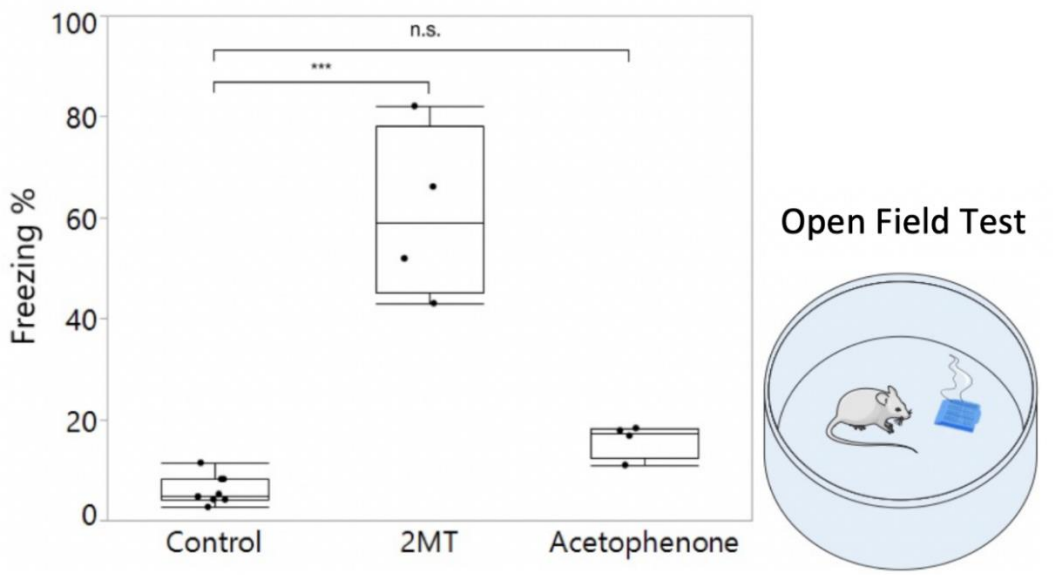

Figure 27: Predator naïve lab mice show freezing behavior towards 2MT. Amount of total freezing time induced by no-odor (control), innate-freezing-inducing (1% 2MT) and neutral (1% ACT) odorants. Data are box and whiskers plots. Global ANOVA, ***p < 0.0001.

We developed an in-house mouse motion analysis software to generate detailed traces of realtime mouse activity (Figure 28). Video recordings of mice presented with different odorants (10 mins per odorant condition) were analyzed for pixel shifts and freeze durations (> 2s). We saw that the wild-type mouse exhibited freezing behavior when presented with 0.5% 2MT, but not 1% ACT (Figure 28A) . However, when the mouse was presented first with 0.5% 2MT which induced freezing, subsequent presentation of 1% ACT also induced freezing behavior (Figure 28B). This is likely because the mouse has learnt to be fearful of the odorant cassette that was presented.

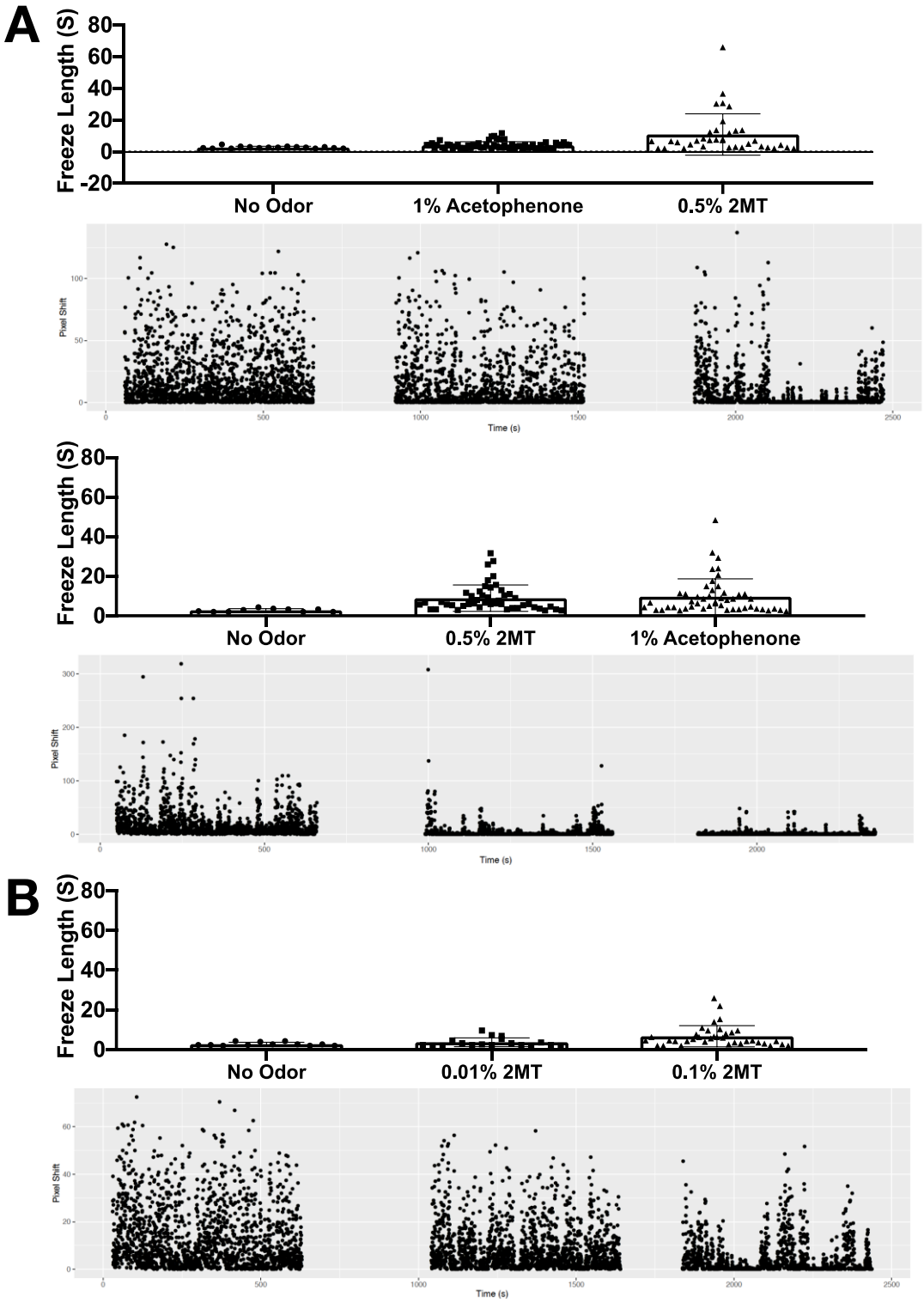

Figure 28: Mice Freezing behavior trials show concentration sensitivity. Freeze events > 2s were plotted into bar graphs at each odorant condition in chronological order. Pixel shifts are computed based on shifts in the centroid position of the recorded mice. Higher pixel shifts mean

more movement and lower pixel shifts indicate freezing. (A) The order of presentation of ACT and 2MT is switched. (B) Different concentrations of 2MT were presented to the mouse.

6.2.2 pS6-IP-Seq of TMT structural analogs

It is known that the expression of ORs on OSNs display a zonal distribution in terms of diversity along the dorsal-ventral axis at both the olfactory epithelium and the olfactory bulb. Although both dorsal and ventral OSNs are activated by TMT, dorsal OSNs preferentially inputs to the cortical amygdala, which was found to be functionally implicated in a neural circuit for TMT avoidance (Miyamichi et al., 2011; Root et al., 2014). It was also reported that OSNs expressing dorsal ORs project to the dorsal domain of the olfactory bub, and ablation of these OSNs inhibited freezing behavior in mice (Kobayakawa et al., 2007). Because OSN axons expressing the same OR converge on common glomerular structures, predator cues have been implicated with particular topographic maps of activated glomeruli. Specifically, a new cluster of glomeruli was identified to respond to heterocyclic odorants with sulfur and nitrogen atoms (eg. TMT) at the posterior D_{II} (dorsal, class II) region of the olfactory bub (Matsumoto et al., 2010). we looked for potential 'fear-OR(s)' amongst D_{II} receptors which are activated by TMT and/or 2MT.

The level of odorant intensity is another important variable to investigate because it is known that the concentration of an odorant could greatly affect how it is perceived emotionally. In the case of TMT, we postulate that odorant concentration is important in determining whether the innate-fear response neural circuit has been activated. we predict that the ORs regulating the innate-fear behavior should be particularly sensitive

to aversive odorants at low concentrations. As such, the OR will have functional significance in facilitating early predator detection while the fox is still at a safe distance. It is known that as odorant concentration goes up, additional ORs with low affinity for the odorant will also be recruited, thus altering the receptor code (Malnic et al., 1999). To narrow my search for the "fear-OR(s)", we focused on D_{II} receptors that respond to equal to 1% TMT and 2MT. We also performed pS6-IP-Seq to identify ORs enriched by SBT (released in dominant mice and endangered conspecifics) and nTMT (non-dihydrogenated TMT).

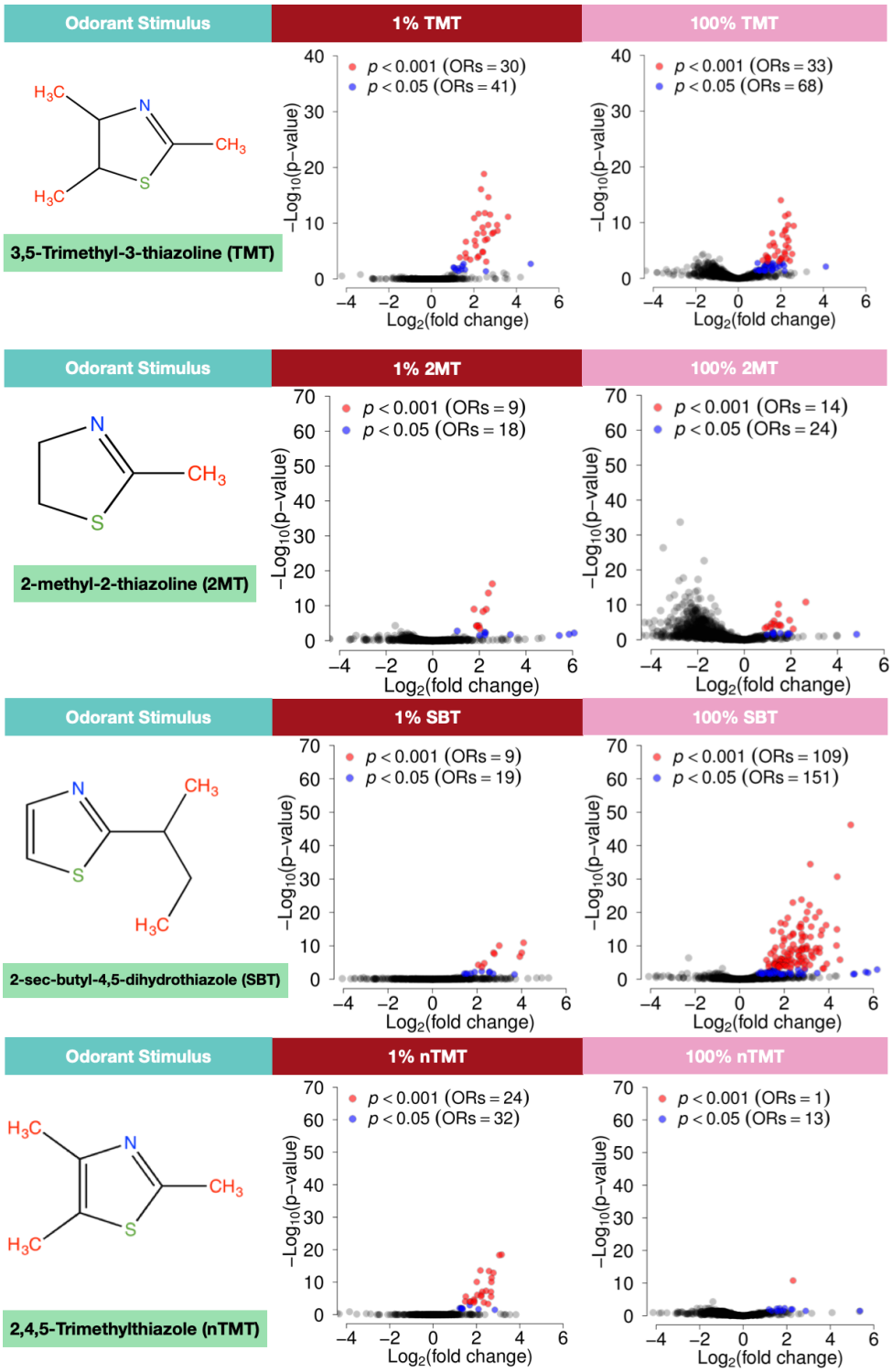

Figure 29: pS6-IP-Seq OR enrichment for TMT and its structural analogs. Volcano plots showing the $\log_2$ fold change and $-\log_{10}$ p-value (FDR corrected) of OR genes for 1% to 100% starting concentrations of odorant. OR differential expression values are based on pS6-IP-Seq comparing odorant stimulated and unstimulated C57BL6 mice. ORs significantly enriched by

pS6-IP-Seq with positive fold change are colored in blue and red based their p-values (FDR corrected). N = 3 mice were used for each odorant condition.

pS6-IP-Seq mRNA profiling revealed 41 and 18 ORs that are sensitive to 1% TMT and 1% 2MT respectively (Figure 29). We identified three 'fear-OR(s)' (Olfr1131 Olfr1132, Olfr376) which respond *in vivo* and *in situ* to both 1% TMT and 1% 2MT. Curiously, based on pS6-IP-Seq, we found Olfr1131 (closely related to Olfr1132) to be uniquely enriched by 1% 2MT but not any other odorants (Figure 29). Given the fact that 1% 2MT triggers more pronounced freezing response than 1% TMT, a possible explanation behind this is perhaps the recruitment of additional 'fear-OR(s) such as Olfr1131.

Olfr1132 show good colocalization with the anti-pS6 signal at both 100% and 1% TMT exposure (Figure 30). A pairwise distances tree of aligned OR amino acid sequences was created and we identified the two D_{II} ORs (Olfr376, Olfr1132) that were activated by both 1% TMT and 1% 2MT (Figure 30, red circles) to be located in distinct clusters across the OR tree.

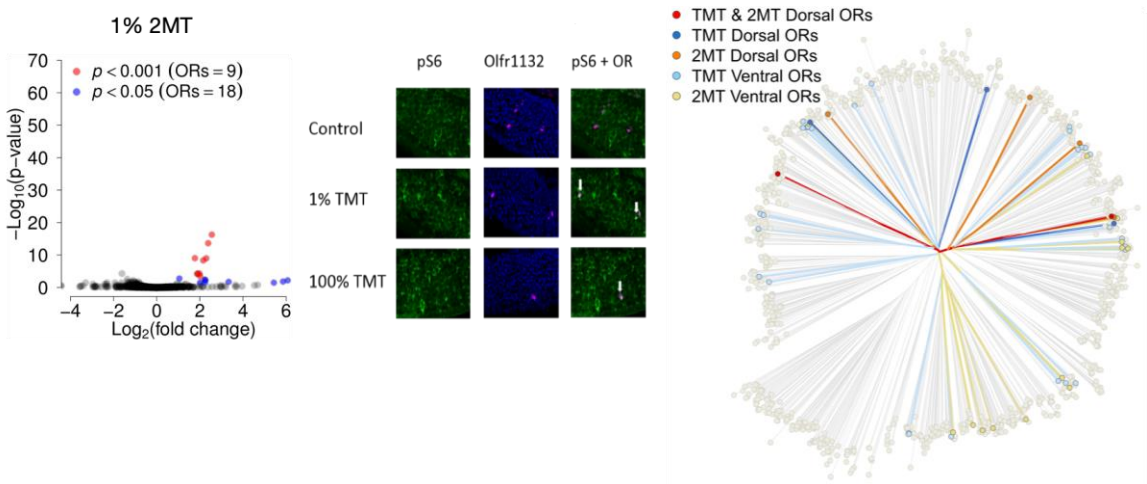

Figure 30: Lists of TMT and 2MT responsive ORs show some overlap. (A) Volcano plots compare 2MT transcriptome data generated by pS6-IP-Seq, between odorant-stimulated (1% 2MT) and unstimulated groups. (B) Coronal section of the mice olfactory epithelium stimulated with 1%

and 100% TMT. Shown in magenta are DIG probes labeling the dorsal TMT OR, Olfr1132, which respond towards TMT. (C) Analysis based on pairwise distances from aligned OR protein sequences using similarity. Color OR labels are based on gene enrichment information from one hour long 1% TMT and 1% 2MT odorant stimulation + pS6-IP RNA-Seq combined with ventral/dorsal zonal expression data. FDR < 0.05 corrected.

6.2.3 CRISPR/Cas9 knockout of TMT activated ORs

To investigate the sensory receptors behind innate fear, we generated triple knockout mice (Olfr1131, Olfr1132, Olfr376) via the CRISPR/Cas9 gene editing system with the overall goal of eliminating or reducing defensive behavior towards 1% TMT and/or 1% 2MT.

With newly popularized CRISPR/Cas9 mouse genome editing tools, it is possible to generate single, and, even more gene knockout mice in a fraction of the original time needed from conventional methods (Fujii et al., 2013; Wang et al., 2013; Platt et al., 2014). The CRISPR/Cas9 gene editing system presents many advantages over the transgenic methods in terms of both cost and time. For instance, early targeted nucleases (eg. Zinc finger) requires meticulous engineering of a series of zinc fingers in order to achieve accurate protein-based DNA-binding (Miller et al., 2007). Whilst with the CIRSPR/Cas9 system, all that needs to be customized is the gRNA and additional standardized reagents can be brought off the shelf (Sander and Joung, 2014).

In collaboration with the Duke Transgenic Core facility, we have initiated the one-step generation of mice carrying multiple OR mutations. The single guide RNAs (sgRNAs) suggested for our target ORs were commercially synthesized and cloned into PX330 plasmids. The different sgRNAs were also screened *in vitro* for optimal nuclease activity in cleaving the target site. The optimal gRNAs with cas9 mRNA were microinjected into around fertilized single-celled mouse embryos, and we got between 9 to 12 viable pups per litter.

We subsequently genotype the mice to see of double-stranded breaks in the OR genes repaired by non-homologues end joining has successfully created loss-of-function frameshift mutations (Lieber, 2010). We found pronuclear injection to be more effective in generating triple homozygous knockout mice. Out of the 9 pups that we obtained from the litter, 6 of them were triple homozygous mutants (Figure 31). Cytoplasmic injection of the Cas9 protein however, did not yield any triple mutants. Instead, 4 double mutants, 4 single mutants and 4 wild-type pups were delivered (Figure 31).

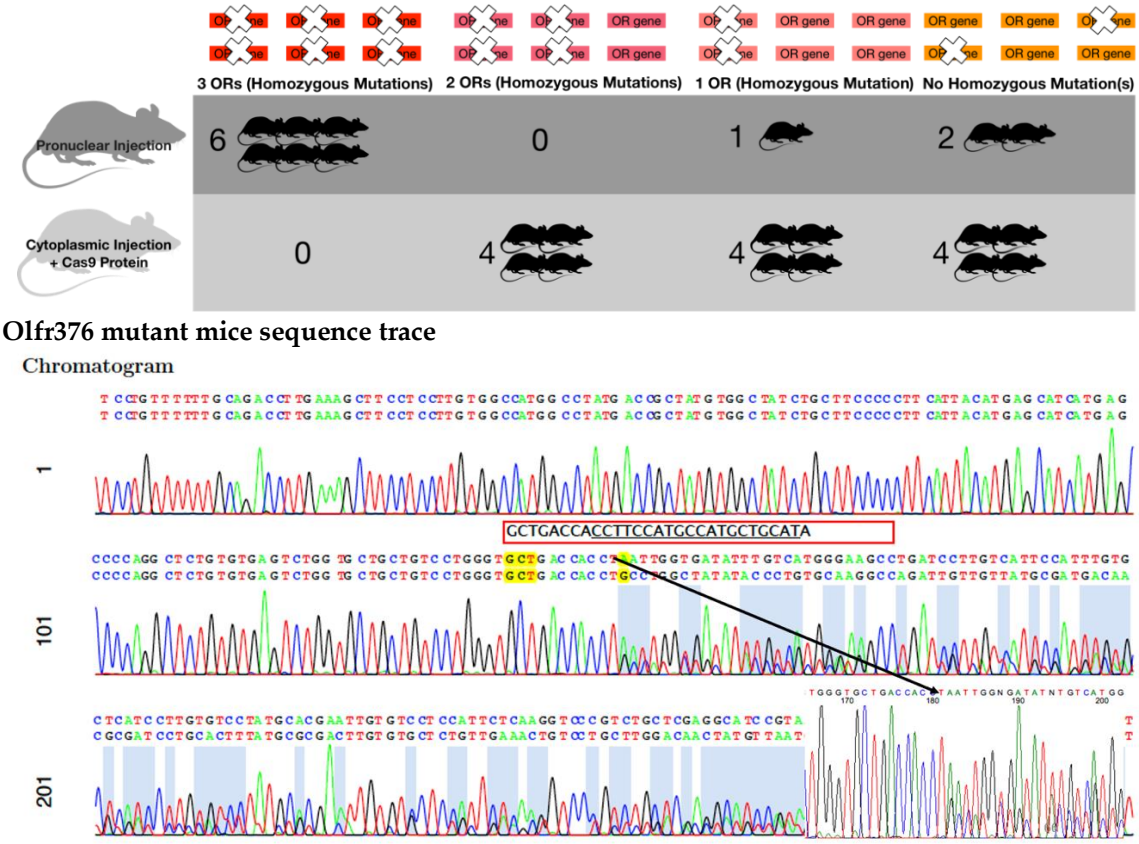

Figure 31: Triple homozygous mutants were generated with CRISPR. Sequence trace shows a mutation of a CRISPR mice for Olfr376. The red box indicates the expected wild-type sequence.

However, unwanted mutations were found also in genes such as Olfr153 with the CRISPR/Cas9 technology generated mice. With pronuclear injection, 44% of the pups had

Olfr153 mutations; with cytoplasmic injection, 58% of the pups had Olfr153 mutations (Figure 32). A variety of online tools offer computational methods to warn users of potential off-target hits that give unwanted indel loci (Marx, 2014). We validated for off-target effects by checking particular genes which share significant sequence homologies to our target ORs and redesigned alternative gRNAs, one particularly useful resource is the Optimized CRISPR Design software (crispr.mit.edu), which the Duke Transgenic Core recommends. See details of the new gRNA design protocol in appendix A. We also checked for mosaicism in the CRISPR generated mice by sequencing from multiple tissues in the brain, the internal organs and the limbs of the pups that were sacrificed. All tissues contained identical mutations to the initial toe clipping used for genotyping (Figure 33).

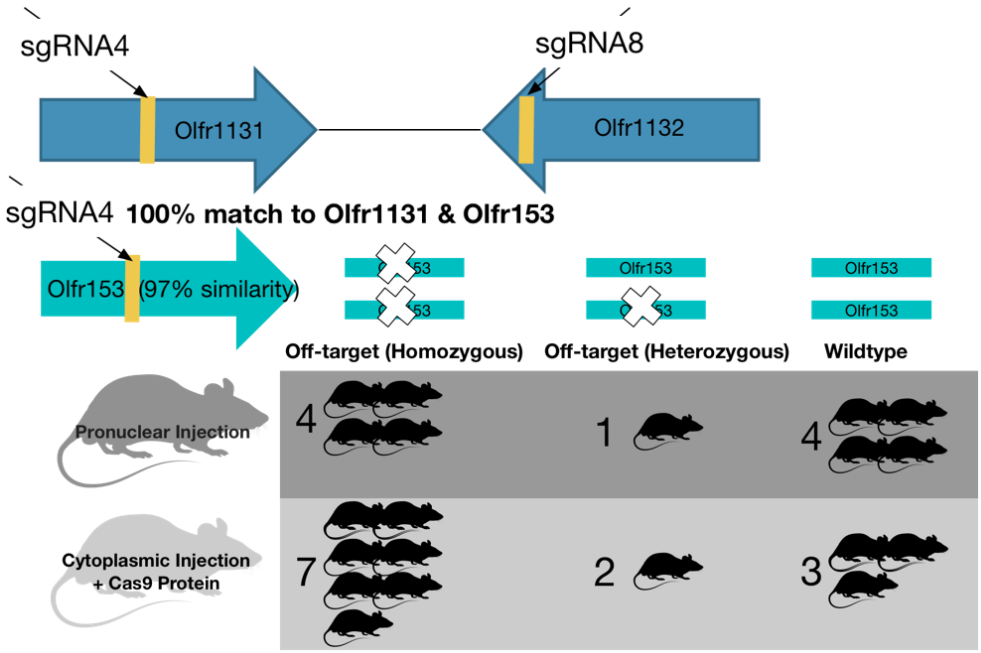

Figure 32: Non-target mutations were detected in genes such as Olfr153

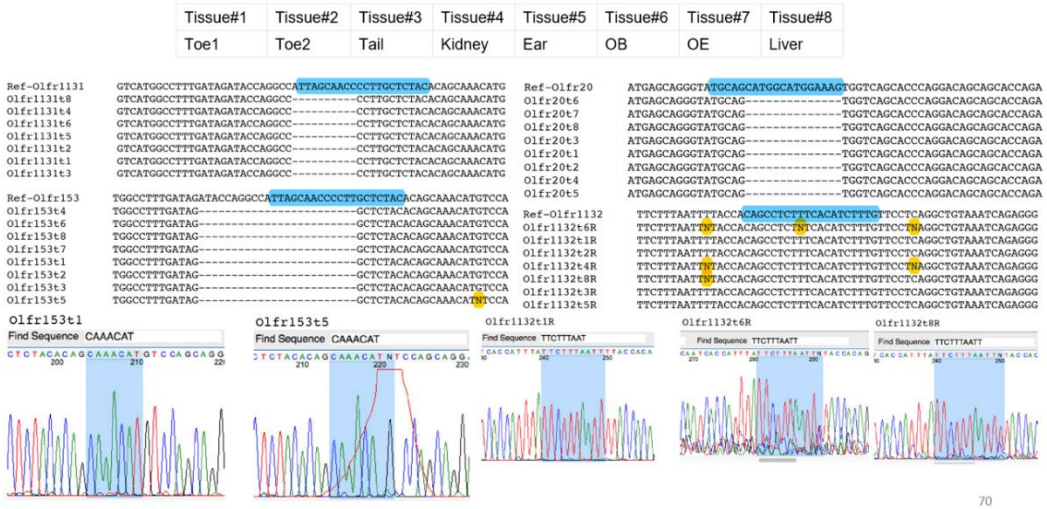

Figure 33: Mosaicism was not detected in the CRISPR mouse with tissue sequenced from 8 different sites.

Single or double knockout mice were then tested in behavior assays to see if individual ORs is contributing to fear response. We saw one mouse that no longer exhibits robust freezing behavior towards 2MT. This mouse is a triple homozygous knockout for Olfr376, Olfr1131 and Olfr1132. It exhibited slight freezing when presented with 0.01% 2MT, and lower freezing behavior when presented with 0.1% 2MT (Figure 34). In wild-type mouse trials, all mice reliably exhibited higher freezing behavior when presented with 0.1% 2MT (Figure 34A).

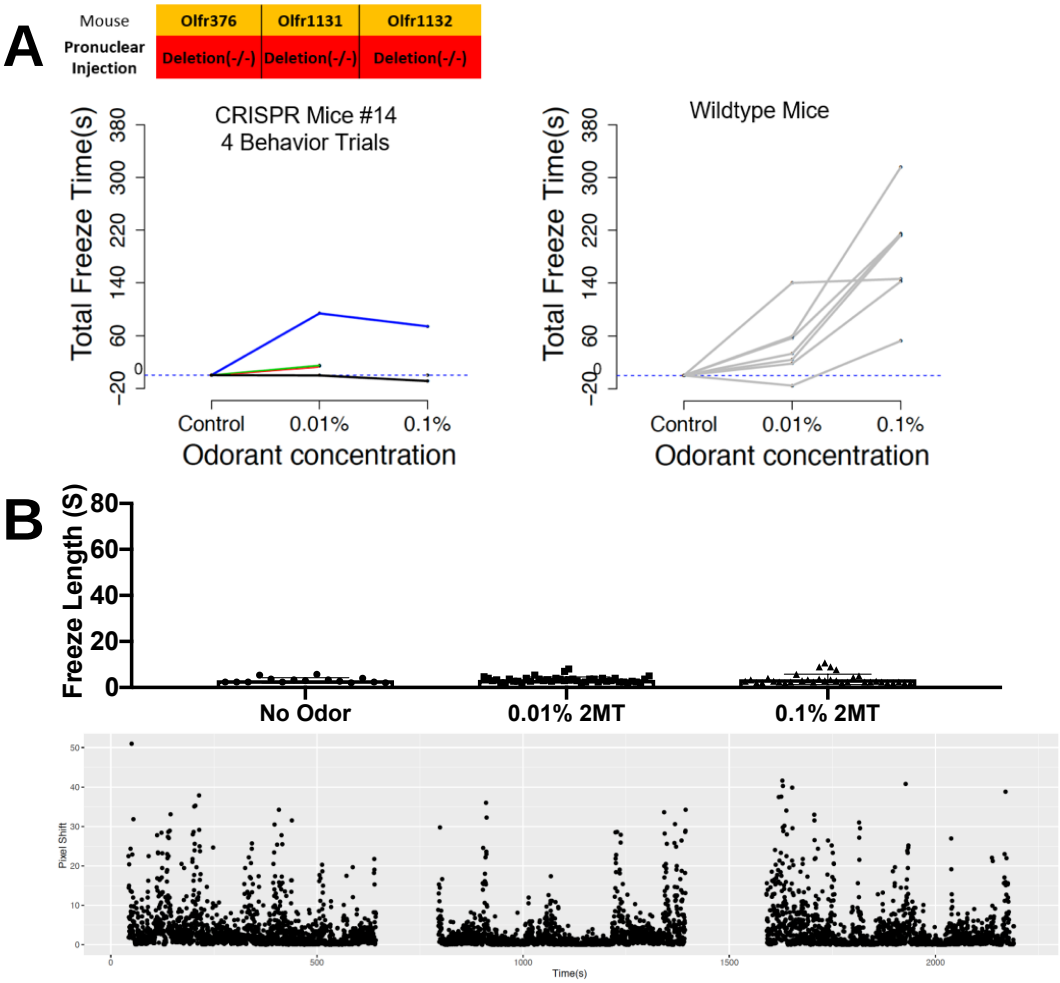

Figure 34: Freezing behavior was reduced in a triple knockout CRISPR mouse.

6.3 Conclusion and Discussion

We expect the OR knockout pups to show impairment in olfaction-mediated innate-fear response, thus suggesting that necessity of our disrupted receptors in mediating defensive behavior. For instance, their freezing behavior towards TMT/2MT may start to resemble that of a neutral odorant. However, no reliable behavior differences were observed in the double or triple knockout mice. This suggests the possibility that instinctive emotions such as predator fear may be anatomically organized in the mammalian brain within pathways beyond the olfactory circuits.

7. Covalent modification of ORs

7.1 Introduction

In 2018, Wang et al., reported a large-scale forward genetics screening that identified Trpa1 as a chemosensor for predator odor-evoked innate fear behaviors (Wang et al., 2018). This suggests that the trigeminal system plays an important part in driving the odor-evoked freezing behavior of mice exposed to TMT and 2MT. Interestingly, they also found that Trpa1 may act as a direct chemosensor for TMT/2MT through covalent modifications of critical cysteine residues of the receptor (Wang et al., 2018). We thus hypothesize that this covalent modification of the Trpa1 receptor may be conserved in a small subset of TMT/2MT responsive ORs. Macpherson et al. reported that 5 mM reducing agent dithiothreitol (DTT) reverses TRPA1 activation induced by the disulfide-forming activator MTSEA inside TRPA1-expressing cells (Macpherson et al., 2007). We thus set out to investigate if DTT can selectively inhibit the activation of certain TMT/2MT responsive ORs. Knowing DTT is a cell-permeable reducing agent that can reverse the disulfide modification of cysteines, we also generated cysteine to serine mutants to test if OR activations can be reversed by DTT.

7.2 Results

7.2.1 DTT inhibits some 2MT responsive ORs

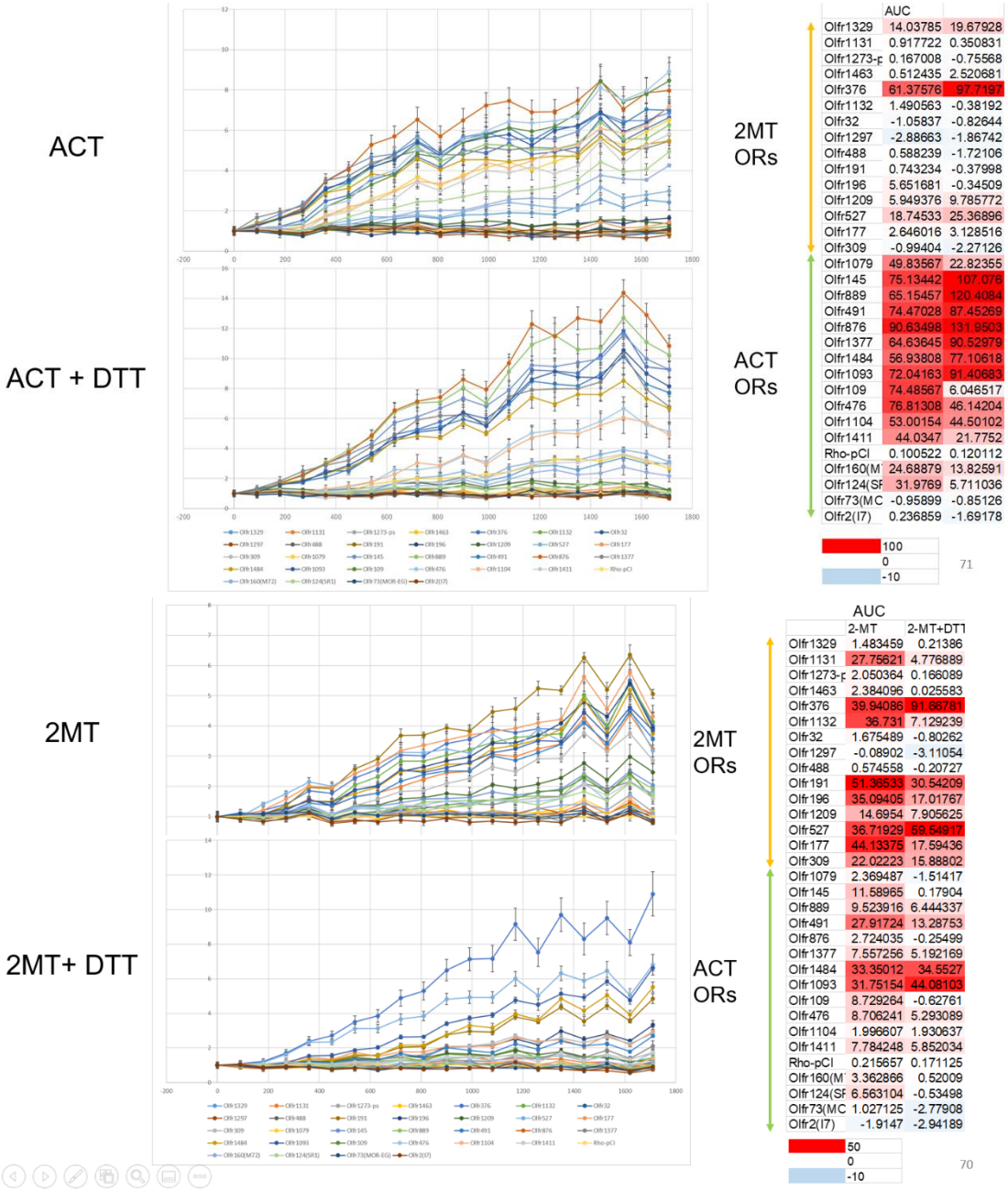

Figure 35: Vapor-phase ACT or 2MT stimulation of pS6-IP-Seq enriched ORs with the GloSensor assay system. Luminescence in each well was measured once every 90 s for 20 cycles and the values were normalized with the initial value for each individual OR and response of the pCI control at the given time point. Error bars indicate SEM (n = 3). 5 mM DTT was administered 5 minutes before inserting the plates into the reading chamber. Table shows the

area under the curve (AUC) of the normalized luminescence for the odorant stimulated plate and odorant + DTT stimulated plate.

With ACT exposure, none of the 2MT responsive ORs (based on pS6-IP-Seq, orange arrow) activation was dampened by DTT (Figure 35). Activation of 7 of the 16 ACT responsive ORs (based on pS6-IP-Seq, green arrow) showed lower (> 5 units) activation with the addition of DTT (Figure 35). With 2MT exposure, 7 of the 15 2MT responsive ORs (based on pS6-IP-Seq, orange arrow) showed inhibition by DTT (> 5 units). In contrast, only 2 of the 16 ACT responsive ORs (based on pS6-IP-Seq, green arrow) showed lower activation with DTT (> 5 units). This suggests that the reducing agent DTT inhibits specific OR activity, and that a disulfide bond may be needed in either odorant-OR binding or in maintaining the integrity of the OR structure.

7.2.2 Inhibition dependent OR and odorant

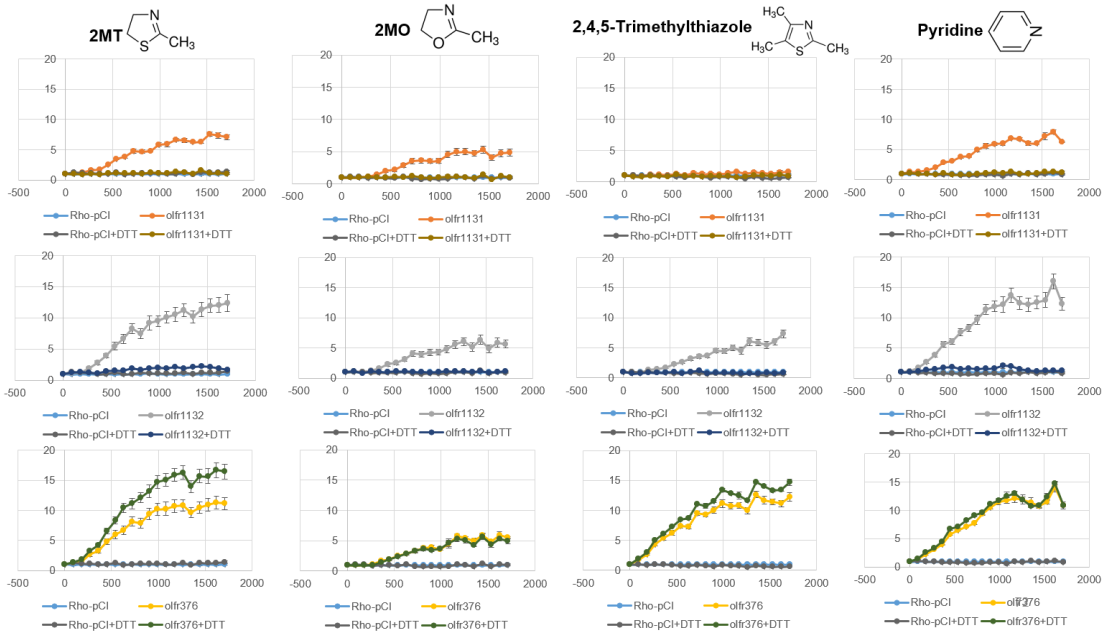

Figure 36: ***In vitro*** **activation and inhibition of 2MT and its analogs is OR specific. Vapor-phase ACT (ACT), 2-methyl-2-oxazoline (2MO), 2,4,5-Trimethylthiazole (nTMT) and pyridine stimulation against Olfr1131, Olfr1132, Olfr376 with the GloSensor assay system. Luminescence in each well was measured once every 90 s for 20 cycles and the values were normalized with the initial value for each individual OR and response of the pCI control at the given time point. Error bars indicate SEM. (n = 3). 5 mM DTT was administered 5 minutes before inserting the plates into the reading chamber.**

We see that Olfr1131 responded to 2MT, 2MO and pyridine; DTT also successfully inhibited the response in all three conditions (Figure 36). Olfr1132 responded strongly to 2MT and pyridine but moderately to 2MO and nTMT, DTT inhibited the response in all four conditions (Figure 36). Olfr376 responds to 2MT, nTMT and pyridine strongly, but DTT surprisingly enhanced the 2MT and nTMT response (Figure 36).

7.2.3 OR mutants show diminished response towards 2MT but not ACT

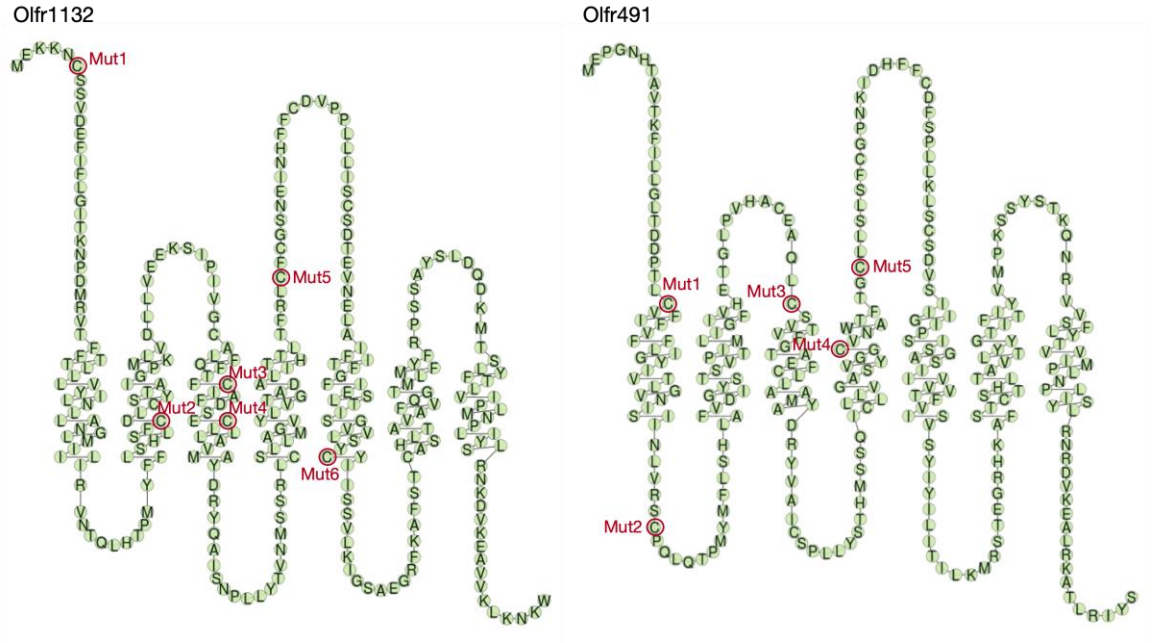

Figure 37: Olfr1132 and Olfr491 cysteines to serine OR mutants. Olfr1132 and Olfr491 GPCR snakeplots show the location of the mutated cysteines.

Figure 38: Olfr1132 and Olfr491 mutants showed a reduced response to 2MT but not ACT. Area under the curve (AUC) for Olfr1132 and Olfr491 cysteine to serine mutants. Sum of normalized luminescence (normalized to pCI vector+ buffer condition) from initial response to final response. Error bars indicate SEM (n = 3).

When select Olfr1132 cysteines were mutated to serine (Figure 37), we saw that only Mut6 retained a similar level of AUC to that of the Olfr1132 wild-type when exposed to 1% 2MT (Figure 38). All six mutants however, were inhibited by DTT when exposed to 1% 2MT (Figure 38). Olfr1132 does not respond to ACT and serves as a negative control.

When select Olfr491 cysteines were mutated to serine (Figure 37), we saw that all mutants had responses to 1% ACT comparable to the wild-type Olfr491 (Figure 38).

However, all mutants showed lower responses towards 1% 2MT than wild-type Olfr491 (Figure 38). DTT did not affect the mutant's response towards ACT and activation remained high, but DTT inhibited these mutant's response towards 2MT (Figure 38). Olfr376 served as a positive control whereby DTT does not inhibit the Olfr376's response towards ACT and 2MT.

7.2.4 Clickable-TMT activated some ORs

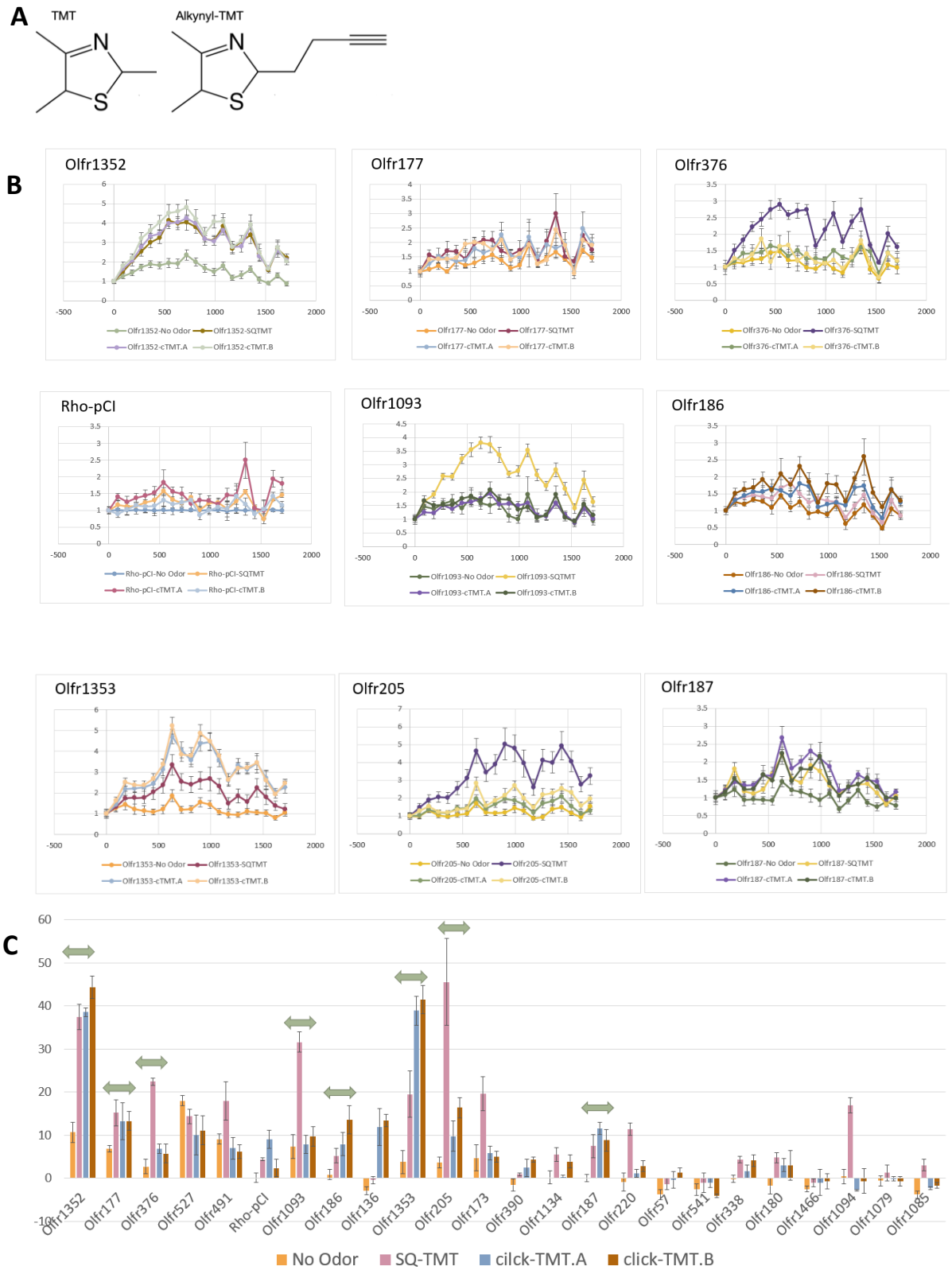

Figure 39: TMT and click-TMT activated slightly different sets of ORs *in vitro*. (A) TMT and click-TMT chemical structures. (B) Vapor-phase TMT and click-TMT stimulation of a panel of TMT S6-IP-Seq enriched ORs with the GloSensor assay system. Luminescence in each well was measured once every 90 s for 20 cycles and the values were normalized with the initial value for each individual OR and response of the pCI control at the given time point. Error bars indicate SEM (n = 3). (C) Area under the curve (AUC) indicates the sum of normalized luminescence (normalized to pCI vector+ buffer condition) from initial response to final response. Error bars indicate SEM (n = 3).

Olfr1352 serves as a good candidate for the testing of TMT's interaction with ORs via covalent modification because it was activated reliably by both click-TMT isomers A and B (Figure 39B, C). Olfr177, Olfr1352, Olfr186, Olfr187 also showed comparable activation for both TMT and click-TMT (Figure 39B, C). Olfr376, Olfr1093, Olfr205, Olfr173 showed some activation with click-TMT isomers, but considerably higher activation with TMT (Figure 39). This points to the precision of ORs in their interactions with distinct chemical ligands.

7.3 Conclusion and Discussion

The covalent interaction of 2MT with Trpa1 opens the possibility that similar covalent modifications might be present in 2MT's interaction with the ORs that it activates. Such covalent modifications have not been found with ORs and their chemical ligands. The ability of DTT to selectively inhibit the odorant of certain but not all ORs, further points to the interesting underlying chemistry that may be behind the interaction of predator related odors and their ORs. Further investigation of the activation mechanisms of click-TMT and click-2MT compounds with receptors such as Olfr1352 and Olfr491 respectively can help unravel novel processes underlying the detection of such predator related odorants.

8. Conclusion

Understanding how the olfactory system is organized at the receptor level to discriminate between odorant concentrations is challenging. This question became accessible with our latest high-throughput next-generation sequencing method which identifies collections of activated mouse ORs in vivo. Research to date found OR repertoires to encode for distinct odors. We provide an additional understanding of this combinatorial code: individual ORs operate over a narrow range of odorant concentrations, but the population can generate distinct OR repertoires across a ten-thousand-fold concentration range. We saw from our ACT and TMT pS6-IP-Seq data that OR repertoires expand with increasing odorant concentrations from 0.01 to 100% odorant. In addition, we found that sensitive ORs responsive at 0.01% odorant may not be most robust responders at higher concentrations such as 1% and 100% odorant. This active recruitment process can allow unique populations of ORs to represent odorant concentrations with flexibility and sensitivity.

Comparing pS6-IP-Seq with existing *in vitro* and *in vivo* OR deorphanization methods, we saw that pS6-IP-Seq enriched ORs tend to show higher *in vitro* activation levels than non pS6-IP-Seq enriched ORs. The DREAM in vivo OR deorphanization approach is based on a different principal from pS6-IP-Seq: it relies on the transcriptional downregulation of individual ORs after five hours of odorant exposure. We found that pS6 induction and downregulation of mRNA expression are moderately correlated. For DREAM ORs reported to be downregulated with ACT, our pS6-IP-Seq data consistently captured higher OR mRNA from these olfactory sensory neurons with the pS6 antibody.

We also explored the activation of Olfr923 as the best ACT responder by exploring the glomeruli response, GloSensor assay activation and *in silico* receptor binding. We saw significant c-Fos induction of periglomerular cells surrounding the Olfr923 glomerulus when mice were exposed to 0.01% ACT. This complement our pS6-IP-Seq enrichment data suggesting Olfr923 to be a sensitive ACT OR. We further confirmed Olfr923's activation *in vitro* using the GloSensor assay system to monitor the real time response of Olfr923 against ACT and heptanal. We saw a dosage-dependent increase in luminescence with ACT, but not heptanal. Further molecular dynamic simulations revealed the high affinity of Olfr923 for ACT and stable association of ACT inside the Olfr923 canonical binding cavity. We also computed a favorable negative free energy of binding of Olfr923 towards ACT but not heptanal.

In summary, our study comprehensively identifies ORs responding to varying concentrations of odorants and contributes to the understanding of how odorant concentration information is encoded at the receptor level in the peripheral olfactory system. Identifying ORs responding to both low to high odorant concentrations will be valuable in future studies evaluating the contribution of high- and low- affinity ORs towards odor perception. For instance, high-affinity may be implicated in concentration invariance and perceived quality, while low-affinity ORs may drive differences in perceived intensity. Further advancements in monitoring the active combinatorial code at the muli-glomeruli level will help to reveal the functional meaning of these ORs in generating an overall olfactory percept.

9. Methods

9.1 Animal protocol

9.1.1 Animals

All animal procedures were performed in accordance with the Duke University animal care committee's regulations. All experiments in this paper were carried out on both male and female mice. C57BL/6J and B6.Cg-Gt(ROSA)26Sor tm9(CAG-tdTomato)Hze/J were obtained from the Jackson Laboratory and crossed in the mouse facility. C57BL/6J mice of 20 to 22 days of age were used for pS6-IP-Seq, RNA-Seq and staining experiments. All experiments in this paper were carried out on both male and female mice. Littermates of the same sex were used for each pS6-IP-Seq replicate (n=3) and data from both sexes were pooled to avoid sex-specific genes being enriched in a given odor exposure. Though we did not formally test between the two sexes for differences, we did not observe any obvious differences between males and females in the experiments.

9.1.2 Odor exposure

Odorant exposures of ACT or TMT was performed on C57BL/6J mice. Mice were habituated in a disposable paper container for 1 hour and exposed to an odor cassette for 1 hour. The starting concentrations of odorants used for stimulations comprise of 10 μl of tested odorant diluted with dW (v/v). Diluted odorants were spotted individually onto a 2cm x 2cm blotting paper and placed into a Uni-cassette (Sakura) for odor stimulation.

The mice stimulation environment was inside a fresh paper container with lid (International Paper) inside the fume hood.

9.2 Olfr923-CRE Transgenic Mouse

9.2.1 Targeting of the Olfr923 locus

A targeting vector expressing Cre under control of the Olfr923 locus was generated by BAC recombineering (Liu et al., 2003) in SW102 cells (Warming et al., 2005). Briefly, an IRES-Cre-frt-neomycin-frt cassette was introduced by homologous recombination into BAC clone bMQ186d17 (SystemBioSciences) containing 147 kb of mouse chromosome 9 immediately downstream of the TGA stop codon within the Olfr923 coding region. Next, the targeting vector containing the IRES-Cre-Neo flanked by homology arms was retrieved by gap repair from the BAC into plasmid pL253. The resulting targeting vector was linearized with NotI restriction endonuclease and purified by phenol:chloroform extraction and ethanol precipitation. Murine ES cell line was electroporated with a linearized targeting vector containing 7 kb of 5′ homology and 2 kb of 3′ homology to the endogenous Olfr923 locus (G4 mES Cells were acquired from Samuel Lunenfeld Research Institute Mount Sinai Hospital).

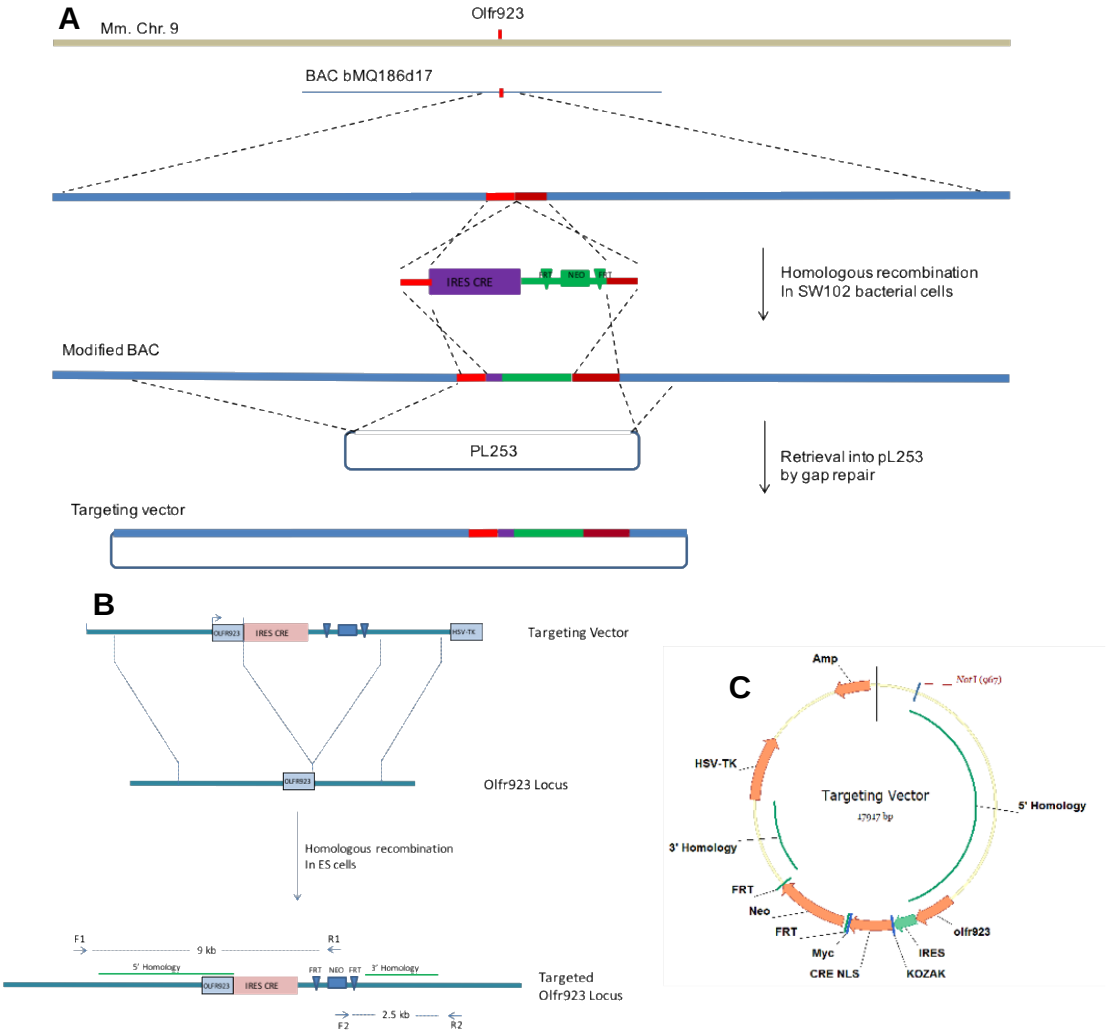

Figure 40: Homologous recombination of the Olfr923 targeting vector. (A) **Targeting vector construction through homologous recombination mediated BAC recombineering** (B**) Schematic of the Olfr-923-IRES-Cre targeting** (C) **Targeting vector map.**

9.2.2 PCR Screening of Targeted ES Cells

Allele-specific primers were used to screen ES cells from genomic DNA for homologous recombination across the 5′ long arm (F1: 5′-ACA GTG CAC AAA ACT AAC CCC-3′, R1: 5′-CTA CCG GTG GAT GTG GAA TGT GTG-3′) and 3′ short arm (F2: 5′-CTA TCG CCT TCT TGA CGA GTT CTT C-3′, R2: 5′-CAA CAG AAG ATG GAC TTC AGA AC-3′) by PCR.

9.2.3 ES Targeting

15 million G4 ES cells (Nagy et al., 1993) passage 13, were electroporated with 35 ◎g of targeting construct in a 4 mm gap cuvette using a Bio-Rad Genepulser II with Bio-Rad Capacitance Extender, set at 0.25 KV, 0.5 UF x 1000 for 2 pulses. Transfected cells were plated onto four 10 cm plates with neomycin resistant feeder cells. Targeted cells were fed selection medium with 250 ◎g/ml active G418 Geneticin at 24 hours after transfection, followed by the addition of 2 Um ganciclovir to the selection medium at 48 hours. Selection medium with G418/Ganc was changed once a day until clones were picked on day 7 after transfection. 142 clones were picked and expanded on 96 well plates. DNA was analyzed by PCR for homologous recombination on the 3′ end. 24/142 clones were identified as positive. 18 clones were expanded to the 6 well size plate, then cryopreserved in duplicate aliquots. Further analysis was done on genomic DNA prepared from these expanded clones by 3′ and 5′ Southern blot and PCR to confirm homologous recombination. Confirmed clones were injected into an ICR morulae host embryo (Nagy et al., 1993). Five clones produced a high percentage of agouti coat color chimeras which were used for breeding and expansion of the colony for this study.

9.2.4 Olfactory bulb glomerulus visualization

3-6 weeks old mice were habituated for 1 hour and then received either control or ACT stimulation by spotting 10◎L of freshly made 0.01% ACT onto blotting paper placed in an

odor cassette for 1 hour. Control conditions consisted of placing clean blotting paper into an odor cassette. The mice were sacrificed, and olfactory bulbs were collected into cold fixative solution consisting of 1X PBS, 4% paraformaldehyde for 2 hours with gentle shaking. Subsequently, olfactory bulbs were washed with cold 1X PBS three times and placed into cryoprotective solution consisting of 1X PBS, 30% sucrose, overnight with gentle shaking (Nutator S0500-VWR). The next day, sunken olfactory bulbs were collected and placed into Optimal Cutting Temperature (OCT) compound and flash frozen with liquid nitrogen. Olfactory bulbs were then sectioned at 20◎m sections using a cryostat. Detection of endogenous TdTomato fluorescence using 554/581 nm (excitation/emission) light was used to confirm glomerulus presence whilst sectioning. For fluorescent labeling of c-Fos-positive periglomerular cells, olfactory bulb sections were immersed in 1X PBS for 5 minutes at room temperature. Slides were then blocked with 4% donkey serum (Jackson Immuno 017-000-121) and 1% Triton X-100 for 1 hour at room temperature. Subsequently, slides were incubated with the primary anti c-Fos antibody (1:400, 9F6 Cell Signaling 2250) overnight at 4°C. The next day, slides were washed in 1X PBS three times at room temperature. Slides were then incubated with secondary donkey anti-rabbit Alexa 488 (1:200, Jackson Laboratories) diluted in 1X PBS, 5% skim milk for 1 hour. Slides were then washed in 1X PBS two times, stained with bisbenzimide (1:1000000) for 5 minutes, washed with 1X PBS, distilled water, and mounted with mowiol. Glomeruli with the greatest density of tdTomato expressing OSN terminals were imaged and periglomeruli cells in the immediate vicinity of the Olfr923 glomerulus were counted. C-Fos signal

intensities were quantified as follows. We obtained 200x magnification Z–stacked images with 2 μm intervals using the Zeiss Axiocam MRm and upright inverted fluorescent microscope. The filter sets used were as follows: Zeiss filter set #38 for Alexa 488, #43 for tdTomado, and #49 for bisbenzimide.

9.3 GloSensor Assay

The liquid-stimulation GloSensor assay was conducted as previously described with slight modification (Kida et al., 2018). Hana3A cells were plated on 96-well plates and placed into a 5% CO2 incubator overnight. 18–24 h after plating, cells were transfected with 80 ng/well of Olfr923-pCI plasmid, 5 ng/well of RTP1S and 10 ng/well of GloSensor plasmid (Promega) placed into a 5% CO2 incubator overnight. 18–24 h later, the medium was replaced with 50 μL of HBSS (Gibco) containing 10 mM HEPES and 1 mM Glucose (wash). This was followed by adding 30 μl of the HBSS containing GloSensor cAMP Reagent (Promega). Plates were kept in a dark place at room temperature for two hours to equilibrate the cells. ACT and heptanal was diluted individually in DMSO (Sigma-Aldrich) to 100 mM working stocks, and further diluted in the GloSensor buffer for dose-response experiments. 30 μl/well of diluted liquid odorants were added and immediately and the test plate was inserted in the plate reader. The luminescence in each well was measured at 90 s intervals for 6 cycles. All luminescence values were normalized by dividing by the value obtained from the wells transfected with the empty pCI vector at the same cycle.

9.4 Immunohistology and in situ hybridizations

Fluorescent in situ hybridization (FISH) and immunohistochemical staining were performed in reference to Jiang et al. (2015) with some modifications (Jiang et al., 2015). Briefly, 18-μm frozen sections of the mouse snout containing the olfactory epithelium were fixed in paraformaldehyde and pretreated. Digoxigenin-labeled (DIG) complementary RNA probes were hybridized to the tissue sections overnight at 58 °C. Unless specified, we used open reading frame of ORs for the RNA probes. We designed 3'UTR specific probe for the labeling of Olfr376 because of OR sequence similarity, and the primers used for cloning into pCI vector were as follows: AAACGCGTCAGTAATATTTTAA CACTGA (Forward) and AAGCGGCCGCCTGAGTGTACAGTTTTTGAG (Reverse). Following washes, the sections were incubated for 45 mins with a horseradish peroxidase (HRP)-conjugated antibody (Roche, 1:1000 in blocking solution) against DIG. Hybridization signals were labeled with a 10 min incubation of tyramide signal amplification (TSA) solution. For immunostaining, the FISH labeled sections were incubated with a polyclonal rabbit anti-phospho-S6 (244/247) (Thermo Fisher Scientific, 1:300 dilution in blocking solution) overnight at 4 °C. Following washes, a 45 min incubation with the donkey Cy3-conjugated anti-rabbit IgG (Jackson Immunologicals, 1:200) was used to visualize pS6 proteins. Olfactory epithelium images were taken using the Zeiss Axiocam MRm and upright inverted fluorescent microscope with ApoTome functionality at 200x magnification. The filter sets used were as follows: Zeiss filter set #38 for fluorescein, #43 for Cy3, and #49 for

bisbenzimide. ImageJ was used in the quantification of colocalization signals, where pS6 pixel intensity of DIG positive OSNs was subtracted from the average pixel pS6 intensity of no odor exposed OSNs labeled with the same OR probe. The resulting normalized intensities were quantified and compared using one-way ANOVA with Dunnett's test.

9.5 Next-generation sequencing

9.5.1 pS6-IP-Seq

Following odor stimulation, the mouse was killed, and the dissected olfactory epithelium was processed for RNA library in reference to the method described by Jiang et al. (2015) with some modifications (Jiang et al., 2015). Pieces of freshly dissected olfactory epithelium were homogenized and centrifuged. 6 μl of a monoclonal Phospho-S6 Ribosomal Protein (Ser240/244) (D68F8) XP Rabbit mAb (Cell Signaling Technologies) was added to the supernatant, and incubated with rotation for 1.5 hours at 4 °C. Protein A Dynabeads (Invitrogen) was added to the antibody mixture and incubated for another hour with rotation at 4 °C. After incubation and washing, the bead-captured RNA was eluted and purified with RNeasy Micro kit (Qiagen). 10 ng of starting RNA was used to make cDNA libraries with the SMART-Seq v4 kit (Clontech) with 11 cycles of PCR. cDNA was purified with AMPure XP beads (Beckman Coulter) and 0.5 ng was used to make cDNA libraries using the Nextera XT DNA Library Preparation Kit (Illumina).

Three weeks old wild-type male and female C57BL/6 mice were used. In phospho-S6 ribosomal protein immunoprecipitation (pS6-IP) experiments, littermates were used for all replicates (n=3). Mice were contained individually in paper buckets and habituated for

1 hour inside a fume hood. Mice were then presented a piece of filter paper kept in an uni-cassette soaked with either 10 μl of odorant (diluted with dW) or a plain piece of filter paper for an hour and we prepared experimental buffers on ice. We staggered the stimulation start time with about 20 minutes in between each mouse. When the 1-hour odorant stimulation was done, the mouse was euthanized according to the institutional protocol (CO2). The olfactory epithelium was dissected in 25 ml of buffer B (1x HBSS+CaCl+MgCl, 2.5 mM HEPES.KOH [pH 7.4], 100 μg/ml cycloheximide, 35 mM Glucose, phosphatase inhibitor cocktail (250 mM Sodium Fluoride, 50 mM Sodium Orthovanadate, 50 mM Sodium Pyrophosphate, 50 mM beta-Glycerophosphate). The olfactory epithelium was broken up into smaller pieces and resuspended in 1350 μl of buffer C (10 mM HEPES.KOH [pH 7.4], 150 mM KCl, 5 mM MgCl2, 100 nM calyculin A, 2 mM DTT, 100 μg/ml cycloheximide,100 U/ml RNasin, protease and phosphatase inhibitor cocktails). The mixture was then transferred to a glass homogenizer chilled on ice. All subsequent steps were performed in a 4°C cold room. The olfactory epithelium mixture was homogenized three times at 30 rpm, and then ten times at 40 rpm. The homogenate was transferred to a 1.5 ml LoBind tube and stored on ice. The above steps were repeated until all other odorant stimulated mice were processed. The homogenates were spun for 10 min at 2100 g. The supernatant was transferred to a new LoBind tube, and we added 90 μl of 10% NP40 and 90 μl of 1,2-diheptanoyl-sn-glycerol-3-phosphocholine (DHPC, 100 mg/0.69 ml). The supernatant was pipette mixed and centrifuged at max speed for 10 minutes before transferring to a new LoBind tube. 20 μl

of the supernatant was added to 350 μl of buffer RLT and stored at −80°C to keep as an input RNA. To each remaining supernatant, we added 1.3 μl cycloheximide (100 mg/ml), 27 μl phosphatase inhibitor cocktail and 6 μl pS6 antibody (Cell Signalling, D68F8). The supernatants were then incubated on a lab rotator (Labnet) for 1.5 hours for immunoprecipitation. 100 μl of magnetic beads were washed three times with buffer A (10 mM HEPES.KOH [pH 7.4], 150 mM KCl, 5 mM MgCl2, 1% NP40, 0.05% BSA) using the magnetic separation stand. During a fourth wash, 500 μl of the leftover buffer C was used. The supernatants were added individually to the washed magnetic beads and incubated on a lab rotator for 1 hour for pS6 antibody binding to the breads. The beads mixtures were moved from the rotator and the supernatant was removed. Target RNA should be bound to the magnetic beads. The beads were then gently washed with 700 μl of Solution D (10 mM HEPES.KOH [pH 7.4], 350 mM KCl, 5 mM MgCl2, 2 mM DTT, 1% NP40, 100 U/ml RNasin, and 100 μg/ml cycloheximide). During the fourth wash, samples were taken back to the lab bench on the magnetic separation stand. Solution D was removed, and the RNA was eluted with during a 5 min incubation with 350 μl of RLT buffer (Qiagen). The elute was aspirated into LoBind tubes and immediately frozen at -80°C. After we a full set of 12 RNA samples (e.g., control, odorant 1, odorant 2) in triplicates were collected, we performed RNA purification according to the RNeasy Micro Kit (QIAGEN) manual. RNA concentration in the samples were quantified using the Qubit Fluorometer. The cDNA library was made using the SMART-Seq® v4 Ultra® Low Input RNA Kit for Sequencing with 10.05 ng of starting purified RNA, and 11 cycles of

PCR (half-reaction). PCR products were purified with magnetic beads (Ampure) on a magnate plate, and cDNA concentrations were quantified using the Qubit Fluorometer. The Illumina DNA library was prepared using the Nextera XT DNA Library Preparation Kit accordingly and purified with magnetic beads, with an expected length ranging from 0.2 to 1.5 kb. 50 base sequencing was performed on the HiSeq 2500 System (Illumina), obtaining 15-38 million reads per sample. Sequence reads were mapped using STAR alignment (Dobin et al., 2013) against the entire transcriptome and newly annotated ORs (UTRs annotations included for all genes). Reads mapped onto 1088 intact OR genes (297 ORs with pseudogene labels removed) were used for the purpose identifying odorant activated OSNs based on differential expression analysis with edgeR (Anders and Huber, 2010; Robinson et al., 2010; McCarthy et al., 2012). ORs with FDR corrected p-value <0.05 and a positive fold-change were considered significantly enriched.

9.5.2 RNA-Seq from dorsal and ventral olfactory epithelium

After the dorsal and ventral olfactory epithelium were dissected, RNA was extracted using the TRIzol reagent (Invitrogen) followed by clean up with RNeasy Mini (Qiagen). 1000 ng of RNA were used for cDNA libraries using the SMART-Seq v4 kit (Clontech), with two cycles of PCR. cDNA was purified with AMPure XP beads (Beckman Coulter) and 0.5 ng was used to make cDNA libraries using the Nextera XT DNA Library Preparation Kit (Illumina). The sequenced reads were then mapped and analyzed using the same bioinformatics pipeline as described above for pS6-IP-Seq.

9.6 OR Mapping

9.6.1 OR gene definitions

Based on the Jiang et al. (2015) publication, mRNAs captured by pS6-IP were mapped based on the Mus musculus (house mouse) genome assembly GRCm38 (mm10) coding exons using Bowtie (Jiang et al., 2015). OR transcript definitions were re-annotated to include 5′ and 3′ UTRs with the coding sequence. This is based on Ibarra-Soria et al.'s work which included new annotations for 1248 mouse ORs (Ibarra-Soria et al., 2014). University of California Santa Cruz genome assembly mRNA sequences were used to visualize transcripts that mapped onto coding and non-coding parts of the exons for all genes (Kent et al., 2002). 58 ORs listed as coding exons in Ibarra-Soria's definition were replaced in the new UTR included OR definitions. Olfr151 was misannotated and corrected as Olfr160; 4 ORs which were not yet annotated were added from the refGene database (O'Leary et al., 2015). In total, we included the gene definitions of 1385 ORs (pseudogenes included) in our new pS6-IP-Seq pipeline.

9.6.2 OR sequence alignment

To analyze the Illumina sequencing read files, we created a customized GTF annotation file. BLAT v. 35 (Kent, 2002) which was used to align intact OR sequences to the mouse genome represented by the Mus_musculus.GRCm38.dna_sm.primary_assembly.fa.gz file from Ensembl release 96 (April 2019). A custom R script was used to remove hits that did not overlap with the coding region of the queried OR and format the results in GTF format. OR pseudogenes and non-OR genes were defined using the ensembl standard file Mus_musculus.GRCm38.96.gtf.gz file. Snakemake v3.5.5 (Köster and Rahmann, 2012)

was used to process read files through alignment and quantification. STAR v2.7.0d (Dobin et al., 2013) was used to generate a genome index using the Ensembl Mus musculus primary assembly genome sequence and custom GTF annotation file. Reads were aligned to this genome index using STAR with default options except for –quantMode TranscriptomeSAM which maps genome alignments to transcript coordinates. STAR output transcriptome SAM files were quantified using RSEM v1.3.1 (Li and Dewey, 2011) using default options to generate gene and transcript level counts for differential expression.

9.7 In silico modelling of Olfr923

9.7.1 Homology modelling

The protocol follows two previously published methods with an optimal alignment which fulfills constraints provided by more than 100 mutants from the literature (Charlier et al., 2013; Yu et al., 2015). Four experimental non-olfactory GPCR structures (1U19, 3ODU, 2YDV, and 2LNL) were selected as templates to build Olfr923 by homology modeling using Modeller (Eswar et al., 2006). The percentage of identity for the seven transmembrane domains of Olfr923 with respect to the four templates were as follows: 22.02% with Rhodospin (1U19), 13.68% with CxCR4 (3ODU), 19.87% with A2a (2YDV), and 25.00% with CxCR1 (2LNL). The N-terminal structure was omitted to avoid perturbing the modeling protocol. Five models were obtained and we kept the one that was consistent with several additional structural constraints (no large folded structure in

extra-cellular loops should be observed, all TMs and H8 folded as α-helices, a short α-helix structure between TM3 and TM4).

9.7.2 Molecular dynamics simulation

All systems were then embedded in a model membrane made up of POPC lipids solvated by TIP3P water molecules using Maestro (Schrödinger, 2013). The total system was made up of ~77,000 atoms. For all systems in this article, molecular dynamics simulations were performed with sander and pmemd.cuda modules of AMBER with the ff03 force-field for the protein the gaff.lipid force-field for the membrane, and the gaff force-field for the ligands (Case et al., 2014). Bonds involving hydrogen atom were constrained using SHAKE algorithm. Long-range electrostatics interactions were handled with the Particle Mesh Ewald (PME) method. The cutoff for non-bonded interactions was set to 8 Å. Temperature was maintained constant with a Langevin thermostat with a collision frequency of 2 ps-1. In addition, a weak coupling anisotropic algorithm with a relaxation time of 1 ps-1 was applied to keep a constant pressure. Snapshots were saved every 2 femtoseconds. The detailed workflow of the simulations was detailed in Figure 7-1C.

Appendix A

A.1 Detailed protocol for the updated pS6-IP-Seq

Materials

Materials	Brand	Cat. No.
5 lb. Chicken Bucket Container	International Paper	DFM85
Uni-Cassette	Sakura	4157-01
NP-40 (10%)	Roche	11332473001
BSA (10%)	Sigma	A2058
HBSS (1x) + CaCl + MgCl	Thermo Fisher	14025-092
HEPES.KOH (1 M)	Sigma	H3375
Cycloheximide (100 mg/ml)	Sigma	C7698
Glucose (45%)	Sigma	G8769
Calyculin A (50 μM, dissolved in DMSO)	Sigma	C5552
DTT (1 M, dissolved in dW)	Sigma	D9779-5G
Protease inhibitor cocktail	Roche	5892970001
1 M KCl	Mallinckrodt	6845-04
1 M MgCl2	Sigma	7786-30-3
1 M HEPES.KOH	Sigma	H3375
DHPC (1,2-diheptanoyl-sn-glycero-3-phosphocholine)	Avanti Polar Lipids	850306P
Recombinant RNasin® Ribonuclease Inhibitor	Promega	N2515
RNeasy Micro Kit	Qiagen	74004
RLT Buffer	Qiagen	1015750
Sodium Fluoride	Sigma	S7920
Sodium Orthovanadate	Sigma	S6508
beta-Glycerophosphate	Sigma	G5422
Agencourt AMPure XP	Beckman Coulter	A63880
Dynabeads® Protein A	Life Technologies	10002D
Qubit™ RNA HS Assay Kit	Invitrogen	Q32855
Qubit assay tubes	Invitrogen	Q32856
SMART-Seq® v4 Ultra® Low Input RNA Kit for Sequencing	Clontech	634891
Nextera XT DNA Library Preparation Kit (96 samples)	Illumina	15032354

Equipment

Item	Brand	Cat. No.
PCR tube 8-strips	Sarstedt	72.991.102
Professional trio thermocycler	Biometra	070-724
Glass homogenizer	Wheaton	358029
MagneSphere® Technology Magnetic Separation Stands	Promega	Z5342
DNA LoBind Tube	Eppendorf	22431021
Mikro 20 Centrifuge	Hettich	2004-01
Revolver Lab Rotator	Labnet	H5600
Filtered tips 1000 µl	Corning (Axygen)	320-01-151
Filtered tips 200 µl	Denville Scientific	P1122
Filtered tips 10 µl	Denville Scientific	P1096-FR
Filtered tips 20 µl	USA Scientific	1120-1810
Qubit® 2.0 Fluorometer	Invitrogen	Q32866

Part 1 - Odor Stimulation

1.1 Subjects

Wildtype male and female C57BL/6 mice are used in all experiments at around three weeks. In pS6-IP experiments, littermates are used for each replicate (n=3), and both males and females are used for a given condition. Data from both sexes are pooled.

1.2 Odor Exposure

Pick up three weeks old mice in the same litter from mouse facility and transfer them to individual paper containers with lids. Let them habituate for 60 minutes in a clean paper tub in a fume hood. The hood should be clean without any other volatile chemicals inside. When the habituation is over, transfer the mice to a fresh paper tub, add a Uni-Cassette containing a 2cm x 2cm filter paper with 10 µl of odorant (diluted with dW or an appropriate solvent) or without an odor (no-odor or solvent only control) for 60 minutes. Stagger the stimulation start time and leave about 15-20 minutes in between. Animal

procedures should be performed in accordance with appropriate institutional approvals and governmental ethics guidelines.

Part 2- Immunoprecipitation

2.1 Buffers

All buffers must be prepared on ice. During the habituation and odorant stimulation, prepare buffers A, B and C. Buffer D will be prepared later during the beads binding step. Wear clean gloves and use RNase-free reagents and equipment.

Solution A

Item Name	Amount (3 Mice)	Amount (4 Mice)
Stock AC (2x)	4500 µl	6000 µl
NP-40 (10%)	900 µl	1200 µl
BSA in dW (10%)	45 µl	60 µl
Distilled water	3555 µl	4740 µl

Solution B

Item Name	Amount (50 ml Vol)	Amount (25 ml Vol)
HBSS (1x) + CaCl + MgCl	48 ml	24 ml
HEPES.KOH (1M)	125 µl	62.5 µl
CHX in methanol (100 mg/ml)	50 µl	25 µl
Phosphatase inhibitor cocktail (50x)	1000 µl	500 µl
Glucose (45%)	700 µl	350 µl

Solution C

Item Name	Amount (3 Mice)	Amount (4 Mice)
Stock AC (2x)	3 ml	4 ml
Distilled water	1978 µl	2637 µl
Calyculin A in DMSO (50 µM)	12 µl	16 µl
DTT (1 M)	12 µl	16 µl
CHX in methanol (100 mg/ml)	6 µl	8 µl
Protease inhibitor cocktail in dW (7x)	857 µl	1143 µl
Phosphatase inhibitor cocktail (50x)	120 µl	160 µl
Recombinant RNasin® (40 U μl^{-1})	15 µl	20 µl

Solution D

Item Name	Amount (3 mice)	Amount (4 mice)
Stock D (2x)	4500 µl	6000 µl
NP-40 (10%)	900 µl	1200 µl
DTT	18 µl	24 µl
Recombinant RNasin® (40 U μl^{-1})	22.5 µl	30 µl
CHX in methanol (100 mg/ml)	9 µl	12 µl
Protease inhibitor cocktail in dW (7x)	180 µl	240 µl
Distilled water	3370 µl	4494 µl

The stock buffers can be made beforehand and stored at 4°C

Stock AC (2x)	**50 ml Stock**	**Final Concentration**
1 M KCl	15 ml	300 mM
1 M $MgCl_2$	0.5 ml	10 mM
1 M HEPES.KOH	1 ml	20 mM
Distilled water	33.5 ml	-
Stock D (2x)	**50 ml Stock**	**Final Concentration**
1 M KCl	35 ml	700 mM
1 M $MgCl_2$	0.5 ml	10 mM
1 M HEPES.KOH	1 ml	20 mM
Distilled water	13.5 ml	-

Phosphatase inhibitor cocktail (store as 2 ml aliquots)	
Sodium Fluoride	0.419 g
Sodium Orthovanadate	0.3678 g
Sodium Pyrophosphate	0.44388 g
beta-Glycerophosphate	0.43208 g
Distilled water	40 ml

2.2 Dissection

Keep buffers, thawed reagents and glass homogenizers in ice. Before starting, cut 5 mm off the front ends of 1 ml pipetteman tips for taking up larger tissue pieces, add 25 ml of solution B to a 25 cm Petri dish, and add 1350 µl of solution C to a 3.5 cm Petri dish. When the odorant stimulation time (1hr) is up, remove odorant cassette inside the fume hood and discard. Euthanize mouse according to the institutional protocol (e.g. CO_2). Clean the mouse by spraying with 70% ethanol, and lay it flat on its belly. Use a pair of scissors to cut off the upper jaw, and remove the skin on the head. Dab specimen with Kimwipes to dry the blood, and bring it under the dissection microscope. Remove the palette and upper front teeth from the jaw. Cut across the bottom side of the head from the posterior to anterior. Flip and cut across the sagittal structure and stop right before the nasal bone.

Switch to a pair of microdissection scissors and cut through the remaining bones. Carefully separate the skull into two halves.

2.3 Isolation of Olfactory Epithelium

Remove the brain by scooping from the posterior (back) of the head.
Cut around olfactory bub to loosen tissue connections, scoop the whole olfactory bub out. Cut around and below the curvature between olfactory bub and olfactory epithelium (dotted lines in Fig. 2) to loosen the basal bone/tissues. Remove the whole olfactory epithelium out of the basal bone, and collect additional dorsal olfactory epithelium pieces into solution B. Repeat steps 1-4 for the other halve of the skull. Gently, wash the tissue pieces in solution B, then transfer them to buffer C inside a 35 mm Petri dish. Break up the tissue into small pieces and remove the bones. Finally, suck up the olfactory epithelium pieces with the 1 ml pipette into a chilled glass homogenizer tube, and then bring to the cold room on ice.

All subsequent steps and equipment are in the 4°C cold-room unless otherwise specified.

2.4 Tissue homogenization

Slide glass grinding vessel containing tissue solution into a piston-type pestle with stainless steel shaft, slowly press the glass vessel on to the pestle with a twisting motion. The pestle is raised and lowered while twisting to help expose the sample to a proper grinding. This helps create shearing forces to break up the tissue. This action is repeated three times at 30 rpm and ~ten times at 40 rpm. The homogenate is then poured into a clean 1.5ml LoBind tube and stored on ice. Rinse out the pestle tissue grinder assemblies and bring another clean glass grinding vessel to the dissection room for tissue collection. Repeat the above steps until all necessary mice homogenates are collected for processing. Balance the homogenates containing LoBind tubes and spin them for 10 minutes at 4600 rpm in a centrifuge chilled at 4°. In the meantime, clean up the dissection room accordingly

5.5 Immunoprecipitation

Transfer the low-speed mice olfactory epithelium supernatant into new LoBind tubes. Add 90 µl of 10% NP40 and 90 µl of 1,2-diheptanoyl-sn-glycerol-3-phosphocholine (DHPC, 100 mg/0.69 ml, 300 mM in dW), pipette up and down to mix the solution, and centrifuge at max speed for 10 minutes. Transfer the spun supernatant to another new LoBind tube. Take 20 µl to another LoBind tube containing 350 µl of buffer RLT, and store at −80°C to keep a record of your input RNA. To each remaining supernatant, add 1.3 µl cycloheximide (100 mg/ml), 27 µl phosphatase inhibitor cocktail, 6 µl monoclonal pS6 antibody. Pipette up and down to mix the solution, gently remove any bubbles. Incubate samples on lab rotator for 1 hour 30 minutes to allow for immunoprecipitations.

2.6 Beads Binding

Shake up the beads well and add 100 µl to a clean LoBind tube. Place LoBind tubes onto a magnetic separation stand, wait for beads to be captured by the magnet and carefully remove the soaking buffer. Remove the LoBind tubes from the magnetic stand, and add 900 µl Solution A. Pipette up and down to mix, capture the washed beads and carefully remove buffer A. Repeat wash twice. During the fourth wash, use 500 µl of leftover buffer C instead. Add homogenate that was incubating on lab rotator to freshly washed beads. Pipette up and down to mix, carefully remove bubbles. Incubate samples on lab rotator for 1 hour to allow for beads binding to pS6 antibody.

2.7 Wash and Elution

Bring all the pipettes and filtered tips out from the cold room to the lab bench. On ice, make solution D. When the 1 hour incubation is complete, remove the beads solution from rotator and place onto magnetic separation stand. Carefully remove the supernatant and freeze it at -80 °C. Target RNA should be bound to the magnetic beads. Gently wash magnetic beads with 700 µl Solution D four times. During the fourth wash, place LoBind tubes onto the magnetic separation stand and bring to the lab bench at room temperature. Carefully remove the remaining solution D and incubate beads in 350 µl RLT solution on a clean tube rack for 5 minutes. Pipette out the RLT buffer containing target RNA into LoBind tubes and freeze at -80°C. Freeze the remaining tubes containing Dynabeads as future references. After you have acquired a full set of RNA samples (e.g. Control, odorant 1, odorant 2) in at least triplicates, perform RNA purification according to the RNeasy Micro Kit (QIAGEN) manual.

2.8 RNA Extraction

Clean the pipettes and centrifuge, and change bench covers. Get the RLT-RNA frozen samples from -80°C freezer and thaw samples on ice. Make 5 ml of fresh 70% and 80% ethanol diluted in distilled water. Add 1 volume (350 µl) of 70% ethanol to the lysate, and mix well by pipetting. Transfer the sample (700 µl), with any precipitate, to an RNeasy MinElute spin column in a 2 ml collection tube (supplied). Close the lid and centrifuge for 30 s at 8000 x g (rcf). Discard the flow-through, dry column on Kimwipes®. Add 350 µl Buffer RW1 to the RNeasy MinElute spin column. Close the lid. Centrifuge for 30 s at 8000 x g. Discard the flow-through. Add DNase we incubation mix (80 µl/sample) directly to the RNeasy MinElute spin column membrane. Place on the benchtop (20–30°C) for 15 minutes. Add 350 µl Buffer RW1 to the RNeasy MinElute spin column. Close the lid, and centrifuge for 15 s at ≥ 8000 x g. Discard the collection tube. Place the RNeasy MinElute spin column into new 2 ml collection tubes (supplied). Add 500 µl Buffer RPE to the spin column. Close the lid, and centrifuge for 15 s at ≥8000 x g. Discard the flow-through. Add 500 µl of 80% ethanol to the RNeasy MinElute spin column. Close the lid, and centrifuge for 2 minutes at ≥8000x g. Discard the collection tube. Place the RNeasy MinElute spin column in new 2 ml numbered collection tubes (supplied). Open the lid of the spin column, with lids along the direction of spin, and centrifuge at full speed for 5 minutes to dry the

membrane. Discard the flow-through and collection tube. Place the RNeasy MinElute spin column in a new 1.5 ml collection tube (supplied). Add 14 µl RNase-free water directly to the center of the spin column membrane. Close the lid gently, wait 2 minutes, then centrifuge for 2.5 minutes (Eppendorf soft start) at full speed to elute the RNA. Store RNA immediately on ice to prevent degradation and label accordingly for long-term storage at -80°C.

	Standard/Sample	**Qubit Master Mix**
Standard 1	10 µl	190 µl (reading ~0 ng/mL)
Standard 2	10 µl	190 µl (reading ~500 ng/mL)
Sample	1 µl	199 µl (reading > *15 ng/mL for Nextera)

Read RNA concentration in the samples using the Qubit Fluorometer. Actual RNA concentration in ng/µl] = ng/mL reading ÷ 1000 x 200 = ng/mL reading ÷ 5

Part 3 - cDNA Preparation

Instructions modified based on SMART-Seq® v4 Ultra® Low Input RNA Kit for Sequencing

3.1 First-Strand cDNA Synthesis

1. Thaw all the reagents needed for first-strand cDNA synthesis (except the enzyme). Keep the 5X Ultra Low First-Strand Buffer at room temperature. Mix everything well before use. Thaw SMART-Seq v4 Oligonucleotide (48 µM). Switch to a set of filtered tips reserved for RNA work.

2. Start the 72°C program. Pause.
Get a cooling block from the cold.

3. Prepare a stock solution of 10X Reaction Buffer by mixing the 10X Lysis Buffer with the RNase Inhibitor as indicated below (scale-up as needed):

10X Reaction Buffer	8 samples	14 samples
10X Lysis Buffer	9.5 µl	17 µl
RNase Inhibitor	0.5 µl	0.9 µl

Mix briefly, then spin down. NOTE: Lysis Buffer contains a detergent; it is critical to avoid bubbles when mixing.

3.1 Make 50 µl of RNase Inhibitor dW (1 µl RNase Inhibitor in 50 µl of nuclease-free water).

3.2 Dilute (use RNAse free dW) 4 µl of RNA samples to 3 ng/µl final concentration.

From 1 µg/µl control RNA, make 2 ng/µl control RNA solution via serial dilutions, as indicated below.

0.5 µl 1 µg/µl Control RNA
24.5 µl RNase Inhibitor dW to make 20 ng/µl

0.5 µl Diluted (+) Control RNA (20 ng/µl)
4.5 µl RNase Inhibitor dW to make 2 ng/µl .

Discard 2 ng/µl solution after use. 20 ng/µl RNA can be stored for further dilutions.

4. Prepare a master mix with the following:

Master Mix	1 sample	8 samples	14 samples
RNAse-free dW	1.4 µl	11.2 µl	19.6 µl
10X Reaction Buffer	0.5 µl	4 µl	7 µl
3′ SMART-Seq CDS Primer II A (12 µM)	1 µl	8 µl	14 µl

5. Add 2.9 µl of master mix, followed by 3.35 µl of 3 ng/µl diluted RNA into 0.2-ml RNase-free PCR tubes. Mix well by gently tapping and then spin the tube(s) briefly to collect the contents at the bottom of the tube.

6. Incubate the tubes at 72°C in a preheated, hot-lid thermal cycler for 3 minutes.

NOTE: Get SMART-Seq v4 Oligonucleotide (48 µM) and SMARTScribe Reverse Transcriptase from -20 ºC freezer.

7. Immediately after the 3-minute incubation at 72°C, place the samples on ice for 2 minutes, then close the tube caps.

8. Preheat the thermal cycler to 42°C.
NOTE: Prepare your Master Mix quickly while your tubes are on ice. The enzyme will be added just before use.

9. Prepare enough Master Mix for all the reactions by combining the following reagents in the order shown at room temperature:

Master Mix	1x	8x	14x

5X Ultra Low First-Strand Buffer	2 µl	16 µl	28 µl
SMART-Seq v4 Oligonucleotide (48 µM)	0.5 µl	4 µl	7 µl
RNase Inhibitor (40 U/µl)	0.25 µl	2 µl	3.5 µl
SMARTScribe Reverse Transcriptase	1 µl	8 µl	14 µl

* Gently mix the Master Mix well and spin the tube briefly.

10. Add 3.75 µl of the Master Mix to each reaction tube. Mix the contents of the tubes by gently pipetting, and spin them briefly to collect the contents at the bottom of the tubes.

12. Place the tubes in a thermal cycler preheated to 42 °C, and with a heated lid. Run the following program:

42°C 90 minutes
70°C 10 minutes
4°C forever

The tubes can be stored at 4°C overnight or at -20°C, but preferentially proceed to the next step (PCR) soon.

3.2 cDNA Amplification

1. Thaw all the reagents needed for PCR (except the enzyme) on ice. Gently mix each reagent tube and spin down briefly. Switch to a set of filtered tips reserved for next-generation sequencing.

2. Prepare enough PCR Master Mix for samples and an additional reaction. Thaw the Elution Buffer early, because it comes in a large volume and takes time.
NOTE: Remove the SeqAmp DNA polymerase from the freezer, gently mix the tube without vortexing, and add to the Master Mix just before use.

	1X	8X	14x
2X SeqAmp PCR Buffer	12.5 µl	100 µl	175 µl
Nuclease-Free water	1.5 µl	12 µl	21 µl
PCR Primer II A (12 µM)	0.5 µl	4 µl	7 µl
SeqAmp DNA Polymerase	0.5 µl	4 µl	7 µl

* Gently mix the Master Mix well and spin the tube briefly.

3. Aliquot 15 µl of PCR Master Mix to new strip tubes. Add 10 µl of first-strand cDNA product from part A. Mix well with multi-channel pipette (avoid bubbles), and briefly spin to collect the contents at the bottom of the tube(s).

4. Place the tube(s) in a preheated thermal cycler with a heated lid and run the following program:

95 °C 1 minute
98 °C 10 sec
65 °C 30 sec
68 °C 3 minutes

For 11 cycles (10 ng starting RNA)

72 °C 10 minutes
4 °C forever

5. Use 5 µl of the PCR product to run a gel for at 100 V for around 30 mins. Amplified cDNAs should show smear signals with molecular size ranging from ~0.5 to 0.3 kb.

6. Transfer PCR (20 µl) products to fresh strip-tubes. Samples can be stored at 4°C overnight or at -20°C for a longer term.

3.3 Purification of Amplified cDNA

Before use, bring AMPure XP beads to room temperature for at least 30 minutes and mix well to disperse. You will need a magnetic separation device for 0.2 ml tubes. Thaw Elution Buffer, and check that > 30 µl is available for each sample. Freshly prepare 7 ml of 80% ethanol in a 15 ml tube.

1. Add 0.4 µl of 10X Lysis Buffer to each PCR product from part B.

2. Vortex AMPure XP beads until evenly mixed, then add 25 µl of AMPure XP beads to each sample.

3. Mix thoroughly by vortexing or pipetting the entire volume up and down at least 10 times. NOTE: The beads are viscous; pipette the entire volume.

4. Incubate at room temperature for 8 minutes to let the cDNA bind to the beads.

5. Briefly, spin the samples to collect the liquid from the side of the tube. Place the samples on the magnetic separation device (press-in) for ~5 minutes or longer, until the liquid appears completely clear.

6. While the samples are on the magnetic separation device, remove the supernatant and discard.

7. On the magnetic stand, wash the beads with freshly prepared 80% ethanol as follows:
Add 190 µl of 80% ethanol to each sample well, then put caps on.
Incubate the strip-tubes on the magnetic stand for 30 seconds.
Carefully remove the ethanol wash.

8. Perform a second ethanol.

9. Briefly, spin the samples to collect the liquid from the side of the tube. Place the samples on the magnetic separation device for 30 seconds, then remove all the remaining ethanol with a p10 pipette.

10. On the magnetic stand, place the samples at room temperature for approximately 2 – 2.5 minutes until the pellet is no longer shiny, but before a crack appears. NOTE: Be sure to dry the pellet only until it is just dry (matte with no shine). If you under-dry or over-dry the pellet, it will reduce your amplified cDNA recovery rate and ultimately your yield.

11. Once the beads are dry, add 27-30 µl of Elution Buffer to cover the bead pellet. Remove the samples from the magnetic separation device and mix thoroughly to resuspend the beads.

12. Incubate at room temperature for 2 minutes to rehydrate.

13. Briefly spin the samples to collect the liquid from the side of the tube or sample well. Place the samples back on the magnetic separation device for 1 minute or longer, until the solution is completely clear.

14. Transfer 28 µl of clear supernatant containing purified cDNA from each well to LoBind tube. Quantify DNA using Qubit Fluorometer. Yield needs to be higher than 1 ng/ml (0.2 ng/µl) and DNA can be stored at –20°C.

Part 4 – Illumina DNA Library Preparation

Instructions modified based on Nextera XT DNA Library Preparation Kit (96 samples)

Tagmentation of Input DNA

1. Thaw ATM (Amplicon Tagment Mix) on ice. Thaw TD (Tagment DNA Buffer), NT-6x (Neutralize Tagment Buffer), and RSB-6x (Resuspension Buffer) at room temperature.

After thawing, mix reagents by gently inverting the tubes 3–5 times, followed by a brief spin.

2. Thaw NPM (Nextera PCR Master Mix) and the index primers on ice.

3. Make 0.2 ng/µl input DNA with RSB (Illumina) or Elution Buffer (Clontech).

4. Visually inspect NT to make sure that there is no precipitate. If there is precipitate, vortex until all particulates are resuspended.

5. Preheat a thermal cycler to 55°C and pause the block.

Tagmentation
NOTE: You do not need to assemble the reaction on ice.

Place new 0.2 ml PCR strip-tubes, now referred as NTA (Nextera XT Tagment Amplicon).

Add 5 µl TD Buffer to each well.

Add 2.5 µl input DNA diluted at 0.2 ng/µl (0.5 ng total) to each sample well and mix.

Add 2.5 µl ATM to the wells containing input DNA and TD Buffer.

Using a multichannel pipette, gently pipette up and down 5 times to mix.

6. Centrifuge briefly and place the NTA tubes in a thermal cycler and run as following indicated. NOTE: Make sure that the thermal cycler lid is heated during the incubation.

55°C 5 minutes
10°C hold

7. When the sample reaches 10 °C, proceed immediately to Neutralize NTA at room temperature by adding 2.5 µl NT Buffer to each well.

9. Using a multichannel pipette, gently pipette up and down 5 times to mix.

10. Centrifuge briefly and place the NTA tubes at room temperature for 5 minutes.

4.2 PCR Amplification

Make sure that the correct index 1 (i7) (N7XX) and identical index 2 (i5) (S5XX) primers have been selected and updated into your laboratory notebook.

1. Place the NTA strip-tubes.

2. Add 7.5 µl NPM to each of the NTA tubes.

3. Add 2.5 µl index 1 **(i7)** primers (unique-orange caps) to each NTA tube.

4. Add 2.5 µl index 2 **(i5)** primers (same-white caps) to each NTA tube.

5. Using a multichannel pipette (10 µl), gently pipette up and down 5 times to mix.

6. Centrifuge briefly and perform PCR using the following program on a thermal cycler:

72 °C for 3 minutes
95 °C for 30 seconds
12 cycles of:
— 95 °C for 10 seconds
— 55 °C for 30 seconds
— 72 °C for 30 seconds
72 °C for 5 minutes
Hold at 4 °C

7. transfer 24 µl of PCR product into new PCR tubes, use 1 µl to run a gel at ~100 V for 30 minutes.

4.3 PCR Product Clean-Up

1. Thaw RSB, check if > 30 µl is available for each sample. Freshly prepare 7 ml of 80% ethanol in 15 ml tube.

2. Vortex the AMPure XP beads for 30 seconds to make sure that the beads are evenly dispersed.

3. Add 15 µl AMPure XP beads to each tube containing 25 µl PCR product.

4. Gently pipette mix up and down ten times and incubate at room temperature without shaking for 5-8 minutes.

5. Spin briefly and place the tubes on a magnetic stand for 2 minutes. Check that supernatant is completely clear before proceeding.

6. Remove and discard the supernatant carefully, put caps back on.

7. On the magnetic stand, wash the beads with freshly prepared 80% ethanol as follows:
Add 190 µl 80% ethanol to each sample well, then put caps on.
Incubate the strip-tubes on the magnetic stand for 30 seconds.
Carefully discard the ethanol wash.

8. Perform a second ethanol wash.

9. Briefly spin the samples to collect the liquid from the side of the tube or sample well. Place the samples on the magnetic separation device for 30 seconds, then remove all the remaining ethanol with a p10 pipette.

10. On the magnetic stand, place the samples at room temperature for approximately 2 – 2.5 minutes until the pellet is no longer shiny, but before a crack appears. NOTE: Be sure to dry the pellet only until it is just dry (matte with no shine). If you under-dry or over-dry the pellet, it will reduce your amplified cDNA recovery rate and ultimately your yield.

11. Immediately, remove the tubes from the magnetic stand to regular rack. Using a multichannel pipette, add 27-30 µl RSB to each tube. Remove the samples from the magnetic separation device and mix thoroughly to resuspend the beads and incubate at room temperature for 2-5 minutes.

12. Briefly spin the samples to collect the liquid from the side of the tube or sample well. Place the samples back on the magnetic separation device for 1 minute or longer, until the solution is completely clear.

13. Carefully transfer 28 µl (take 20 µl, then 8 µl) of the supernatant to fresh LoBind tubes.

14. Take1 µl of supernatant and quantify DNA using Qubit Fluorometer. Yield should be ~15 ng/ml.

15. Take 1 µl of the Illumina library and run a gel at 100 V for 30 minutes. The library can be stored at -20 ºC.

16. Submit the library to a sequencing core. Samples can be processed on the HiSeq 2500 or 4000 platform.

Part 5 – mRNA Profiling

We obtain high-throughput sequencing reads as FASTA files. Kallisto is then used to quantify abundances of transcripts via pseudoalignment of reads to target genes (Bray et al., 2016). Refer to https://pachterlab.github.io/kallisto/manual for software installation

and usage instructions. The user can build an index from a FASTA formatted file of target mRNA sequences containing ORs and other annotated genes.

After the mapping, TSV files are generated for each mouse, and the est_counts are used for differential expression analysis. Refer to https://rawgit.com/Yue-Jiang/achems/master/rnaseq_demo.html for a detailed guide using edgeR to identify over-represented mRNA transcripts in odorant stimulated samples (Robinson et al., 2010). The ORs with a positive fold-change and FDR corrected p-value < 0.05 are considered to be significantly enriched and activated by a given odor.

A.2 Detailed protocol for immunohistology and *in situ* hybridization

Materials

Distilled water (Gibco, cat. no. 15230-147)
PCR buffer (10x, 15 mM MgCl2) (Qiagen, cat. no. 203205)
PCR nucleotide mix (10 mM) (Roche, cat. no. 04 638 956 001)
PCR primers (5 μM) (Integrated DNA Technologies)
HotStarTaq DNA polymerase (5 U μl−1) (Qiagen, cat. no. 203205)
OR Plasmid DNA (10 ng μl−1)
MinElute PCR purification kit (Qiagen, cat. no. 28006)
Agarose (Promega, cat. no. P1181)
DTT (100 mM) (Promega, cat. no. P117A)
DIG RNA labelling mix (10x) (Roche, cat. no. 11277073910)
Anti-Digoxigenin-POD (Roche, cat. no. 11207733910)
Recombinant RNasin® (40 U μl−1) (Promega, cat. no. N2515)
MOWIOL® 4-88 reagent (Calbiochem, cat. no. 475904)
RNase Inhibitor (Qiagen, cat. no. 129916)
T3 RNA polymerase (17 U μl−1) (Promega, cat. no. P208C)
Agarose (Denville, cat. no. CA3510-8)
TissueTek O.C.T. compound (Sakura, cat. no. 4583)
Paraformaldehyde (J.T.Baker, cat. no. S89807)
Kroger Instant Nonfat Dry Milk (Kroger)
Deionized formamide (Millipore Sigma, cat. no. 4610-100ML)
Phospho-S6 Antibody (Thermo Fisher, cat. no. 44-923G)
Micro Bio-Spin® Columns with Bio-Gel® P-30 (Bio-rad, cat. no. 7326223)
Bisbenzimide (Sigma-Aldrich, cat. no. B2883-100MG)
Triton™ X-100 solution (American Bioanalytical, cat. no. AB02025)
Bovine Albumin Fraction V (7.5% BSA solution) (Life Technologies, cat. no. 15260037)
UltraPure™ Formamide (Invitrogen, cat. no. 15515-026)
OmniPur® Formamide, Deionized (EMD Millipore, cat. no. 4610-100ML)
SSC buffer, 20x solution (America Bioanalytical, cat. no. AB13156)
Ribonucleic acid from baker's yeast (10 mg/ml) (Sigma-Aldrich, cat. no. R6750)
DL-Dithiothreitol (dissolve in DTT distilled water to 1M) (Sigma-Aldrich, cat. no. D9779-5G)
Heparin sodium salt from porcine intestinal mucosa (30000 U/ml) (Sigma-Aldrich, cat. no. H3149-100KU)
Deoxyribonucleic acid from herring sperm (Sigma-Aldrich, cat. no. D7290-1ML)
Blocking reagent (Roche, cat. no. 11096176001)
Maleic acid (Sigma-Aldrich, cat. no. M0375-500G)

Sodium Hydroxide, Pellet (Macron Chemicals, cat. no. MAL-7708-10)

Equipment

5 lb. Paper bucket container (International Paper, cat. no. DFM85)
500 mL Bottle Top Filter (Nalgene, cat. no. 291-4520)
Superfrost™ plus microscope slides (Fisherbrand, cat. no. 48311703)
100-place slide box (Port City Diagnostics, Inc., cat. no. M1000BOX)
Mini-mouse microfuge (Denville, cat. no. C1301)
PCR tube 8-strips (Sarstedt, cat. no. 72.991.102)
Professional trio thermocycler (Biometra, cat. no. 070-724)
MinElute PCR purification kit (Qiagen, cat. no. 28004)
Staining dish (Tissue-Tek, cat. no. 4456)
Mini stirrer (VWR, cat. no. 12620-998)
Pipet-aid (Drummond, cat. no. DP-100)
Blotting pad (VWR, cat. no. 28297-996)
60x15mm petri-dish (VWR, cat. no. 351007)
100x15mm petri-dish (VWR, cat. no. 25384-070)
Tupperware (Rubbermaid, cat. no. Walmart 001409703)
Labnet proBlot Hybridization Oven L6 (Labnet, cat. no. Labnet 9050577)
Dry block heater (VWR, cat. no. 13259-030)
Water bath (Fried Electric, cat. no. TEP-1)
Glass coverslip (VWR, cat. no. 48311-703)
Stereomicroscope stemi 305 (Zeiss, cat. no. 435425-9000-000)
Glass homogenizer (Wheaton, cat. no. 358029)
Uni-Cassette (Sakura, cat. no. 4157-01)
Zeiss Axioskop 2 microscope
Vertical Retiga 2000R camera
Cryostat (Leica, cat. no. CM1850)
3100 Genetic Analyzer (Applied Biosystems, cat. no. 4359571)

Animals and Odor Exposure

Animal handling and tissue collection procedures in this paper were approved by Institutional Animal Care and Use Committee of Duke University. Both wild-type male and female 21-day-old ±1 C57BL/6 mice were used for staining. Data from both sexes were pooled in the statistical analysis. Group housed C57BL/6 mice were transported individually inside paper containers to the lab and habituated for 1 hour inside the fume hood (cleaned with 70% ethanol before use). After habituation was over, to a piece of 2cm x 2cm filter paper, we add either 10 µl of odorant diluted with dW (stimulated condition) or nothing (control condition). The filter paper was then contained inside an uni-cassette. The odorant cassette was then placed inside a new paper container, and a mouse was

added for a 1-hour odorant stimulation. If more than one mouse were to be stimulated, the odorant exposure was staggered with 10-minute intervals.

Tissue Section

Control or odorant exposed mice were sacrificed, and snouts were dissected and fixed in O.C.T. compound contained in 2 cm2 aluminum foil cubes. 18 μm frozen sections of the olfactory epithelium were cryosectioned and collected on Superfrost™ plus microscope slides and stored in a 100-place slide box for long-term storage in the 80 °C freezer. Around 6 serial tissues were collected on a glass slide per mice, with 20 slides in total. We typically combine the tissues from two mice onto two separate rows in single slide (control mice & 0.1% odorant mice) or (0.01% odorant mice & 1% odorant mice).

PCR amplification of ORs

Prepare enough master mix for all the reactions by combining the reagents in order shown: For 1 sample, add 6 μl of distilled water, 1 μl of PCR Buffer (10x, 15 mM MgCl2), 1 μl of forward PCR primer (5 μM, pCI5'A primer – CTC CAC AGG TGT CCA CTC), 1 μl of reverse PCR primer (5 μM, T3pCI3' primer –GAA ATT AAC CCT CAC TAA AGG CAC TGC ATT CTA GTT GTGG), 0.05 μl of HotStarTaq DNA polymerase (5 U μl−1). We adjusted the volumes accordingly to our samples number. The master mix was mixed via pipetting, and 10 μl of the mix was added into individual PCR tubes, followed by 1 μl of Plasmid DNA (10 ng μl−1). Based on the OR(s) of interest cloned into pCI vectors (Promega), plasmids were verified via Sanger's sequencing.

The reaction was incubated in a thermal cycler with a heated lid, as described below. The PCR products were examined by running 1 μl of purified DNA to 5 μl of loading dye on a 1.1% agarose gel.

Cycle	Denature	Anneal	Extend	Hold
1	95 °C, 15 min	-	-	-
2-26	95 °C, 15 s	55 °C, 15 s	72°C, 1 min	-
27	-	72°C, 5 min	-	
28	-	-	4 °C	

PCR purification

MinElute columns were placed inside 2 ml collection tubes. 200 μl of Buffer PB was then added to each 10 μl PCR reaction and added to individual columns. The columns were centrifuged at full speed for 30 s and the flow-through discarded. Another 750 μl of Buffer PE was added to the column and centrifuged for 30 s, flow-through was discarded and columns were centrifuged for another 2 min. Each column was then placed into a clean 1.5 ml microcentrifuge tube and 10 μl Buffer EB was added to elute DNA by centrifuging for 2 min at full speed. The purified PCR products were examined by running 1 μl of purified DNA to 5 μl of loading dye on a 1.1% agarose gel.

Reverse transcription

We prepared the RT mix for all reactions by combining the reagents in the order show: For each sample, add 4 µl of distilled water, 2 µl Transcription optimized buffer (5x), 1 µl DTT (100 mM), 1 µl DIG RNA labelling mix (10x), 0.25 µl Recombinant RNasin® (40 U µl−1), 0.25 µl Qiagen RNase Inhibitor, 0.5 µl T3 RNA polymerase (17 U µl−1). We adjusted the volumes accordingly to our samples number. The master mix was mixed via pipetting, and 9 µl of the mix was added into individual PCR tubes, followed by 1 µl of purified OR PCR product. The tubes were briefly spun down to collect any liquid at the bottom. The RT reaction was incubated at 37 °C for 120 min, 4 °C hold in a thermocycler with a heated lid. The RNA probes could be stored after this step at −20 °C (wrapped in aluminum foil) for a few days.

Alkaline hydrolysis

An alkaline buffer was made by mixing 24µl of 1M NaHCO3 and 36µl of 1M Na2CO3 with 240 µl of distilled water. 25 µl of the alkaline buffer was added to individual RNA probes inside the PCR tubes from the step above and pipette mixed. The samples were briefly spun in a microfuge and incubated at 60 °C for 15 min, 4 °C hold in a thermocycler with a heated lid.

RNA probe purification

The Micro Bio-Gel® P-30 columns were inverted a few times sharply and tapped gently to let any gel settle. The tips were then snapped off, and the columns were placed into 2 ml collection tubes. The top caps were then removed to allow the excess packing buffer to drain by gravity and the flow-through was discarded. We then centrifuge the columns at 3400 rpm for 2 mins to drain the remaining packing buffer. The columns were placed into new 1.5 ml microcentrifuge tubes. 35 µl of RNA probe sample was carefully applied to the center of the column and centrifuged at 3400 rpm for 4 mins. To the purified probe, we added 35µl of deionized formamide. Finally, we check the expected size of the probes (around 100 bp) by running 5 µl of purified probes with 1 µl of loading dye on a 1.1% agarose gel. The RNA probes were stored after this step permanently at −80 °C.

Immunohistochemistry and in situ hybridizations

Buffers

Maleic Acid 5% Blocking Solution

To 440 ml of 1X Maleic Acid Buffer (0.1M Maleic Acid, 0.15M NaCl, adjust to pH7.5 with NaOH pellets), we added 22 g of blocking reagent and autoclaved before use.

Hybridization Buffer: 25 ml OmniPur® Formamide, 12.5 ml 20x SSC solution, 1.5 ml RNA from baker's yeast (10 mg/ml), 0.5 ml DTT (1M), 10 ml distilled water, 0.5 ml Heparin (30000U/ml), 0.5 ml DNA from herring sperm (10mg/ml). Can store buffer in 50 ml tube at − 20 °C for up to 1 year.

20x SSC buffer: 350.8 g NaCl, 176.4 g Sodium citrate, top up to 4 L of autoclaved deionized water.

20x PBS buffer: 640 g NaCl, 92 g Na2HPO4, 16 g KCl, 16 g KH2PO4, top up to 4 L of autoclaved deionized water.

Fresh paraformaldehyde (PFA) (4%, wt/vol)

To avoid RNase contamination that may degrade the RNA probe we wore clean gloves and used RNase-free reagents and equipment. To a glass beaker reserved for dissolving RNase-free PFA, we added 300 ml of autoclaved deionized water. In the chemical hood, we carefully weighed out 16g of powdered PFA and added it to the glass beaker. 1 ml of 10 N NaOH was also added to raise the PH and dissolve PFA faster. 17 ml of 20x PBS was also added to obtain a final NaCl concentration of 150 mM. The PFA beaker was covered with aluminum foil to reduce evaporation and stirred on low speed for at least an hour. After all the PFA dissolves, the solution became transparent. The pH was adjusted to between pH 7-8 with about 1 ml of 10 N HCl. HCl was slowly added dropwise towards the end to avoid over adjusting. The volume of the final solution was topped up to 400 ml with deionized water, and finally, vacuum filtered into a clean glass bottle.

Slide holders & humidified hybridization chamber

We placed 2 rails across a 25 cm petri-dish and added a small piece of blotting pad on top. The blotting pad was soaked with premade formamide wash buffer (50 ml of 20x SSC, 50 ml of autoclaved deionized water and 100 ml of formamide). Also, we prepared a humidified hybridization chamber using a clean Tupperware and soaked another blotting-pad with some formamide wash buffer placed on the bottom.

Sections pretreatment

olfactory epithelium glass slides were taken from the -80°C freezer, gently dried with a hairdryer and allowed to dry briefly at room temperature. The slides were then into a staining dish, and tissue sections were fixed by immersing fully in freshly made (< 1-day old) 4% PFA for 15 min. The slides were washed inside a clean staining dish containing 1x PBS for 5 min, repeat this step once. While waiting, in a glass beaker, we dissolved 8.2 ml of triethanolamine in 700 ml of autoclaved deionized water and kept the mixture stirring. Next, we immersed the washed slides into the gently stirring triethanolamine solution. Within one minute, 1.75 ml of acetic anhydride was added dropwise to the triethanolamine solution. We let slides soak in this solution for 10 min. Finally, we washed the slide in another clean staining dish containing 1x PBS. We then drained off the 1x PBS buffer by tapping the slides gently on a blotting pad. Each slide was placed evenly on two rails inside the petri-dish. 500 µl of hybridization buffer was then added to each slide, covering the entire tissue sections and incubated in the humidified hybridization chamber at 58°C for at least 1 hour.

Hybridization

A dry block heater was pre-heated to 85°C while we dilute the appropriate probe solutions in a hybridization buffer. We typically add around 0.03 µl to 0.5 µl of mRNA probe (individually optimized) per 200 ◎l of hybridization buffer per slide. The RNA probes were thawed on ice, added to appropriate volumes of hybridization buffers and heated for 5 min at 85°C before use. 200 µl of probe solution was added per slide, covering the entire tissue. A small piece of parafilm was also used to exactly cover the glass slide and prevent evaporation. The slide was then evenly placed on the rails inside a petri-dish and incubate in the humidified hybridization chamber at 58°C overnight.

Subsequent steps were no longer RNAse free.

Washing

The next day, we washed away any excess probe and hybridization buffer with heated SSC at 72°C. Bottles of 5x SSC and 0.2x SSC (diluted from 20x SSC in autoclaved deionized water) were equilibrated for around 45 mins in the water bath. Heated 0.2x SSC was poured into two staining dishes and placed into a 72°C incubation oven. Picking up each slide with a pair of tweezers, we drained off the probe solution by tapping the slides gently against a blotting pad. The slide was then fully immersed in heated 5x SSC inside a staining dish. The parafilm would fall out and was gently removed. We next transferred the slide to a second 5x SSC staining dish and finally into a 5x SSC staining dish. We did this for all the subsequent slide(s) and loaded all the slides into a 0.2x SSC staining dish. The slides were placed into a 72°C incubation oven for 30 mins. The previous step was repeated with a second staining dish for another 30 mins. In the meantime, we placed 2 rails across 25-cm tissue culture dish(s) and added a small piece of paper towel soaked with autoclaved deionized water below. When the second 30 mins incubation was done, we transferred the slide(s) into coplin staining jar(s), and immersed with 1x PBS for 5 min.

Double label in situ hybridization

The 1x PBS wash was replaced with 0.5% maleic acid blocking solution diluted in 1x PBS. The slides were incubated in coplin staining jar(s) for 30 min at room temperature. While waiting, we made anti-DIG-POD (HRP) (1:1000 in maleic acid blocking solution). The 0.5% maleic acid blocking solution was replaced with 300µl anti-DIG solution per slide and incubate for 45 min. The slide(s) were rinsed twice with 1x PBS (< 1 min) and washed by immersing in 1x PBS for 10 mins (repeat this step 3 times). We then replaced the wash with 0.1% BSA-PBS (50 ml 1x PBS, 667 µl BSA) and waited briefly before adding 200 µl tyramide signal amplification (TSA) working solution per slide, kept them inside water humidified 25-cm petri-dish(s). The slides were incubated for 10 mins at room temperature, and we covered the slides to protect the fluorophore from light exposure. The slide(s) were rinsed inside coplin staining jar(s) with 1x PBS twice (< 1 min) before proceeding.

Subsequent procedures were kept in the dark when possible.

Immunostaining we

We replaced the 1x PBS wash with 0.1% Triton X-100 PBS (99 ml 1x PBS, 1 ml Triton™ X-100 solution) and waited for 1 min. The slides were then rinsed twice with 1x PBS (< 1 min). The slides were equilibrated with Triton X-100 blocking solution (2.5g instant dry milk, 49 ml of 0.1% Triton X-100 PBS) for 30 mins. We drained off the Triton X-100 blocking solution and added phospho-S6 polyclonal antibody (1:300 dilution) to the blocking solution. 300 µl of the primary antibody mix was added directly onto each slide. The slide was covered with a fitting piece of parafilm to prevent evaporation and incubated overnight at 4˚C in the cold room.

Immunostaining II

The slide(s) were rinsed twice with 1x PBS (<1 min) inside staining dishes to wash off any excess antibody and the Triton X-100 blocking solution. The parafilm covers were removed and we transferred the slides(s) to coplin staining jar(s) filled with 1x PBS. We washed the slides three times in 1x PBS for 5 mins and incubated them in milk blocking solution (2.5g instant dry milk, 49 ml 1x PBS), for another 5 mins. The blocking solution was then drained off, and we added 200 µl of the donkey Cy3-conjugated anti-rabbit IgG (1:200 dilution in blocking solution) and incubated for 45 mins at room temperature. The slide(s) were rinsed twice with 1x PBS (> 1 min) and transferred to Coplin staining jar(s) containing 1x PBS and washed twice for 5 mins. For nuclear staining, we incubated the slides in 1% bisbenzimide (1: 100000 dilutions in 1x PBS) for 5 min. The slides were washed in 1x PBS for 5 mins and then rinsed in autoclaved deionized water. The slides were finally mounted with a few drops of mowiol and carefully covered with a glass coverslip. Slides were dried overnight before imaging.

Microscopy

Images of the olfactory epithelium were taken at 200x magnification using the Zeiss Axioskop 2 microscope with an attached HBO 100 fluorescent lamp. The vertical Retiga 2000R camera was used to capture the images. On the Zeiss microscope, the filter set 38 was used for DIG-signal detection, the filter set 43 was used for pS6-signal detection, and the filter set 49 was used for nuclear-staining detection. Z-stacked images were taken with 2-µm intervals. Images were obtained at 200× magnification with the ApoTome functionality on the low grid and 1x1 binning. Within the same experiment, the same exposure should be used for all slides containing the pS6 signal. Also, the same exposure was used for the same probe across multiple olfactory epithelium sections. The ApoTome image was used alongside with orthogonal projection transformation to stitch the different slices and generate a maximum intensity projection image for colocalization analysis. FIJI. was then used for the quantification of colocalization signals, the mask of individual DIG signals was overlaid onto the pS6-signal image and the average intensity

of the pixels in all selected areas was multiplied by its area in arbitrary square units to yield an integrated density value by FIJI. To subtract the background fluorescence, these numbers were divided by the average pixel intensity of all DIG positive cells in the control condition for that probe.

A.3 Protocol for Olfr376 gRNA designs

1. NCBI nucleotide search for Olfr376 to get 1000+ bp ORF
2. Split 1000+ bp into 4 segments of 250 bp sequences (20bp overlap)
3. Run each of the segments through http://crispr.mit.edu/
4. For each of the generated reports, look at the green 'gRNA'

	score	sequence	
Guide #1	57	AACAGGTGTTGATGCTCTGT	GGG
Guide #2	53	GAACAGGTGTTGATGCTCTG	TGG
Guide #3	53	GGCAGTTTGATTCCTTTCTG	TGG
Guide #4	47	CATCATCATCCTTATTCATC	TGG

5. Compile the list of 'green' gRNAs (prioritize segment 3 & 4) and identify their positions within the OR GPCR structure

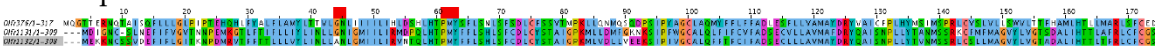

6. Only gRNAs after TM1 and before TM7 are considered

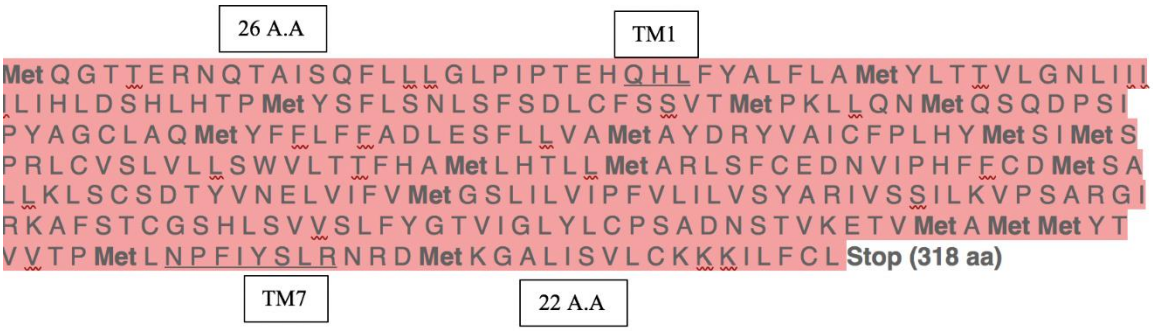

1. The remaining gRNAs are then blasted for off-target effects
   - http://www.sanger.ac.uk/htgt/wge/find_off_targets_by_seq
   - https://blast.ncbi.nlm.nih.gov/Blast.cgi

Segment	gRNA	Score	gRNA Position (From AUG)	Within TM1-7	Off-target
Olfr376-sgRNA2	CCTTCCATGCCATGCTGCAT	Nil	467bp-F	Yes	Olfr19(1mis)
Olfr376-sgRNA3	ATGTTAATGAATTGGTGATA	Nil	587bp-F	Yes	Olfr20(2mis)
Olfr376-A1-57	AACAGGTGTTGATGCTCTGT	57	70bp-R	No	N/A
Olfr376-A2-53	GAACAGGTGTTGATGCTCTG	53	71bp-R	No	N/A
Olfr376-A3-53	GGCAGTTTGATTCCTTTCTG	53	14bp-R	No	N/A
Olfr376-B1-72	GATCCATCAATTCCCTATGC	72	274bp -F	Yes	Olfr1(2mis)
Olfr376-B2-67	CATAGGGAATTGATGGATCC	67	273bp-R	Yes	Olfr394(3mis)
Olfr376-B3-61	AATTCCCTATGCAGGCTGCC	61	282bp-F	Yes	Olfr1(2mis)
Olfr376-B4-55	TTTCAAGGTCTGCAAAAAAC	55	336bp-R	Yes	Cep162(3mis)

Olfr376-B5-55	CAGCCTGCATAGGGAATTGA	55	280bp-R	Yes	Olfr1(2mis)
Olfr376-C1-63 (sgRNA1)	TGACACCTATGTTAATGAAT	63	579bp-F	Yes	Olfr20(2mis)
Olfr376-C2-51	CAATTCGTGCATAGGACACA	51	666bp-R	Yes	OLfr20(1mis)
Olfr376-D1-56	TCTTGCAAAGAACACTAATT	56	924bp-R	No	N/A
Olfr376-D2-55	CTTGCAAAGAACACTAATTA	55	923bp-R	No	N/A

A.4 Cloning CRISPR guide sequences into pX330

1. Dissolve oligo's in STE buffer (10mM Tris pH 8.0, 50mM NaCl, 1mM EDTA) to a final concentration of 0.1 nMoles/ul (100 uM)
    - To 98ml of dW, we add 1ml of 100X Tris-EDTA buffer solution + 1ml of 5M NaCl (Glass bottle next to SSC)
2. Add 1 ul of each sense and antisense oligo pair into a PCR tube and label carefully.
    - Alternatively, to 2ul of STE buffer, add 1ul of dW diluted oligos each
3. Heat oligo mix to 94°C for 2 min. Cycle to cool the block to <30C over a 20-30 min. period (~0.1C/2 sec).
    - Add 198ul/196ul dH2O to dilute the guide duplex.
4. Linearize pX330 (BbsI) using Protocol from Cornell University Transgenic Core
    - 1 µl pX330 (0.8µg/µl stock)
    - µl 10X NEBuffer 2.1
    - 1 µl *Bbs*I (NEB)
    - 16 µl H2O to volume of 20 µl
    - Incubate the digestion reaction at 37°C for 1.5 hour. Heat inactivate (65°C for 20 min) the enzyme.
5. Set up a ligation rxn with T4 ligase using 1ul (~5ng) of linearized pX330 (BbsI) and 0.5ul of the diluted guide duplex in a 10 ul rxn

Reagent	Vol/Rxn
dW	6.5µl
T4 Ligase Buffer [Modifying enzyme blue ice-box] Shake to dissolve white ppt.	1µl
Vector(Digested pCI) *frozen stock	**1µl**
T4 ligase [Modifying enzyme blue ice-box]	1µl
Insert diluted Oligos	**0.5µl**
Total (Kept reaction at room temperature for 15 mins)	10µl

6. Transform plasmids using 1-3 ul of ligation reaction. Plate entire cell pellet on Amp.
    - Pipette 2 µl of ligation product into the competent cells on ice
        - +ve control: Dip pipette tip in (100ng/µl) plasmid mixture, dip tip in competent cells
        - -ve control: ligated digested pCI vector without any insert
        - Incubate on ice for 30 min to transform the cells
        - Streak 30µl of the transformed *E. coli* and incubate plate for ~ 11 hours.

7. Confirm CRISPR guide insert via sequencing with hU6 primer: taatttcttgggtagtttgcag

A.5 Freezing Behavior Assay

8. Mice were place in home cage and habituated for ~ 30 mins in the dissection room before testing.
9. Set up the test arena -> clean hood -> new bench paper -> clear plastic plate> camera on tripod.
10. Make 0.01% odorant -> 1μl 100% odorant + 99 μl dW = 1% -> 1μl 1% odorant + 99 μl dW = 0.01%.
11. Using tweezers, pick up and habituate mouse in paper tub in fume hood for ~ 2 minutes.
12. Check for decent basal activity, start video recording, show coverlid info, using another tweezer, add square of filter paper into white/blue plastic cassette, place plastic lid on and record for 10 mins.
13. After at least 10 mins is up, place mouse into a new paper bucket (tweezers1) and let mouse run around briefly to habituate.
14. Go to fume hood and prepare a fresh 0. 1% odorant cassette (10μl of diluted odorant).
15. With another tweezer, drop 0.1% odorant cassette into bucket, place plastic lid on top and record for 10 mins.
16. After at least 10 mins is up, repeat step 5 to 7 if necessary.
17. Change bench paper, tub, lid, glove, discard all into trash.
18. Let hood stay empty for 10 mins for odorants to clear/ wipe the hood down with ethanol.

19. Go to step 3 and repeat experiment for next mice. Careful to change gloves before handling and adding new odor cassettes.
20. Mice are nocturnal, which means they are most active at dusk ~(5.30pm), after dark and at dawn (~7am).

Appendix B

B.1 Olfr1132 and Olfr491 cystine mutants

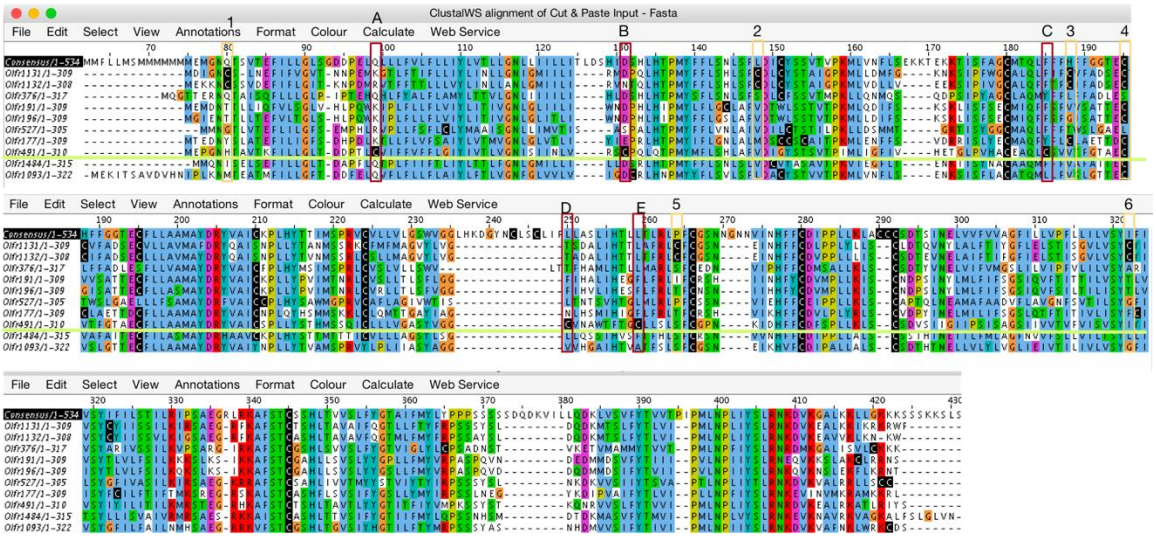

Figure 41: Alignment of amino acid residues for 2MT responsive ORs. Olfr1132 specific cysteines boxed in yellow, Olfr491 specific cysteines boxed in red.

Olfr1132 amino acids
MEKKNCSSVDEFIFLGITKNPDMRVTFFTTLLLVYLINLLANLGMIILIRVNTQLHTPM
YFFLSHLSFCDLCYSTAIGPKMLVDLLVEEKSIPIVGCALQFFTFCIFADSECLLLAVMA
YDRYQAISNPLLYTVNMSSRLCSLLMAGVYLVGTADALIHTTLTFRLCFCGSNEINHFF
CDVPPLLLISCSDTEVNELAIFTIFGFIELSTISGVLVSYCYIISSVLKIGSAEGRFKAFSTCA
SHLTAVAVFQGTMLFMYFRPSSAYSLDQDKMTSLFYTLVIPMLNPLIYSLRNKDVKEA
VVKLKNKW

Six cysteine to serine mutants for Olfr1132

atg**gaaaagaaaaat**tgc**tcctcagtag**atgaattcatcttcttgggaattaccaagaac
M E K K N C S S V D E F we F L G we T K N
cctgacatgagagtgaccttcttcaccacactcctacttgtttatctcattaatcttctg
P D M R V T F F T T L L L V Y L we N L L
gccaaccttgggatgatcatcttaattagagtgaacactcagctgcacacacccatgtac
A N L G M we we L we R V N T Q L H T P M Y
tttttcctcagcca**cctctctttc**tgt**gacctctgc**tattccacagcaattggacccaag
F F L S H L S F C D L C Y S T A we G P K
atgttggtggatcttttagttgaggagaaatcgattcccattgttggttgtgctttgcag
M L V D L L V E E K S we P we V G C A L Q
t**tttttacgttc**tgc**atctttgcag**attctgag**tgtctactgctgg**cagtgatggcctat
F F T F C we F A D S E C L L L A V M A Y

gacagataccaggccatcagtaacccattgctctacacagtgaacatgtccagccggctg
D R Y Q A we S N P L L Y T V N M S S R L
tgctccctcctgatggctggagtttacctggtgggaacagcagatgctttgatacataca
C S L L M A G V Y L V G T A D A L we H T
accctgacc**ttccgcttg**tgt**ttctgtggat**ccaatgagatcaaccactttttgtgat
T L T F R L C F C G S N E we N H F F C D
gtgcctcctcttctattaatatcttgctcagatacagaggtcaatgagttagctatattc
V P P L L L we S C S D T E V N E L A we F
acaattttcgggttcattgagctgagtaccatttctggagtc**cttgtttcttat**tgc**tac**
T we F G F we E L S T we S G V L V S Y C Y
atcatatcatcagtcttgaagatcggttctgctgaggggcggtttaaagctttctctacc
we we S S V L K we G S A E G R F K A F S T
tgtgcttcccacctgactgctgttgcagtattccaggggactatgctcttcatgtatttc
C A S H L T A V A V F Q G T M L F M Y F
cggccaagttctgcctactctctagatcaagacaaaatgacctcactcttctacaccctg
R P S S A Y S L D Q D K M T S L F Y T L
gtgattccaatgttgaaccctctgatttacagcctgaggaacaaagatgtgaaagaggct
V we P M L N P L we Y S L R N K D V K E A
gtggtaaaattaaagaataaatggtga
V V K L K N K W -
WEBSEQUENCE Length: 308
WEBSEQUENCE Number of predicted TMHs: 7
WEBSEQUENCE Exp number of AAs in TMHs: 145.94173
WEBSEQUENCE Exp number, first 60 AAs: 23.42666
WEBSEQUENCE Total prob of N-in: 0.23922
WEBSEQUENCE POSSIBLE N-term signal sequence

WEBSEQUENCE	TMHMM2.0	outside	1	26
WEBSEQUENCE	TMHMM2.0	TMhelix	27	49
WEBSEQUENCE	TMHMM2.0	inside	50	60
WEBSEQUENCE	TMHMM2.0	TMhelix	61	83
WEBSEQUENCE	TMHMM2.0	outside	84	97
WEBSEQUENCE	TMHMM2.0	TMhelix	98	120
WEBSEQUENCE	TMHMM2.0	inside	121	139
WEBSEQUENCE	TMHMM2.0	TMhelix	140	162
WEBSEQUENCE	TMHMM2.0	outside	163	198
WEBSEQUENCE	TMHMM2.0	TMhelix	199	221
WEBSEQUENCE	TMHMM2.0	inside	222	240
WEBSEQUENCE	TMHMM2.0	TMhelix	241	260
WEBSEQUENCE	TMHMM2.0	outside	261	274
WEBSEQUENCE	TMHMM2.0	TMhelix	275	292
WEBSEQUENCE	TMHMM2.0	inside	293	308

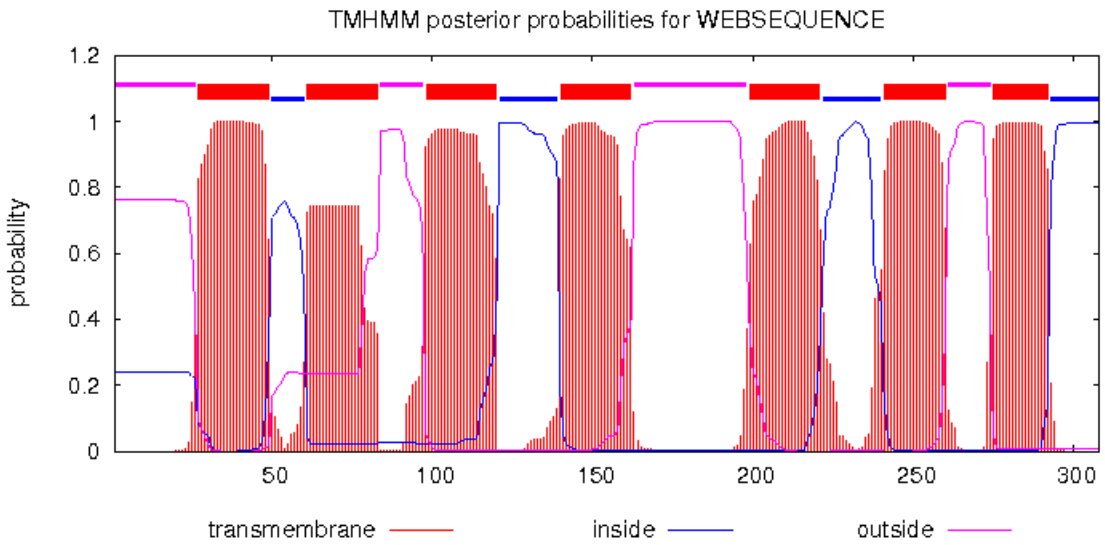

Olfr491 amino acids

MEPGNHTAVTKFILLGLTDDPTL**C**VIFFVFFLGIYIVTLVGNISI**I**NLVRSCPQLQTPMY
MFLSH**L**AFVDIGYSTSVTPIMLIGFIV**H**ETGLPVHACEAQLC**S**VVTFGTAECFLLAAMA
YDRYVAICSPLLYSTHMSSQ**I**CLLLVGASYVGGCVNAWT**F**TGCLLSLSFCGPNKIDHFF
CDFSPLLKLSCSDVS**I**IGIIPSISAGSIIVVTVFVIS**V**SYIYILITILKMRSTEGRHK**A**FSTCTS
HLTAVTLYYGTITFI**Y**VMPKSSYSTKQNRV**V**SLFYTVVIPMLNPLIYS**L**RNRDVKEALRK
ATLRIYS

Five cysteine mutants for Olfr491

atggaacctggaaaccacactgcagtgacaaagttcatccttttggggttaacagatgat
M E P G N H T A V T K F we L L G L T D D
cctacactc**tgt**gtcatcttctttgtgtttttttcttggaatatacattgtcaccttagta
P T L **C** V we F F V F F L G we Y we V T L V
ggaaatatcagcataataaatttagtaagaagc**tgt**cctcagctccaaacccccatgtac
G N we S we we N L V R S **C** P Q L Q T P M Y
atgtttcttagccatctggcttttgtggacattggctattcaacatcagttacacctata
M F L S H L A F V D we G Y S T S V T P we
atgttaataggattcattgtacatgaaacaggcctccctgtgcatgcctgtgaagcacaa
M L we G F we V H E T G L P V H A C E A Q
ctc**tgt**tctgttgtgactttgggacagctgaatgcttcctgctggctgccatggcctat
L **C** S V V T F G T A E C F L L A A M A Y
gacagatatgttgctatttgctctcccttgctctactccacacatatgtcttcccaaatc
D R Y V A we C S P L L Y S T H M S S Q we
tgtctcctcttagttggggcatcctatgtgggtggc**tgt**gtgaatgcatggacatttact
C L L L V G A S Y V G G **C** V N A W T F T
ggc**tgt**ttgttaagtctgtccttttgtggaccaaataagatagatcacttcttctgtgat
G **C** L L S L S F C G P N K we D H F F C D

ttctcccctttgttgaaactttcatgctcagatgtctccattattggaatcatcccctct
F S P L L K L S C S D V S we we G we we P S
atctctgctggctccattattgtagtgacagtgtttgtcatatctgtctcctacatctac
we S A G S we we V V T V F V we S V S Y we Y
atccttatcaccatcctgaagatgcgctccactgagggtcgccacaaggccttctccacc
we L we T we L K M R S T E G R H K A F S T
tgcacctcccacctcactgcagtcactctctactatggaactattactttcatttatgtg
C T S H L T A V T L Y Y G T we T F we Y V
atgcccaagtccagctactcaactaagcagaacagggtggtgtctctgttctacacagtg
M P K S S Y S T K Q N R V V S L F Y T V
gtgatccccatgttgaatcccctcatctatagtttgaggaacagagatgttaaggaagcg
V we P M L N P L we Y S L R N R D V K E A
ctgaggaaggcaactcttagaatatattcatag
L R K A T L R we Y S -

WEBSEQUENCE Length: 310
WEBSEQUENCE Number of predicted TMHs: 7
WEBSEQUENCE Exp number of AAs in TMHs: 155.845
WEBSEQUENCE Exp number, first 60 AAs: 22.9487
WEBSEQUENCE Total prob of N-in: 0.02578
WEBSEQUENCE POSSIBLE N-term signal sequence

WEBSEQUENCE	TMHMM2.0	outside	1	23
WEBSEQUENCE	TMHMM2.0	TMhelix	24	46
WEBSEQUENCE	TMHMM2.0	inside	47	65
WEBSEQUENCE	TMHMM2.0	TMhelix	66	88
WEBSEQUENCE	TMHMM2.0	outside	89	102
WEBSEQUENCE	TMHMM2.0	TMhelix	103	120
WEBSEQUENCE	TMHMM2.0	inside	121	139
WEBSEQUENCE	TMHMM2.0	TMhelix	140	159
WEBSEQUENCE	TMHMM2.0	outside	160	193
WEBSEQUENCE	TMHMM2.0	TMhelix	194	216
WEBSEQUENCE	TMHMM2.0	inside	217	236
WEBSEQUENCE	TMHMM2.0	TMhelix	237	259
WEBSEQUENCE	TMHMM2.0	outside	260	273
WEBSEQUENCE	TMHMM2.0	TMhelix	274	292
WEBSEQUENCE	TMHMM2.0	inside	293	310

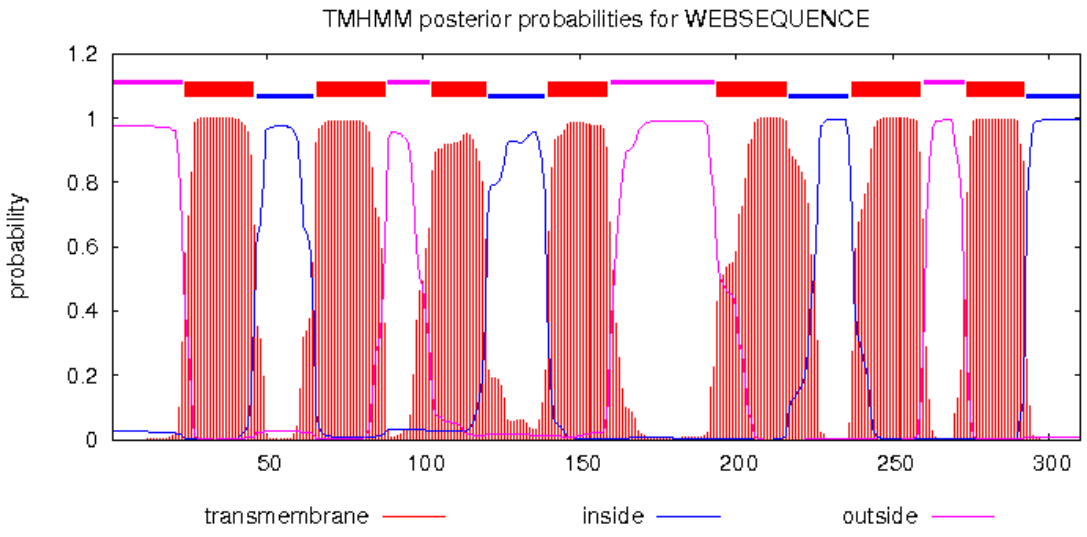
TMHMM posterior probabilities for WEBSEQUENCE
probability
1.2
1
0.8
0.6
0.4
0.2
0
50
100
150
200
250
300
transmembrane
inside
outside

References

Adipietro KA, Mainland JD, Matsunami H (2012) Functional evolution of mammalian odorant receptors. PLoS Genet 8:e1002821.

Ahmed L, Zhang Y, Block E, Buehl M, Corr MJ, Cormanich RA, Gundala S, Matsunami H, O'Hagan D, Ozbil M (2018) Molecular mechanism of activation of human musk receptors OR5AN1 and OR1A1 by (R)-muscone and diverse other musk-smelling compounds. Proceedings of the National Academy of Sciences 115:E3950-E3958.

Alexander RW, Davis JN, Lefkowitz RJ (1975) Direct identification and characterisation of beta-adrenergic receptors in rat brain. Nature 258:437-440.

Anderson AK, Christoff K, Stappen I, Panitz D, Ghahremani DG, Glover G, Gabrieli JD, Sobel N (2003) Dissociated neural representations of intensity and valence in human olfaction. Nat Neurosci 6:196-202.

Apfelbach R, Blanchard CD, Blanchard RJ, Hayes RA, McGregor IS (2005) The effects of predator odors in mammalian prey species: A review of field and laboratory studies. Neuroscience and Biobehavioral Reviews 29:1123-1144.

Asakawa M, Fukutani Y, Savangsuksa A, Noguchi K, Matsunami H, Yohda M (2017) Modification of the response of olfactory receptors to acetophenone by CYP1a2. Sci Rep 7:10167.

Ballesteros JA, Weinstein H (1995) Integrated methods for the construction of three-dimensional models and computational probing of structure-function relations in G protein-coupled receptors. In: Methods in neurosciences, pp 366-428: Elsevier.

Bargmann CI (1998) Neurobiology of the Caenorhabditis elegans genome. Science 282:2028-2033.

Bargmann CI (2006a) Comparative chemosensation from receptors to ecology. Nature 444:295-301.

Bargmann CI (2006b) Chemosensation in C. elegans. WormBook:1-29.

Bautista DM, Movahed P, Hinman A, Axelsson HE, Sterner O, Högestätt ED, Julius D, Jordt S-E, Zygmunt PM (2005) Pungent products from garlic activate the sensory ion channel TRPA1. Proceedings of the National Academy of Sciences 102:12248-12252.

Beets MG (1970) The molecular parameters of olfactory response. Pharmacol Rev 22:1-34.

Bhandawat V, Reisert J, Yau KW (2005) Elementary response of olfactory receptor neurons to odorants. Science 308:1931-1934.

Biever A, Valjent E, Puighermanal E (2015) Ribosomal Protein S6 Phosphorylation in the Nervous System: From Regulation to Function. Front Mol Neurosci 8:75.

Bozza T, Feinstein P, Zheng C, Mombaerts P (2002) Odorant receptor expression defines functional units in the mouse olfactory system. J Neurosci 22:3033-3043.

Bray NL, Pimentel H, Melsted P, Pachter L (2016) Near-optimal probabilistic RNA-seq quantification. Nat Biotechnol 34:525-527.

Breer H, Boekhoff I (1992) Second messenger signalling in olfaction. Curr Opin Neurobiol 2:439-443.

Buck L, Axel R (1991) A novel multigene family may encode odorant receptors: a molecular basis for odor recognition. Cell 65:175-187.

Bushdid C, Magnasco MO, Vosshall LB, Keller A (2014) Humans Can Discriminate More than 1 Trillion Olfactory Stimuli. Science 343:1370-1372.

Chess A, Simon I, Cedar H, Axel R (1994) Allelic inactivation regulates olfactory receptor gene expression. Cell 78:823-834.

Christensen TA, Mustaparta H, Hilderbrand JG (1989) Discrimination of sex pheromone blends in the olfactory system of the moth. Chemical Senses 14:463-477.

Clyne PJ, Warr CG, Freeman MR, Lessing D, Kim J, Carlson JR (1999) A novel family of divergent seven-transmembrane proteins: candidate odorant receptors in Drosophila. Neuron 22:327-338.

D'Hulst C, Mina RB, Gershon Z, Jamet S, Cerullo A, Tomoiaga D, Bai L, Belluscio L, Rogers ME, Sirotin Y, Feinstein P (2016) MouSensor: A Versatile Genetic Platform to Create Super Sniffer Mice for Studying Human Odor Coding. Cell Rep 16:1115-1125.

de March CA, Yu Y, Ni MJ, Adipietro KA, Matsunami H, Ma M, Golebiowski J (2015) Conserved Residues Control Activation of Mammalian G Protein-Coupled Odorant Receptors. J Am Chem Soc 137:8611-8616.

Dobin A, Davis CA, Schlesinger F, Drenkow J, Zaleski C, Jha S, Batut P, Chaisson M, Gingeras TR (2013) STAR: ultrafast universal RNA-seq aligner. Bioinformatics 29:15-21.

Dohlman HG, Thorner J, Caron MG, Lefkowitz RJ (1991) Model systems for the study of seven-transmembrane-segment receptors. Annu Rev Biochem 60:653-688.

Dryer L (2000) Evolution of odorant receptors. Bioessays 22:803-810.

Dryer L, Berghard A (1999) Odorant receptors: a plethora of G-protein-coupled receptors. Trends in pharmacological sciences 20:413-417.

Duchamp-Viret P, Duchamp A (1997) Odor processing in the frog olfactory system. Prog Neurobiol 53:561-602.

Eltz T, Whitten W, Roubik D, Linsenmair K (1999) Fragrance collection, storage, and accumulation by individual male orchid bees. J Chem Ecol 25:157-176.

Feinstein P, Mombaerts P (2004) A contextual model for axonal sorting into glomeruli in the mouse olfactory system. Cell 117:817-831.

Feinstein P, Bozza T, Rodriguez I, Vassalli A, Mombaerts P (2004) Axon guidance of mouse olfactory sensory neurons by odorant receptors and the beta2 adrenergic receptor. Cell 117:833-846.

Fendt M, Endres T, Lowry CA, Apfelbach R, McGregor IS (2005) TMT-induced autonomic and behavioral changes and the neural basis of its processing. Neuroscience and Biobehavioral Reviews 29:1145-1156.

Firestein S (1996) Scentsational ion channels. Neuron 17:803-806.

Fried HU, Fuss SH, Korsching SI (2002) Selective imaging of presynaptic activity in the mouse olfactory bulb shows concentration and structure dependence of odor responses in identified glomeruli. Proc Natl Acad Sci U S A 99:3222-3227.

Fujii W, Kawasaki K, Sugiura K, Naito K (2013) Efficient generation of large-scale genome-modified mice using gRNA and CAS9 endonuclease. Nucleic Acids Research 41:9.

Godfrey PA, Malnic B, Buck LB (2004) The mouse olfactory receptor gene family. Proceedings of the National Academy of Sciences of the United States of America 101:2156-2161.

Grosmaitre X, Vassalli A, Mombaerts P, Shepherd GM, Ma M (2006) Odorant responses of olfactory sensory neurons expressing the odorant receptor MOR23: a patch clamp analysis in gene-targeted mice. Proc Natl Acad Sci U S A 103:1970-1975.

Gross-Isseroff R, Lancet D (1988) Concentration-dependent changes of perceived odor quality. Chemical senses 13:191-204.

Guthrie KM, Anderson AJ, Leon M, Gall C (1993) Odor-induced increases in c-fos mRNA expression reveal an anatomical "unit" for odor processing in olfactory bulb. Proc Natl Acad Sci U S A 90:3329-3333.

Hanchate NK, Kondoh K, Lu Z, Kuang D, Ye X, Qiu X, Pachter L, Trapnell C, Buck LB (2015) Single-cell transcriptomics reveals receptor transformations during olfactory neurogenesis. Science 350:1251-1255.

Healy MD, Smith JE, Singer MS, Nadkarni PM, Skoufos E, Miller PL, Shepherd GM (1997) Olfactory receptor database (ORDB): a resource for sharing and analyzing published and unpublished data. Chemical senses 22:321-326.

Horowitz LF, Saraiva LR, Kuang D, Yoon K-h, Buck LB (2014) Olfactory receptor patterning in a higher primate. Journal of Neuroscience 34:12241-12252.

Ibarra-Soria X, Levitin MO, Saraiva LR, Logan DW (2014) The olfactory transcriptomes of mice. PLoS Genet 10:e1004593.

Ibarra-Soria X, Nakahara TS, Lilue J, Jiang Y, Trimmer C, Souza MA, Netto PH, Ikegami K, Murphy NR, Kusma M, Kirton A, Saraiva LR, Keane TM, Matsunami H, Mainland J, Papes F, Logan DW (2017) Variation in olfactory neuron repertoires is genetically controlled and environmentally modulated. Elife 6.

Isosaka T, Matsuo T, Yamaguchi T, Funabiki K, Nakanishi S, Kobayakawa R, Kobayakawa K (2015) Htr2a-Expressing Cells in the Central Amygdala Control the Hierarchy between Innate and Learned Fear. Cell 163:1153-1164.

Iurilli G, Datta SR (2017) Population coding in an innately relevant olfactory area. Neuron 93:1180-1197. e1187.

Jabba S, Goyal R, Sosa-Pagán JO, Moldenhauer H, Wu J, Kalmeta B, Bandell M, Latorre R, Patapoutian A, Grandl J (2014) Directionality of temperature activation in mouse TRPA1 ion channel can be inverted by single-point mutations in ankyrin repeat six. Neuron 82:1017-1031.

Jiang Y, Matsunami H (2015) Mammalian odorant receptors: functional evolution and variation. Curr Opin Neurobiol 34:54-60.

Jiang Y, Gong NN, Hu XS, Ni MJ, Pasi R, Matsunami H (2015) Molecular profiling of activated olfactory neurons identifies odorant receptors for odors in vivo. Nat Neurosci 18:1446-1454.

Jones DT, Reed RR (1989) Golf: an olfactory neuron specific-G protein involved in odorant signal transduction. Science 244:790-795.

Kajiya K, Inaki K, Tanaka M, Haga T, Kataoka H, Touhara K (2001) Molecular bases of odor discrimination: Reconstitution of olfactory receptors that recognize overlapping sets of odorants. J Neurosci 21:6018-6025.

Kasumyan A (2004) The olfactory system in fish: structure, function, and role in behavior. Journal of Ichthyology 44:S180.

Katada S, Nakagawa T, Kataoka H, Touhara K (2003) Odorant response assays for a heterologously expressed olfactory receptor. Biochem Biophys Res Commun 305:964-969.

Kato A, Katada S, Touhara K (2008) Amino acids involved in conformational dynamics and G protein coupling of an odorant receptor: targeting gain-of-function mutation. Journal of neurochemistry 107:1261-1270.

Kavaliers M, Choleris E (2001) Antipredator responses and defensive behavior: ecological and ethological approaches for the neurosciences. Neuroscience and Biobehavioral Reviews 25:577-586.

Khan AG, Parthasarathy K, Bhalla US (2010) Odor representations in the mammalian olfactory bulb. Wiley Interdiscip Rev Syst Biol Med 2:603-611.

Kida H, Fukutani Y, Mainland JD, de March CA, Vihani A, Li YR, Chi Q, Toyama A, Liu L, Kameda M, Yohda M, Matsunami H (2018) Vapor detection and discrimination with a panel of odorant receptors. Nat Commun 9:4556.

Knight ZA, Tan K, Birsoy K, Schmidt S, Garrison JL, Wysocki RW, Emiliano A, Ekstrand MI, Friedman JM (2012) Molecular profiling of activated neurons by phosphorylated ribosome capture. Cell 151:1126-1137.

Kobayakawa K, Kobayakawa R, Matsumoto H, Oka Y, Imai T, Ikawa M, Okabe M, Ikeda T, Itohara S, Kikusui T, Mori K, Sakano H (2007) Innate versus learned odour processing in the mouse olfactory bulb. Nature 450:503-U505.

Koerte S, Keesey IW, Khallaf MA, Cortes Llorca L, Grosse-Wilde E, Hansson BS, Knaden M (2018) Evaluation of the DREAM Technique for a High-Throughput Deorphanization of Chemosensory Receptors in Drosophila. Front Mol Neurosci 11:366.

Krone D, Mannel M, Pauli E, Hummel T (2001) Qualitative and quantitative olfactometric evaluation of different concentrations of ethanol peppermint oil solutions. Phytother Res 15:135-138.

Laberge F, Hara TJ (2001) Neurobiology of fish olfaction: a review. Brain Res Brain Res Rev 36:46-59.

Langmead B, Trapnell C, Pop M, Salzberg SL (2009) Ultrafast and memory-efficient alignment of short DNA sequences to the human genome. Genome Biol 10:R25.

Lee-Thorp J, Thackeray JF, van der Merwe N (2000) The hunters and the hunted revisited. J Hum Evol 39:565-576.

Li H, Handsaker B, Wysoker A, Fennell T, Ruan J, Homer N, Marth G, Abecasis G, Durbin R, Genome Project Data Processing S (2009) The Sequence Alignment/Map format and SAMtools. Bioinformatics 25:2078-2079.

Liberles SD, Buck LB (2006) A second class of chemosensory receptors in the olfactory epithelium. Nature 442:645-650.

Lieber MR (2010) The mechanism of double-strand DNA break repair by the nonhomologous DNA end-joining pathway. Annu Rev Biochem 79:181-211.

Lindemann B (1996) Taste reception. Physiol Rev 76:719-766.

Lobue V, DeLoache JS (2008) Detecting the snake in the grass - Attention to fear-relevant stimuli by adults and young children. Psychological Science 19:284-289.

Lu M, Echeverri F, Moyer BD (2003) Endoplasmic reticulum retention, degradation, and aggregation of olfactory G-protein coupled receptors. Traffic 4:416-433.

Ma M, Shepherd GM (2000) Functional mosaic organization of mouse olfactory receptor neurons. Proceedings of the National Academy of Sciences 97:12869-12874.

Macpherson LJ, Dubin AE, Evans MJ, Marr F, Schultz PG, Cravatt BF, Patapoutian A (2007) Noxious compounds activate TRPA1 ion channels through covalent modification of cysteines. Nature 445:541.

Madisen L, Zwingman TA, Sunkin SM, Oh SW, Zariwala HA, Gu H, Ng LL, Palmiter RD, Hawrylycz MJ, Jones AR, Lein ES, Zeng H (2010) A robust and high-throughput Cre reporting and characterization system for the whole mouse brain. Nat Neurosci 13:133-140.

Mainland JD, Lundstrom JN, Reisert J, Lowe G (2014) From molecule to mind: an integrative perspective on odor intensity. Trends Neurosci 37:443-454.

Malnic B, Godfrey PA, Buck LB (2004) The human olfactory receptor gene family. Proc Natl Acad Sci U S A 101:2584-2589.

Malnic B, Hirono J, Sato T, Buck LB (1999) Combinatorial receptor codes for odors. Cell 96:713-723.

Marx V (2014) Gene editing: how to stay on-target with CRISPR. Nat Meth 11:1021-1026.

Matsumoto H, Kobayakawa K, Kobayakawa R, Tashiro T, Mori K, Sakano H (2010) Spatial Arrangement of Glomerular Molecular-Feature Clusters in the Odorant-

Receptor Class Domains of the Mouse Olfactory Bulb. Journal of Neurophysiology 103:3490-3500.

McClintock TS, Adipietro K, Titlow WB, Breheny P, Walz A, Mombaerts P, Matsunami H (2014) In vivo identification of eugenol-responsive and muscone-responsive mouse odorant receptors. J Neurosci 34:15669-15678.

McKenzie SK, Kronauer DJC (2018) The genomic architecture and molecular evolution of ant odorant receptors. Genome Res 28:1757-1765.

Miller JC, Holmes MC, Wang J, Guschin DY, Lee YL, Rupniewski I, Beausejour CM, Waite AJ, Wang NS, Kim KA, Gregory PD, Pabo CO, Rebar EJ (2007) An improved zinc-finger nuclease architecture for highly specific genome editing. Nat Biotechnol 25:778-785.

Milner ES, Do MTH (2017) A Population Representation of Absolute Light Intensity in the Mammalian Retina. Cell 171:865-876 e816.

Minic J, Persuy MA, Godel E, Aioun J, Connerton I, Salesse R, Pajot-Augy E (2005) Functional expression of olfactory receptors in yeast and development of a bioassay for odorant screening. FEBS J 272:524-537.

Mitko L, Weber MG, Ramirez SR, Hedenstrom E, Wcislo WT, Eltz T (2016) Olfactory specialization for perfume collection in male orchid bees. J Exp Biol 219:1467-1475.

Miyamichi K, Serizawa S, Kimura HM, Sakano H (2005) Continuous and overlapping expression domains of odorant receptor genes in the olfactory epithelium determine the dorsal/ventral positioning of glomeruli in the olfactory bulb. J Neurosci 25:3586-3592.

Miyamichi K, Amat F, Moussavi F, Wang C, Wickersham I, Wall NR, Taniguchi H, Tasic B, Huang ZJ, He ZG, Callaway EM, Horowitz MA, Luo LQ (2011) Cortical representations of olfactory input by trans-synaptic tracing. Nature 472:191-196.

Mombaerts P, Wang F, Dulac C, Chao SK, Nemes A, Mendelsohn M, Edmondson J, Axel R (1996) Visualizing an olfactory sensory map. Cell 87:675-686.

Moskowitz HOUR, Dravnieks A, Klarman LA (1976) Odor intensity and pleasantness for a diverse set of odorants. Perception & Psychophysics 19:122-128.

Nara K, Saraiva LR, Ye X, Buck LB (2011) A large-scale analysis of odor coding in the olfactory epithelium. J Neurosci 31:9179-9191.

Nathans J (1987) Molecular biology of visual pigments. Annu Rev Neurosci 10:163-194.

Niimura Y, Matsui A, Touhara K (2014) Extreme expansion of the olfactory receptor gene repertoire in African elephants and evolutionary dynamics of orthologous gene groups in 13 placental mammals. Genome Research 24:1485-1496.

Norlin EM, Alenius M, Gussing F, Hägglund M, Vedin V, Bohm S (2001) Evidence for gradients of gene expression correlating with zonal topography of the olfactory sensory map. Molecular and Cellular Neuroscience 18:283-295.

O'Leary NA, Wright MW, Brister JR, Ciufo S, Haddad D, McVeigh R, Rajput B, Robbertse B, Smith-White B, Ako-Adjei D (2015) Reference sequence (RefSeq) database at NCBI: current status, taxonomic expansion, and functional annotation. Nucleic acids research 44:D733-D745.

Oka Y, Katada S, Omura M, Suwa M, Yoshihara Y, Touhara K (2006) Odorant receptor map in the mouse olfactory bulb: in vivo sensitivity and specificity of receptor-defined glomeruli. Neuron 52:857-869.

Parabucki A, Bizer A, Morris G, Munoz AE, Bala ADS, Smear M, Shusterman R (2019) Odor Concentration Change Coding in the Olfactory Bulb. eNeuro 6.

Peterlin Z, Firestein S, Rogers ME (2014) The state of the art of odorant receptor deorphanization: a report from the orphanage. J Gen Physiol 143:527-542.

Peterlin Z, Li Y, Sun G, Shah R, Firestein S, Ryan K (2008) The importance of odorant conformation to the binding and activation of a representative olfactory receptor. Chemistry & biology 15:1317-1327.

Pierce KL, Premont RT, Lefkowitz RJ (2002) Seven-transmembrane receptors. Nat Rev Mol Cell Biol 3:639-650.

Platt RJ et al. (2014) CRISPR-Cas9 Knockin Mice for Genome Editing and Cancer Modeling. Cell 159:440-455.

Polak EH (1973) Multiple profile-multiple receptor site model for vertebrate olfaction. Journal of Theoretical Biology 40:469-484.

Reed RR (1992) Signaling pathways in odorant detection. Neuron 8:205-209.

Ressler KJ, Sullivan SL, Buck LB (1993) A zonal organization of odorant receptor gene expression in the olfactory epithelium. Cell 73:597-609.

Ressler KJ, Sullivan SL, Buck LB (1994) Information coding in the olfactory system: evidence for a stereotyped and highly organized epitope map in the olfactory bulb. Cell 79:1245-1255.

Restrepo D, Okada Y, Teeter JH (1993) Odorant-regulated Ca2+ gradients in rat olfactory neurons. J Gen Physiol 102:907-924.

Robinson MD, McCarthy DJ, Smyth GK (2010) edgeR: a Bioconductor package for differential expression analysis of digital gene expression data. Bioinformatics 26:139-140.

Root CM, Denny CA, Hen R, Axel R (2014) The participation of cortical amygdala in innate, odour-driven behaviour. Nature 515:269-U274.

Rospars JP, Lansky P, Duchamp-Viret P, Duchamp A (2000) Spiking frequency versus odorant concentration in olfactory receptor neurons. Biosystems 58:133-141.

Rubin BD, Katz LC (1999) Optical imaging of odorant representations in the mammalian olfactory bulb. Neuron 23:499-511.

Saito H, Kubota M, Roberts RW, Chi Q, Matsunami H (2004) RTP family members induce functional expression of mammalian odorant receptors. Cell 119:679-691.

Saito H, Chi Q, Zhuang H, Matsunami H, Mainland JD (2009) Odor coding by a Mammalian receptor repertoire. Sci Signal 2:ra9.

Saito H, Nishizumi H, Suzuki S, Matsumoto H, Ieki N, Abe T, Kiyonari H, Morita M, Yokota H, Hirayama N, Yamazaki T, Kikusui T, Mori K, Sakano H (2017) Immobility responses are induced by photoactivation of single glomerular species responsive to fox odour TMT. Nat Commun 8:16011.

Sander JD, Joung JK (2014) CRISPR-Cas systems for editing, regulating and targeting genomes. Nat Biotechnol 32:347-355.

Saraiva LR, Ibarra-Soria X, Khan M, Omura M, Scialdone A, Mombaerts P, Marioni JC, Logan DW (2015) Hierarchical deconstruction of mouse olfactory sensory neurons: from whole mucosa to single-cell RNA-seq. Sci Rep 5:18178.

Schneider RA, Schmidt CE, Costiloe JP (1966) Relation of odor flow rate and duration to stimulus intensity needed for perception. J Appl Physiol 21:10-14.

Scholz P, Kalbe B, Jansen F, Altmueller J, Becker C, Mohrhardt J, Schreiner B, Gisselmann G, Hatt H, Osterloh S (2016) Transcriptome Analysis of Murine Olfactory Sensory Neurons during Development Using Single Cell RNA-Seq. Chem Senses 41:313-323.

Sharma R, Ishimaru Y, Davison I, Ikegami K, Chien MS, You H, Chi Q, Kubota M, Yohda M, Ehlers M, Matsunami H (2017) Olfactory receptor accessory proteins play crucial roles in receptor function and gene choice. Elife 6.

Sirotin YB, Shusterman R, Rinberg D (2015) Neural Coding of Perceived Odor Intensity. eNeuro 2.

Soini HA, Linville SU, Wiesler D, Posto AL, Williams DR, Novotny MV (2012) Investigation of scents on cheeks and foreheads of large felines in connection to the facial marking behavior. J Chem Ecol 38:145-156.

Sosulski DL, Bloom ML, Cutforth T, Axel R, Datta SR (2011) Distinct representations of olfactory information in different cortical centres. Nature 472:213-216.

Stettler DD, Axel R (2009) Representations of Odor in the Piriform Cortex. Neuron 63:854-864.

Storace DA, Cohen LB (2017) Measuring the olfactory bulb input-output transformation reveals a contribution to the perception of odorant concentration invariance. Nat Commun 8:81.

Tan L, Xie XS (2018) A Near-Complete Spatial Map of Olfactory Receptors in the Mouse Main Olfactory Epithelium. Chem Senses 43:427-432.

Tan L, Li Q, Xie XS (2015) Olfactory sensory neurons transiently express multiple olfactory receptors during development. Mol Syst Biol 11:844.

Tareilus E, Noe J, Breer H (1995) Calcium signals in olfactory neurons. Biochim Biophys Acta 1269:129-138.

Tobin DM, Madsen DM, Kahn-Kirby A, Peckol EL, Moulder G, Barstead R, Maricq AV, Bargmann CI (2002) Combinatorial expression of TRPV channel proteins defines their sensory functions and subcellular localization in C. elegans neurons. Neuron 35:307-318.

Touhara K, Sengoku S, Inaki K, Tsuboi A, Hirono J, Sato T, Sakano H, Haga T (1999) Functional identification and reconstitution of an odorant receptor in single olfactory neurons. Proc Natl Acad Sci U S A 96:4040-4045.

Troemel ER, Chou JH, Dwyer ND, Colbert HA, Bargmann CI (1995) Divergent seven transmembrane receptors are candidate chemosensory receptors in C. elegans. Cell 83:207-218.

Tsuboi A, Yoshihara S-i, Yamazaki N, Kasai H, Asai-Tsuboi H, Komatsu M, Serizawa S, Ishii T, Matsuda Y, Nagawa F (1999) Olfactory neurons expressing closely linked and homologous odorant receptor genes tend to project their axons to neighboring glomeruli on the olfactory bulb. Journal of Neuroscience 19:8409-8418.

Uchida N, Mainen ZF (2007) Odor concentration invariance by chemical ratio coding. Front Syst Neurosci 1:3.

Vassar R, Ngai J, Axel R (1993) Spatial segregation of odorant receptor expression in the mammalian olfactory epithelium. Cell 74:309-318.

Vassar R, Chao SK, Sitcheran R, Nunez JM, Vosshall LB, Axel R (1994) Topographic organization of sensory projections to the olfactory bulb. Cell 79:981-991.

von der Weid B, Rossier D, Lindup M, Tuberosa J, Widmer A, Col JD, Kan C, Carleton A, Rodriguez I (2015) Large-scale transcriptional profiling of chemosensory neurons identifies receptor-ligand pairs in vivo. Nat Neurosci 18:1455-1463.

Vosshall LB, Amrein H, Morozov PS, Rzhetsky A, Axel R (1999) A spatial map of olfactory receptor expression in the Drosophila antenna. Cell 96:725-736.

Wachowiak M, Cohen LB (2001) Representation of odorants by receptor neuron input to the mouse olfactory bulb. Neuron 32:723-735.

Wang F, Nemes A, Mendelsohn M, Axel R (1998) Odorant receptors govern the formation of a precise topographic map. Cell 93:47-60.

Wang HY, Yang H, Shivalila CS, Dawlaty MM, Cheng AW, Zhang F, Jaenisch R (2013) One-Step Generation of Mice Carrying Mutations in Multiple Genes by CRISPR/Cas-Mediated Genome Engineering. Cell 153:910-918.

Wang Y, Cao L, Lee C-Y, Matsuo T, Wu K, Asher G, Tang L, Saitoh T, Russell J, Klewe-Nebenius D (2018) Large-scale forward genetics screening identifies Trpa1 as a chemosensor for predator odor-evoked innate fear behaviors. Nature communications 9:2041.

Weth F, Nadler W, Korsching S (1996) Nested expression domains for odorant receptors in zebrafish olfactory epithelium. Proc Natl Acad Sci U S A 93:13321-13326.

Wilson CD, Serrano GO, Koulakov AA, Rinberg D (2017) A primacy code for odor identity. Nat Commun 8:1477.

Yu YQ, de March CA, Ni MJJ, Adipietro KA, Golebiowski J, Matsunami H, Ma MH (2015) Responsiveness of G protein-coupled odorant receptors is partially attributed to the activation mechanism. Proceedings of the National Academy of Sciences of the United States of America 112:14966-14971.

Zhang XM, Firestein S (2002) The olfactory receptor gene superfamily of the mouse. Nature Neuroscience 5:124-133.

Zhao H, Ivic L, Otaki JM, Hashimoto M, Mikoshiba K, Firestein S (1998) Functional expression of a mammalian odorant receptor. Science 279:237-242.

Zhuang H, Matsunami H (2008) Evaluating cell-surface expression and measuring activation of mammalian odorant receptors in heterologous cells. Nature Protocols 3:1402-1413.

Biography

Xiaoyang Serene Hu graduated with a Bachelor of Science in microbiology from the University of Wisconsin-Madison in 2014. She completed her undergraduate senior honors thesis under the guidance of Dr Kalin Vetsigian. She is pursuing her doctoral thesis under Dr Hiroaki Matsunami, and is scheduled to receive her Doctor of Philosophy degree in Molecular Genetics and Microbiology from Duke University in 2019.

Publications

Xiaoyang Serene Hu, Kentaro Ikegami, Aashutosh Vihani, Kevin W. Zhu, Marcelo Zapata, Claire de March, Matthew Do, Natasha Vaidya, Gary Kucera, Cheryl Bock, Yue Jiang, Masafumi Yohda, and Hiroaki Matsunami. "Concentration-dependent recruitment of mammalian odorant receptors." eNeuro (2019) Manuscript submitted for publication.

Xiaoyang Serene Hu, and Hiroaki Matsunami. "High-Throughput Odorant Receptor Deorphanization Via Phospho-S6 Ribosomal Protein Immunoprecipitation and mRNA Profiling." In Olfactory Receptors, pp. 95-112. Humana Press, New York, NY, 2018.

Jiang, Yue, Naihua Natalie Gong, Xiaoyang Serene Hu, Mengjue Jessica Ni, Radhika Pasi, and Hiroaki Matsunami. "Molecular profiling of activated olfactory neurons identifies odorant receptors for odors in vivo." Nature neuroscience 18, no. 10 (2015): 1446.

Scherf, Jacob M., Xiaoyang Serene Hu, William H. Tepp, Konstantin Ichtchenko, Eric A. Johnson, and Sabine Pellett. "Analysis of gene expression in induced pluripotent stem cell-derived human neurons exposed to botulinum neurotoxin A subtype 1 and a type A atoxic derivative." PloS one 9, no. 10 (2014): e111238.

Awards

European Chemoreception Research Organization Travel Award – ECRO (2017)
Chairman's Travel Awards – Duke Department of Molecular Genetics & Microbiology (2017)
Trice Predoctoral Fellowship – Duke University School of Medicine (2016)
Nomination, Howard Hughes Medical Institute (HHMI) International Student Research Fellowships (2016)
Neurogenetics Travel Award - Duke Neurogenetics (2016)
Duke Graduate School Conference Travel Award (2016)